AD-A051 584 BATTELLE COLUMBUS LABS OHIO F/G 20/11
THE DEVELOPMENT OF AN ANALYTICAL PREDICTION TECHNIQUE FOR VARIA--ETC(U)
JUN 77 M F KANNINEN, C ATKINSON, J C BELL N62269-76-C-0316
UNCLASSIFIED BATT-8-6490 NADC-77255-30 NL

1 OF 2
AD A051584

NADC-77255-30

12 SC

THE DEVELOPMENT OF AN ANALYTICAL PREDICTION TECHNIQUE FOR VARIABLE AMPLITUDE FATIGUE PROPAGATION

M. F. Kanninen
C. Atkinson
J. C. Bell
W. I. Griffith
D. W. Schmueser

Applied Solid Mechanics Section
Battelle
Columbus Laboratories
505 King Avenue
Columbus, Ohio 43201

30 June 1977

Final Report for Period 1 July 1976 - 30 June 1977
Airtask WR02303001, Work Unit DG-602

Prepared for

NAVAL AIR DEVELOPMENT CENTER
Warminster, Pennsylvania 18974

NADC Contract No. N62269-76-C-0316

THE DEVELOPMENT OF AN ANALYTICAL PREDICTION TECHNIQUE FOR VARIABLE AMPLITUDE FATIGUE CRACK PROPAGATION

M. F. Kanninen
C. Atkinson*
J. C. Bell
W. I. Griffith
D. W. Schmueser

Applied Solid Mechanics Section
Battelle
Columbus Laboratories
505 King Avenue
Columbus, Ohio 43201

30 June 1977

Final Report for Period 1 July 1976 - 30 June 1977
Airtask WR02303001, Work Unit DG-602

Prepared for

NAVAL AIR DEVELOPMENT CENTER
Warminster, Pennsylvania 18974

NADC Contract No. N62269-76-C-0316

* Department of Mathematics
Imperial College
London, England
Consultant to Battelle

NOTICES

REPORT NUMBERING SYSTEM — The numbering of technical project reports issued by the Naval Air Development Center is arranged for specific identification purposes. Each number consists of the Center acronym, the calendar year in which the number was assigned, the sequence number of the report within the specific calendar year, and the official 2-digit correspondence code of the Command Office or the Functional Department responsible for the report. For example: Report No. NADC-76015-40 indicates the fifteenth Center report for the year 1976, and prepared by the Crew Systems Department. The numerical codes are as follows:

CODE	OFFICE OR DEPARTMENT
00	Commander, Naval Air Development Center
01	Technical Director, Naval Air Development Center
02	Program and Financial Management Department
07	V/STOL Program Office
09	Technology Management Office
10	Naval Air Facility, Warminster
20	Aero Electronic Technology Department
30	Air Vehicle Technology Department
40	Crew Systems Department
50	Systems Department
60	Naval Navigation Laboratory
81	Technical Support Department
85	Computer Department

PRODUCT ENDORSEMENT — The discussion or instructions concerning commercial products herein do not constitute an endorsement by the Government nor do they convey or imply the license or right to use such products.

APPROVED BY: _____ DATE: 11/29/77

SECURITY CLASSIFICATION OF THIS PAGE (When Data Entered)

REPORT DOCUMENTATION PAGE

READ INSTRUCTIONS BEFORE COMPLETING FORM

1. REPORT NUMBER: NADC-77255-30

2. GOVT ACCESSION NO.

3. RECIPIENT'S CATALOG NUMBER

Final Rept. 1 Jul. 76 - 30 Jun. 77

4. TITLE (and Subtitle)
The Development of an Analytical Prediction Technique for Variable Amplitude Fatigue Crack Propagation

5. TYPE OF REPORT & PERIOD COVERED
Final Report
7-1-76 to 6-30-77

6. PERFORMING ORG. REPORT NUMBER
G-6490

7. AUTHOR(s)
M. F. Kanninen, C. Atkinson, J. C. Bell, W. I. Griffith, D. W. Schmueser

8. CONTRACT OR GRANT NUMBER(s)
N62269-76-C-0316 new

9. PERFORMING ORGANIZATION NAME AND ADDRESS
Battelle
505 King Avenue
Columbus, Ohio 43201

10. PROGRAM ELEMENT, PROJECT, TASK AREA & WORK UNIT NUMBERS
BATT-G-6490

11. CONTROLLING OFFICE NAME AND ADDRESS
Naval Air Development Center
Warminster, Pennsylvania 18974

12. REPORT DATE
30 JUNE 1977

13. NUMBER OF PAGES
30 Jun. 77

14. MONITORING AGENCY NAME & ADDRESS (if different from Controlling Office)
DCASO, Columbus
Building 1, Section 1
Defense Construction Supply Agency
Columbus, Ohio 43215

15. SECURITY CLASS. (of this report)
Unclassified

15a. DECLASSIFICATION/DOWNGRADING SCHEDULE

16. DISTRIBUTION STATEMENT (of this Report)

Approved for public release--distribution unlimited.

17. DISTRIBUTION STATEMENT (of the abstract entered in Block 20, if different from Report)

Approved for public release--distribution unlimited.

18. SUPPLEMENTARY NOTES

19. KEY WORDS (Continue on reverse side if necessary and identify by block number)

Fatigue crack propagation, spectrum loading, retardation

20. ABSTRACT (Continue on reverse side if necessary and identify by block number)

The development of a fatigue crack-growth predictive technique for variable amplitude loading, initiated under previous NADC support, was continued. Attention was focused on a simple version of the general model. This provided a crack growth predictive formula for constant amplitude loading. Comparisons with experimental results and a semiempirical crack-growth law show that the prediction is quite realistic. The work has also indicated how improvements in the general model can be made to cope with more realistic

cont'd

DD FORM 1 JAN 73 1473 EDITION OF 1 NOV 65 IS OBSOLETE
S/N 0102-LF-014-6601

407 080

SECURITY CLASSIFICATION OF THIS PAGE (When Data Entered)

serivce conditions. The further steps required to develop an efficient model that can cope with both variable amplitude loading and environmental effects are outlined.

SUMMARY

The development of a mathematical model for fatigue crack growth under arbitrarily varying cyclic loads was initiated under work previously supported by NADC, as documented in report NADC-76076-30. This model utilized the inclined strip yield superdislocation representation of crack-tip plasticity. While in good agreement with experimental results in predicting steady-state crack-growth rates for constant ΔK loading, the model was found to be inadequate in other aspects. Specifically, the mean stress (R effect) was not properly reproduced. Also, because the model retained one superdislocation pair for each load cycle, the computational procedure was quite cumbersome.

Steps to overcome these deficiencies are described in this report. These were undertaken using a simpler model in which one superdislocation pair was used to represent the residual plasticity left behind by the growing crack. In addition to providing results for constant crack growth rates that compare well with experimental results, this work has given some basic insights into the problem. It has also indicated how improvements in the model formulation for general load sequences can be made. Tests of the model show that the main features of the experimental observations--crack closure included--can now be reproduced. While not yet to the point where crack growth calculations for engineering purposes can be routinely performed, it is believed that the model development is well on its way to this goal.

PREFACE

This research program has been conducted by the Applied Solid Mechanics Section, Structures and Mechanics Research Department, Battelle's Columbus Laboratories, Columbus, Ohio. The work was performed under Contract No. N62269-76-C-0316. The program was administered by the Air Vehicle Technology Department, Naval Air Development Center, Warminster, Pennsylvania. Mr. Paul Kozel provided the technical liaison. This report summarizes the work performed during the period from July 1, 1976 to June 30, 1977.

TABLE OF CONTENTS

LIST OF ILLUSTRATIONS

LIST OF ILLUSTRATIONS

LIST OF TABLES

1. INTRODUCTION

A vast amount of experimental and empirical analysis work has been done on fatigue crack growth over the years. The field is sufficently well-documented that comprehensive accounts are now available in basic text books--for examples, see Broek [1], Hertzberg [2], and Rolfe and Barsom [3]--and in various popularized accounts [4-6]. Yet, at present, it is nevertheless true that the fatigue process is simply not well understood. As a consequence, there are many situations in which fatigue crack growth behavior cannot be quantitatively anticipated. Perhaps the most outstanding example is the current inability to predict crack growth in cyclic loading sequences that include load level excursions. To treat this and related situations properly, there is a distinct need for a quantitative predictive method arising from a fundamental mechanics point of view. This report describes a model which is aimed at fulfilling this need.

A predictive model for fatigue crack growth under variable amplitude loading is faced with two conflicting requirements. The first is that the crack tip deformation must be accurately predicted in the presence of the residual crack tip plasticity generated in previous load cycles. This is necessary for the model to be realistic. The second requirement is that the model must be simple enough to permit a great many load cycles to be calculated. This is necessary for the model to be useful for practical applications.

A mathematical model that is an effective compromise between these requirements was initiated in previous work supported by NADC [7-9]. The model is based upon the inclined strip yield superdislocation representation of crack tip plasticity. This gives rise to a number of extremely desirable features: (1) it admits load levels that can vary arbitrarily from cycle to cycle, (2) it automatically takes account of the crack closure phenomenon, and (3) it is capable of predicting crack growth increments solely from readily available mechanical property data. Thus, of most significance, no disposable parameters connected with specific load spectra are required to perform crack growth computations using the model.

Predictions made using the initial version of the model were not completely satisfactory. This work was undertaken to remove the deficiencies. To test the results, specific attention was placed on the steady state crack growth rates resulting from simple constant amplitude loading. As shown in this report, a closed form relation can be extracted from the model for these conditions. It is found that the result closrely resembles the semiemprical fatigue crack growth relation developed by McEvily, et al, [10-11]. McEvily's relation has been found to be in quite good accord with experimental data for many different materials under a range of loading and environmental conditions. Consequently, the correspondance is taken as confirmation that the model is now in good agreement with well established experimental results. Other experimental comparisons are provided which reinforce this conclusion.

The agreement between the crack growth rate predictions of the present model formulation and constant amplitude fatigue crack growth data constitutes the most significant result contained in this report. Nevertheless, it is important only insofar that it demonstrates the correctness of the basic approach taken in this work. It is but one milepost on the road towards the development of a general predictive technique for fatigue crack propagation under variable amplitude loading.

The work presented in this report demonstrates that the model is fundamentally sound and strongly suggests that it is capable of providing an engineering tool suitable for fatigue crack growth calculations in service conditions. However, at the present stage of development, the model is too cumbersome to be used routinely for complex load spectra. Further work is required to develop suitable representations of the residual plasticity associated with arbitrary loading histories. The simple model developed in this report for a uniform cyclic loading shows how this can be accomplished. This, together with an approach that will incorporate environmental effects into the model, will provide a broadly applicable fatigue crack growth predictive model.

2. PRELIMINARY DISCUSSION

Fatigue crack growth predictions made using the preliminary version of the model were found to be at variance with certain well established experimental trends. In subsequent work undertaken to remove these deficiencies, specific attention was placed on the crack growth rates resulting from constant amplitude loading. A large amount of experimental data exists for this case that can be used for comparison with the model. Also, a closed form crack growth relation can be extracted from the model to facilitate these comparisons. In fact, when this is done, it is found that the result approximates the fatigue crack growth relation developed and verified by McEvily and his associates [10,11].

In this section, McEvily's semiempirical crack growth equation is first given. Following this, the basic equations for the model are described together with the procedures for obtaining relations appropriate for linearized small-scale yielding conditions. These discussions are intended to provide background for the material presented in subsequent sections of this report.

McEvily's Semiempirical Crack Growth Relation

McEvily and his associates have examined the various power law and other relationships that have been advanced for constant amplitude cyclic loading in the light of experimental data for a wide range of materials, load levels, and environments. From this work, and also partly guided by theoretical considerations, they have evolved a new crack growth law of great generality. This law can be written

$$\frac{da}{dN} = \frac{A}{EY}\left[\Delta K - (\Delta K)_T\right]^2 \left[1 + \frac{\Delta K}{K_{Ic} - K_{max}}\right] , \qquad (1)$$

where E, Y, ΔK, K_{Ic}, K_{max}, K_{min}, and R have their usual meanings, here and elsewhere in this report, as follows:

K_{max} = stress intensity factor at maximum load
K_{min} = stress intensity factor at minimum load
$R = K_{min}/K_{max}$

E = elastic modulus

Y = the tensile yield stress

K_{Ic} = the plane strain fracture toughness

$\Delta K = K_{max} - K_{min}$.

Also, A is an empirically determined environment sensitive material parameter and $(\Delta K)_T$ is the threshold value of ΔK below which no crack growth is possible.

Values of the coefficients in Equation (1) for several different materials and environmental conditions are given in Table 1. A comparison between the predictions of Equation (1) and experimental data on Ti-6Al-4V at two different R values, in air and in vacuum, which exemplifies the accuracy of this relation, is shown in Figure 1.

Equation (1) contains a stronger R dependence than it might appear since, according to McEvily, et al,

$$(\Delta K)_T = \left(\frac{1 - R}{1 + R}\right)^{\frac{1}{2}} (\Delta K)_o \quad , \qquad (2)$$

where $(\Delta K)_o$ is the threshold value at R = 0. The equation also exhibits a strong yield stress dependence. However, the parameter A can depend on yield stress. Specifically, in inert atmospheres, A is proportional to the ratio Y/E. Inserting this into the above equation and rearranging then gives a result of the form

$$\frac{da}{dN} = C\left[\frac{\Delta K}{E} - \left(\frac{\Delta K}{E}\right)_T\right]^2 \left[\frac{K_{Ic} - K_{min}}{K_{Ic} - K_{max}}\right] \quad . \qquad (3)$$

While this evidently is independent of yield stress, it should be kept in mind that it is not a general result, but holds only for tests conducted in a vacuum.

The most significant point about McEvily's formula is the fact that, in contrast to the conventional power law formulation, the ΔK dependence is quadratic. This is important because the mathematical model being developed here is associated with a crack opening displacement, strain energy release rate point of view and, as is well known in fracture mechanics, these two quantities

TABLE 1. VALUES OF COEFFICIENTS IN SEMI-EMPIRICAL FATIGUE CRACK GROWTH RELATION OF McEVILY, ET AL.

Material	Y (ksi)	E (ksi)	K_c ksi $in^{1/2}$	A (dimensionless)	$(\Delta K)_o$ ksi $in^{1/2}$
		Titanium Alloys			
Ti-6Al-4V Forging in Air	120	17×10^3	65	.05	6
Ti-6Al-4V Forging in Vacuum	120	17×10^3	80	.02	12
Ti-6Al-4V Sheet in Air	140	17×10^3	100	.08	5
		Aluminum Alloys			
2024-T3	57	10.8×10^3	100	.03	5
L64	52	10.6×10^3	60	.18	6
RR58	60	10.7×10^3	21-24	.04	4
		Steels			
A514-B	129	30×10^3	200	.02	8
X65	65	30×10^3	150	.02	5
En30a Unembrittled	107	30×10^3	200	.026	7
En30a Embrittled	107	30×10^3	50	.026	7
		Stainless Steel			
316L	41	30×10^6	90	.01	8

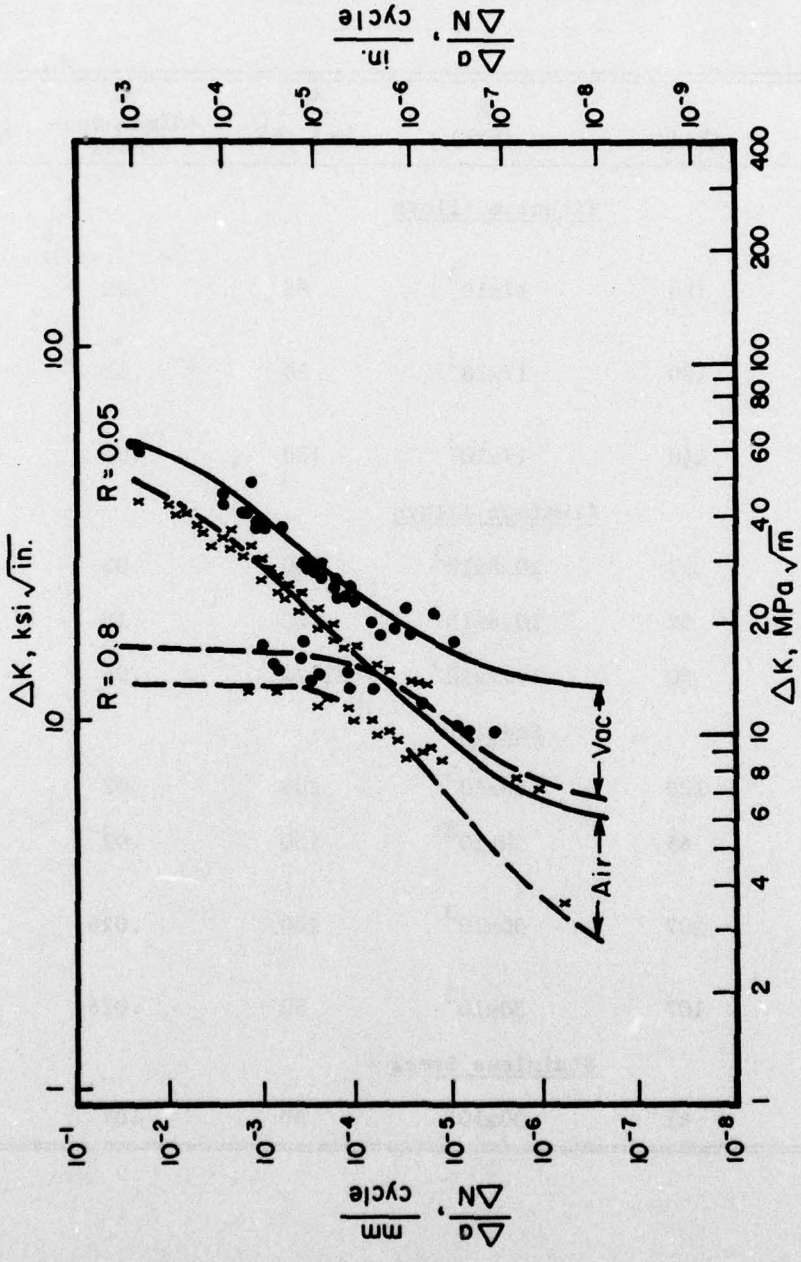

FIGURE 1. COMPARISON OF EXPERIMENTAL CRACK PROPAGATION RATES FOR Ti-6Aℓ-4V FORGING IN AIR AND VACUUM FOR TWO DIFFERENT R VALUES WITH PREDICTION OF EQUATION (1): DATA OF McEVILY, ET AL [10-11]

are related to the second power of the stress intensity factor. Thus, as shown in the following, the model will produce a result similar to that given by Equation (1). One difference is that the K_{Ic} dependence--which may be due to a crack growth mechanism occurring at high load levels that differs from the mechanism that predominates in the near threshold to moderate load regions--is not taken into account.

Basic Equations of the Model

A complete derivation of the equations governing the superdislocation representation of crack-tip plasticity have been given in references [7-9]. For present purposes it will suffice to recapitulate the key results. First, for a tensile loading applied in the direction normal to the crack plane, for plane-strain conditions, the shear stress τ acting on each superdislocation is

$$\tau = \sigma h_n + \frac{E}{8\pi(1-\nu^2)} \sum_{j=1}^{M} b_j (g_{jn} + k_{jn}) , \quad n = 1, 2, \ldots M , \qquad (4)$$

while the stress-intensity factor K is given by

$$K = (\pi a)^{\frac{1}{2}} \left\{ \sigma - \frac{1}{8\pi a} \frac{E}{1-\nu^2} \sum_{j=1}^{M} b_j f_j \right\} , \qquad (5)$$

where

σ = applied tensile stress

a = half crack length

M = number of load cycles imposed

b_j = strength of the dislocation created in the $j^{\underline{th}}$ load cycle

with the remaining undefined quantities in Equations (4) and (5) being known functions of the dislocation positions. These are given in terms of the complex variable representation

$$z_j = a_j + \ell_j e^{i\vartheta} , \quad j = 1, 2, \ldots M ,$$

where

θ = angle between the crack plane and slip plane (constant)
a_j = crack length at the time that the $j^{\underline{th}}$ dislocation was emitted
ℓ_j = distance from the crack plane along the slip plane to the $j^{\underline{th}}$ dislocation.

It is considered that the material provides an intrinsic friction stress which resists the movement of the superdislocation. This parameter is denoted τ_i (for internal) and is related to Y, the tensile yield stress by

$$\tau_i = \varepsilon Y \quad , \tag{6}$$

where ε is a numerical constant. The equations of force equilibrium that are the basis for the mathematical model are formed by setting the right-hand side of Equation (4) equal to τ_i for each of the M superdislocations in the problem.

An expression for the crack-opening displacements can also be determined. Again omitting the details, the result is found to be

$$v = 4\sigma \frac{1-\nu^2}{E} (a^2 - x^2)^{\frac{1}{2}} + \sin\theta \sum_{j=1}^{M} b_j d_j \quad , \tag{7}$$

where $v = v(x)$ is the crack-opening displacement at a position on the crack face $x \leq a$. In Equation (7), x is measured from the center of the crack and d_j is again a function of the superdislocation positions.

For most fatigue crack-propagation problems, a linearized or "small-scale yielding" approximation is valid. For a plastic zone that is represented by a single superdislocation pair, the governing equations are for the force equilibrium of the dislocations (only one needs to be considered because of symmetry) and the singularity canceling equation. The unknowns are the superdislocation strength, b, and the position, ℓ. Setting $\tau = \tau_i$ in Equation (4) and using Equation (6), it is found that

$$\varepsilon Y = \sigma h\ (\ell) + \frac{Eb}{8\pi(1-\nu^2)}\ [g\ (\ell) + k\ (\ell)]\quad , \tag{8}$$

and

$$a\sigma = \frac{Eb}{8\pi(1-\nu^2)}\ f\ (\ell)\quad . \tag{9}$$

In small-scale yielding where $\ell \ll a$, the functions appearing in Equations (8) and (9) are simply

$$f(\ell) = 6\left(\frac{2a}{\ell}\right)^{\frac{1}{2}} \sin\theta \cos\frac{\theta}{2} \tag{10}$$

$$g(\ell) = -\frac{1}{\ell}\ (1 - \cos 2\theta) \tag{11}$$

$$h(\ell) = \frac{1}{4}\left(\frac{2a}{\ell}\right)^{\frac{1}{2}} \sin\theta \cos\frac{\theta}{2} + \sin\theta\cos\theta \tag{12}$$

$$k(\ell) = -\frac{1}{\ell}\cos 2\theta\quad . \tag{13}$$

Substituting Equations (10-13) into Equations (8) and (9) and eliminating b gives the following relation for the superdislocation position

$$\frac{\ell}{a} = \frac{\varepsilon^2}{8}\left\{3\sin\theta\cos\frac{\theta}{2} - \frac{1}{\sin\theta\cos\frac{\theta}{2}}\right\}^2 \left(\frac{\sigma}{Y}\right)^2 \left\{1 - \frac{1}{\varepsilon}\frac{\sigma}{Y}\sin\theta\cos\theta\right\}^{-2} \tag{14}$$

In this work, the particular angle θ selected was that which maximizes the extent of yielding (equivalently, the plane of maximum shear). From Equation (14), this is $\theta = \cos^{-1}(1/3) = 70.53°$.

The superdislocation will not give precise information about the size and shape of the plastic zone. However, this is unimportant because it accurately represents the plastic deformation occurring at the crack tip. Consider the prediction of δ, the crack-tip-opening displacement. This can be written as

$$\delta = 2b \sin \theta \ . \tag{15}$$

Upon solving for b and substituting into the above for plane strain under fixed load for small-scale yielding conditions, it is found that

$$\delta = \frac{2\epsilon}{3} \frac{1-\nu^2}{\cos \theta/2} \left\{ 3 \sin\theta \cos\frac{\theta}{2} - \frac{1}{\sin\theta \cos\frac{\theta}{2}} \right\} \frac{K^2}{EY} \cdot \left\{ 1 - \frac{1}{\epsilon} \frac{\sigma}{Y} \sin\theta \cos\theta \right\}^{-1} \tag{16}$$

where, for an infinite medium, $K = \sigma\sqrt{\pi a}$. Hence, $\delta = \alpha \frac{K^2}{EY}$, where $\alpha = 0.433$ for $\epsilon = 1/\sqrt{3}$ and $\nu = 0.3$. A comparison with the results obtained from a variety of both approximate and highly rigorous calculations of the crack-opening displacement are given in References [7-9]. These results verify the fidelity of the superdislocation representation in the area of main concern here--in its prediction of the crack-tip crack-opening displacement. Further validation of this approach is given in the following section of this report.

3. COMPUTATION OF CRACK-OPENING DISPLACEMENTS

Two areas have been identified from which the inadequacies of the model developed initially have stemmed. These are, (1) the treatment of a residual dislocation in the unloading phase of the load cycle, and (2) the role of the singularity canceling equation in determining an equilibrium state. The key to improving the model in regard to these two areas has been the development of correct expressions for the crack-opening displacements. The procedure and results are completely described in Appendix A of this report. For present purposes it is enough to say that, although these results were derived in the previous work, because no use was made of them earlier, their deficiencies were not recognized. It is now certain, however, that the expressions for the crack-opening displacements, which now play a crucial role, are correct.

When a maximum load is imposed in the model, the nascent superdislocation's strength and position are determined by specifying that (1) the superdislocations are in force equilibrium and (2) the crack-tip singularity is abolished. This is just the same as in previous work. However, when the load is reduced, where previously the strength was modified while the position was held fixed, now the strength is fixed (or moderately reduced) while the position is increased. The reason for the change is based upon the effective representation of the crack-face displacements thereby obtained.

A series of elastic-plastic finite element computations were performed to determine the exact shape of the crack faces in a load-unload sequence. A complete description of the finite element method, the computational procedure, and the results obtained are given in Appendix B of this report. Typical results are given in Table 2. The values of the crack-opening displacement at the center of the crack, for heuristic purposes, are shown in Figure 2 for several load-unload sequences. The idea was to see if this information could be used to test (and perhaps improve upon) the superdislocation representation of the residual plasticity in cyclic loading. In fact, this procedure has revealed a way in which this could be done.

The set of calculations shown in Figure 3 demonstrated the necessity of modifying the superdislocation position during unloading. In these calculations, the superdislocation generated at a maximum applied stress of 29,780 psi (roughly equal to half the yield stress) was allowed to retain its full strength and was kept at the same position while the applied stress was relaxed to zero.

TABLE 2. CRACK OPENING DISPLACEMENTS FOR 2024-T3 ALUMINUM CENTER CRACKED PANELS FOR A LOAD-UNLOAD SEQUENCE OBTAINED FROM AN ELASTIC-PLASTIC FINITE ELEMENT ANALYSIS (PLANE STRESS)

a = 1.18 inches W = 6.0 inches

Data Set Designation	Applied Stress (psi)	Crack Opening Displacement (Inches) At Various Positions On Crack Face (Inches From Center)				
		x = 0	x = .383	x = .709	x = .774	x = 1.063
	(a) Maximum Applied Stress = 29,780 psi					
	Loading Phase					
1	15,190	.00322	.00311	.00257	.00231	.00122
2	20,050	.00433	.00418	.00349	.00315	.00181
3	24,920	.00551	.00533	.00450	.00408	.00253
4	29,780	.00679	.00659	.00562	.00515	.00340
	Unloading Phase					
16	22,330	.00521	.00507	.00436	.00402	.00280
17	14,890	.00364	.00354	.00310	.00289	.00221
18	7,440	.00206	.00202	.00184	.00176	.00161
19	0	.00048	.00050	.00058	.00063	.00100
	(b) Maximum Applied Stress = 35,100 psi					
	Loading Phase					
1	15,190	.00322	.00311	.00257	.00231	.00122
2	20,050	.00433	.00418	.00349	.00315	.00181
3	24,920	.00551	.00533	.00450	.00408	.00253
4	29,780	.00679	.00659	.00652	.00515	.00340
5	35,100	.00836	.00814	.00705	.00652	.00459
	Unloading Phase					
12	26,330	.00651	.00634	.00556	.00519	.00388
13	17,550	.00465	.00455	.00407	.00385	.00318
14	8,770	.00279	.00276	.00259	.00252	.00247
15	0	.00093	.00096	.00110	.00119	.00177
	(c) Maximum Applied Stress = 43,200 psi					
	Loading Phase					
1	15,190	.00322	.00311	.00257	.00231	.00122
2	20,050	.00433	.00418	.00349	.00315	.00181
3	24,920	.00551	.00533	.00450	.00408	.00253
4	29,780	.00679	.00659	.00561	.00515	.00340
5	35,100	.00836	.00814	.00705	.00652	.00459
6	39,150	.00978	.00953	.00836	.00780	.00574
7	43,200	.01150	.01120	.00999	.00934	.00716
	Unloading Phase					
8	32,400	.00890	.00873	.00789	.00748	.00611
9	21,600	.00661	.00651	.00605	.00584	.00523
10	10,800	.00432	.00431	.00423	.00420	.00436
11	0	.00187	.00193	.00219	.00234	.00307

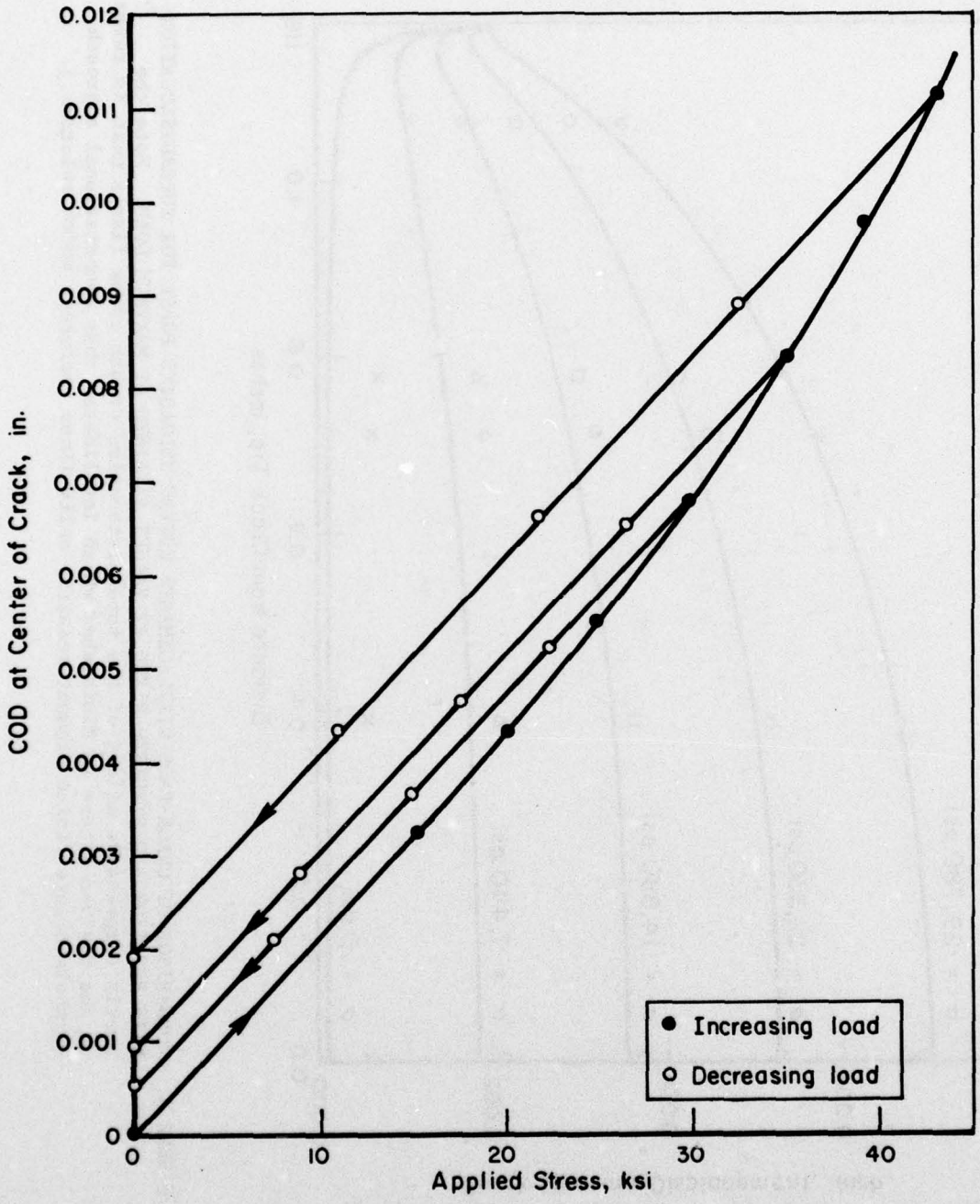

FIGURE 2. CRACK-OPENING DISPLACEMENT AT CENTER OF THE CRACK IN A LOAD-UNLOAD SEQUENCE AS OBTAINED FROM AN ELASTIC-PLASTIC FINITE ELEMENT ANALYSIS

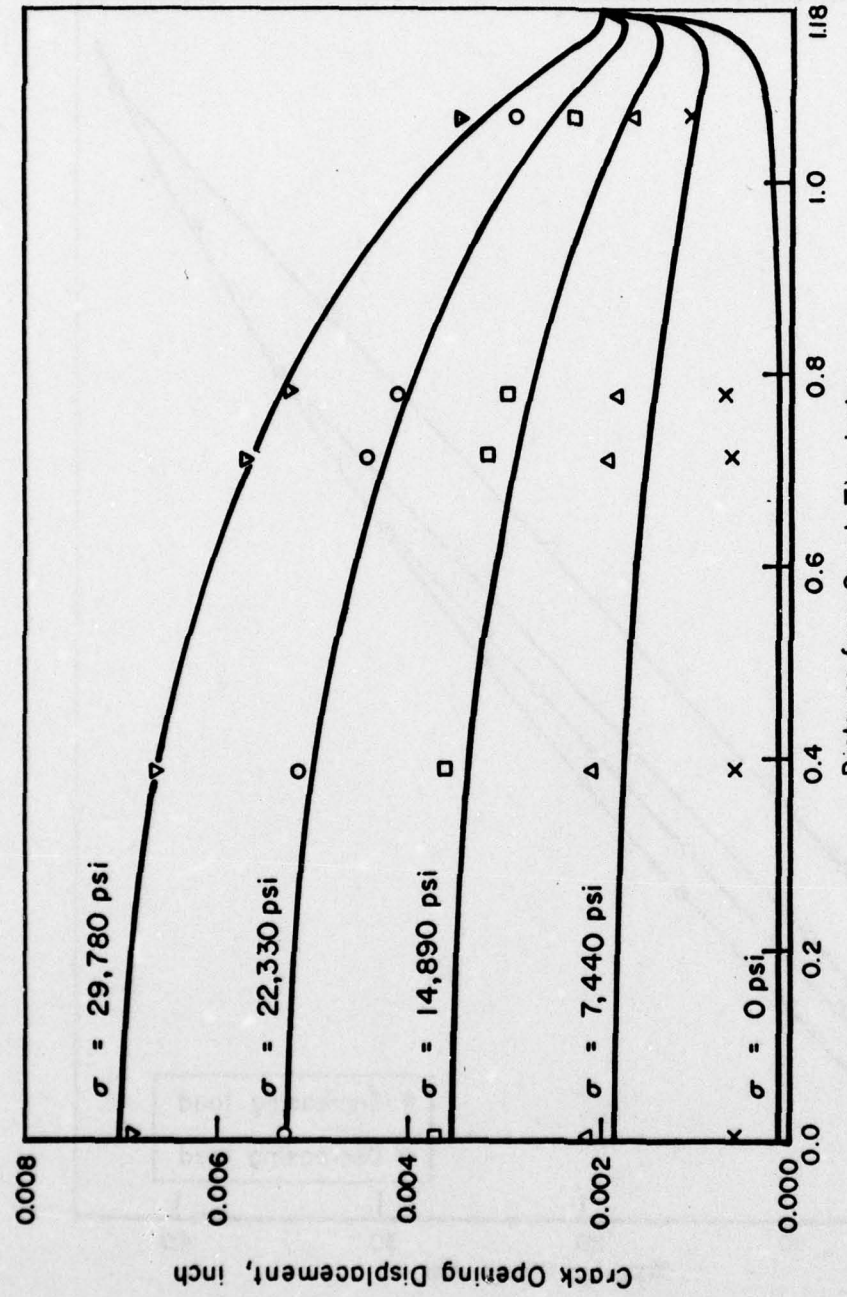

FIGURE 3. COMPARISON OF CRACK-FACE DISPLACEMENTS DURING UNLOADING PHASE FOR SUPERDISLOCATION WITH POSITION AND STRENGTH FIXED AT VALUES ATTAINED AT MAXIMUM LOAD. Note the overly compressive effect of the superdislocation on the crack flanks that is revealed as the applied stress is diminished which invalidates this computational approach. (Symbols denote finite element results, solid lines represent model solution.)

It was seen that, while little discrepancy existed in the beginning stages of the unloading, this eventually became untenable. In particular, at zero load the compressive effect of the superdislocation on the crack flanks was far too great; nb, the crack-tip displacement is about right. Clearly, to reduce this effect, the superdislocation strength must be decreased, or it must be pushed further away from the crack, or both.

The set of calculations shown in Figure 4 demonstrated the inadequacy of reducing the dislocation strength while keeping its position fixed. For these results the strength was reduced by a factor of two, as would be given by the procedure used previously for a zero load level. The position was then increased to determine if a combination change would suffice. It was found that agreement with the finite element results could be obtained for redical strength changes, but only with highly unrealistic changes in the superdislocation position.

The results shown in Figure 4 indicated that focusing on the superdislocation position is the only plausible alternative. There is a physical rationale for this which stems from the point of view that the superdislocation is an idealization of a dislocation pile-up. Specifically, its position represents the "center of gravity" of such a pile-up. In such a pile-up, the dislocations near the crack will slip backwards and will vanish into the crack as the applied stress is reduced. In contrast, the dislocations in the pile-up away from the crack will be locked into position. Thus, the "center of gravity" of the pile-up will shift as the load diminishes. Equivalently, the superdislocation representing the pile-up will shift outwards. This, of course, must be accompanied by a modest decrease in the strength.

While this argument is appealing, it unfortunately cannot easily be made quantitative. An alternative is to use the finite element results to learn just how the superdislocation must be shifted. The result of a trial and error calculation demonstrated that a monotonic increase in ℓ, the distance between the superdislocation position and the crack tip, as the load is decreased to zero gives excellent agreement with the finite element results. Denoting the maximum applied stress as σ_{max} and the superdislocation position at that stress as ℓ_o, the positions ℓ required for good agreement with this set of finite element crack-opening displacements for a maximum load of 29,780 psi are estimated in Table 3.* The crack-opening displacement comparison resulting from movements

* Note that these results are valid only for the particular geometry, load level, and mechanical properties used to generate the finite element results of Table 2; NB, the fairly large aspect ratio used in these calculations.

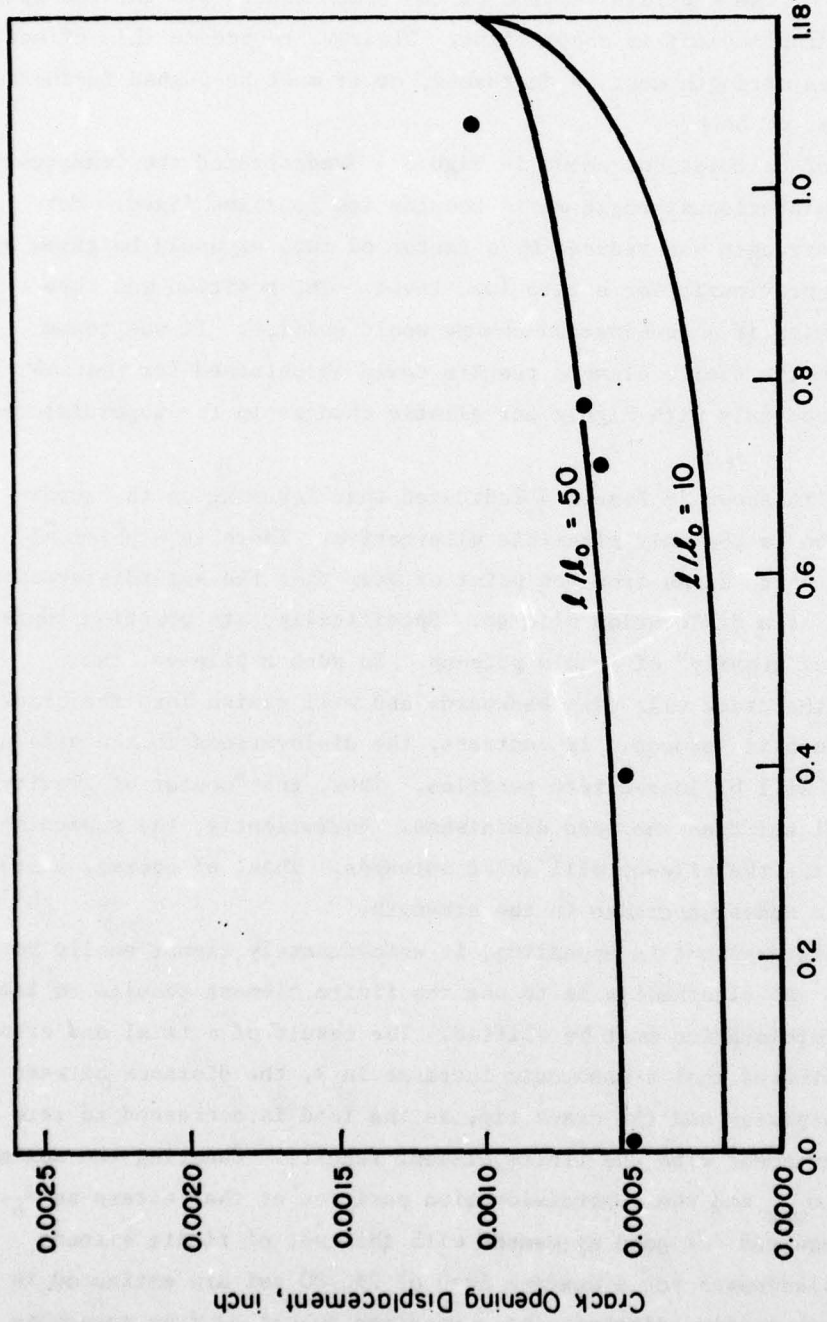

FIGURE 4. COMPARISON OF CRACK-FACE DISPLACEMENTS AT ZERO LOAD FOR SUPERDISLOCATION WITH STRENGTH REDUCED TO ONE-HALF OF THAT ATTAINED AT MAXIMUM LOAD AND POSITION ARBITRARILY VARIED FOR HEURISTIC PURPOSES. Note that position must be increased to an unreasonable extent to achieve agreement with finite-element results which invalidates this computational approach. (Symbols denote finite element solutions, solid lines represent superdislocation model solution.)

of the superdislocations in accord with Table 3 are shown in Figure 5. The results shown in Figure 5 can be readily seen to offer a significant improvement over those of Figure 3.

TABLE 3. RELATIVE SUPERDISLOCATION POSITION IN THE UNLOADING PHASE OF A LOAD-UNLOAD SEQUENCE REQUIRED FOR CORRECT PREDICTION OF THE CRACK-OPENING DISPLACEMENTS (See Figure 5)

$R = \sigma_{min}/\sigma_{max}$	ℓ/ℓ_o
1.00	1.0
0.75	1.5
0.50	3.0
0.25	10.0
0	13.0

The approach to be taken in the following section is based on the point of view that the residual plasticity created during an extended period of steady-state crack growth under constant ΔK load cycles can be represented by a single superdislocation pair. The strength of the "residual" superdislocations is governed by Equations (8) and (9). Its position initially arises from these same equations but is modified to match the finite-element solutions for the crack faces during unloading. An aid in obtaining these results is the linearized relation for the crack-opening displacement at the center of the crack. This is obtained by using the relation

$$d(\ell,0) = 2 - \frac{2}{\pi}\left(\frac{2\ell}{a}\right)^{\frac{1}{2}} \cos\frac{\theta}{2} \quad , \tag{17}$$

where $d = d(\ell,x)$ is the one-superdislocation version of the function of a complex variable included in Equation (7). Substituting Equation (17) into (7) then gives

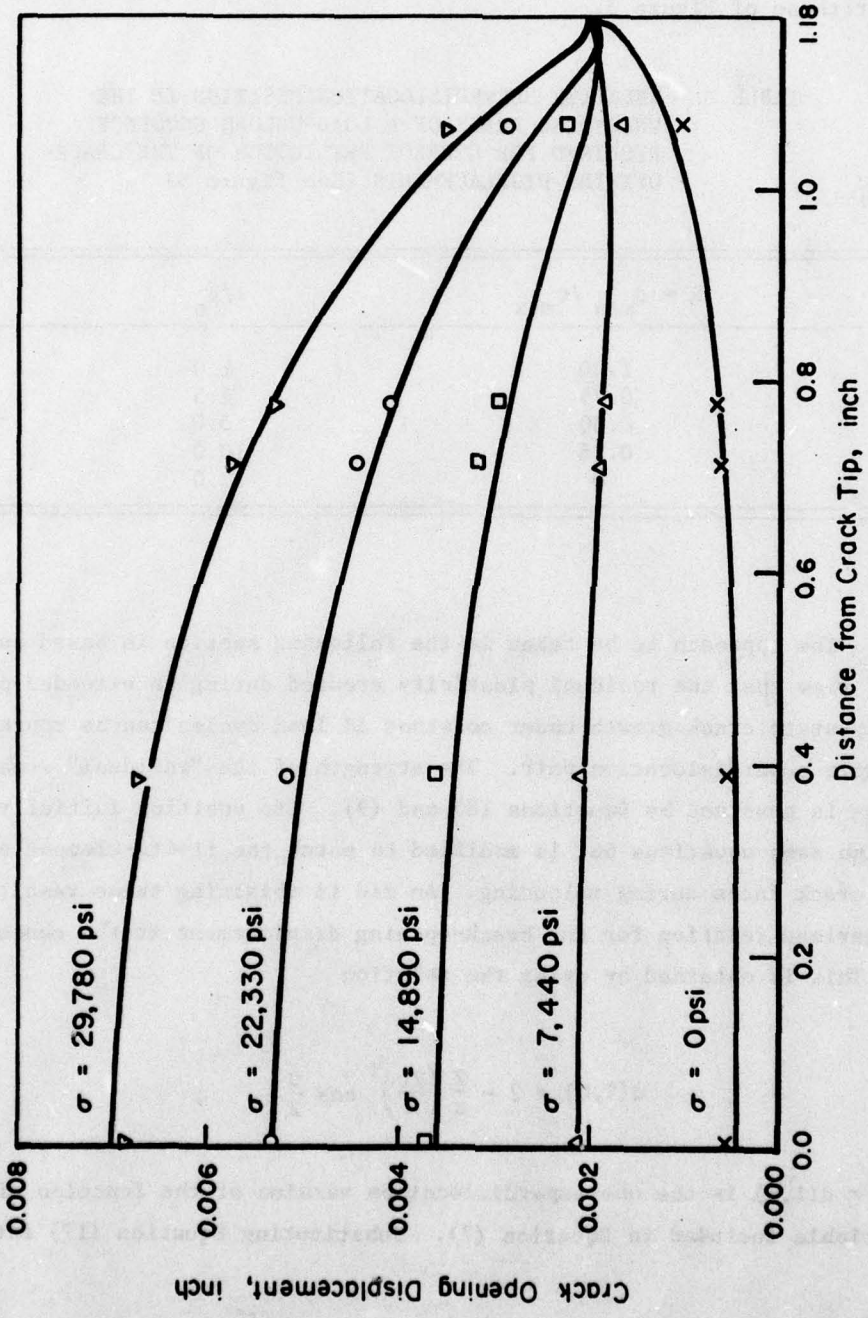

FIGURE 5. COMPARISON OF CRACK-FACE DISPLACEMENTS DURING UNLOADING PHASE FOR SUPERDISLOCATION WITH STRENGTH FIXED AT VALUE ATTAINED AT MAXIMUM LOAD BUT POSITION VARIED AS A FUNCTION OF LOAD TO FIT DATA OF TABLE 2. Note excellent agreement obtained with this computational approach. (Symbols denote finite element solution, solid lines represent superdislocation model solution.)

$$v(0) = 4\sigma a \frac{1-\nu^2}{E} + 2b \left\{ 1 - \frac{1}{\pi} \left(\frac{2\ell}{a} \right)^{\frac{1}{2}} \cos \frac{\theta}{2} \right\} \sin \theta \quad . \qquad (18)$$

Note that v represents here the <u>total</u> distance between the crack faces and is twice the distance from the crack faces to the symmetry plane.

4. FATIGUE CRACK-GROWTH CALCULATIONS

In previous work, fatigue crack growth computations were carried out using one superdislocation pair to represent the crack-tip plasticity in each and every load cycle. This can be referred to as the "cycle-by-cycle" model. In contrast, the following calculations will be performed using a much simpler two superdislocation model. This is motivated by the necessity of working with a less cumbersome computational scheme in the formative stages of the work and the fact that, in the cycle-by-cycle model, one of the superdislocations left behind by the growing crack invariably dominates. This suggests that a suitable model for steady-state crack growth under constant ΔK load cycles would be one composed of one "residual" superdislocation pair and a nascent superdislocation pair. This model is illustrated in Figure 6.

Formulation of the Simplified Model

The relations given earlier apply to the single superdislocation pair representation of residual crack-tip plasticity. For the steady-state crack-growth situation (which will occupy the balance of this section), it is the interaction of a nascent superdislocation pair with the residual plasticity that is of chief concern. The relations for the interaction between two superdislocations are also necessary, therefore. Linearized versions of the dislocation interaction terms can be deduced by assuming that both dislocations are on the same slip plane and that they occupy positions such that $a >> \ell_1 >> \ell_2$. Hence, the interaction terms are found to be

$$g_{12} + k_{12} = -\frac{2}{\ell_1}(1 - \cos 4\theta) - \frac{3}{(\ell_1 \ell_2)^{\frac{1}{2}}} \sin^2\theta \cos^2\frac{\theta}{2} \qquad (19)$$

and

$$g_{21} + k_{21} = 3\frac{\ell_2^{\frac{1}{2}}}{\ell_1^{\frac{3}{2}}} \sin^2\theta \cos^2\frac{\theta}{2} + 2\frac{\ell_2}{\ell_1^2}(1 - \cos 4\theta) \qquad (20)$$

from which it can be seen that

$$g_{21} + k_{21} = -\frac{\ell_2}{\ell_1}(g_{12} + k_{12}) \quad .$$

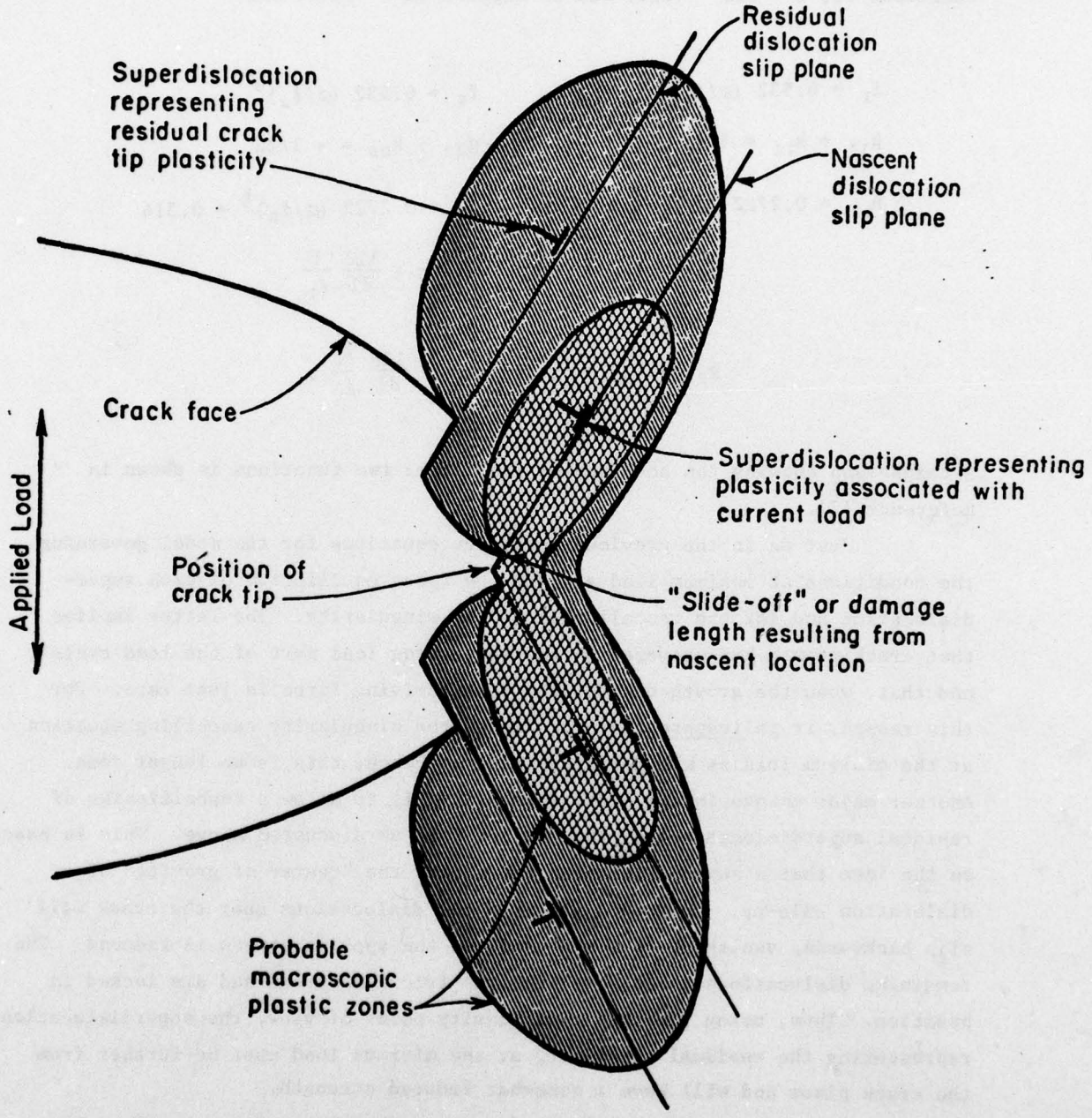

FIGURE 6. SIMPLIFIED TWO SUPERDISLOCATION MODEL FOR STEADY-STATE FATIGUE CRACK GROWTH

For convenience in the following, the specific values for all the linearized functions for $\theta = \cos^{-1}(1/3)$ can be written out. These are

$$f_1 = 6.532\ (a/\ell_1)^{\frac{1}{2}} \qquad f_2 = 6.532\ (a/\ell_2)^{\frac{1}{2}}$$

$$g_{11} + k_{11} = 1/\ell_1 \qquad g_{22} + k_{22} = -\ 1/\ell_2$$

$$h_{11} = 0.2722\ (a/\ell_1)^{\frac{1}{2}} + 0.314 \qquad h_2 = 0.2722\ (a/\ell_2)^{\frac{1}{2}} + 0.314$$

$$g_{12} + b_{12} = -\frac{16}{9}\frac{1}{(\ell_1\ell_2)^{\frac{1}{2}}} - \frac{128}{81}\frac{1}{\ell_1}$$

$$g_{21} + k_{21} = \frac{16}{9}\frac{(\ell_1\ell_2)^{\frac{1}{2}}}{\ell_1^{\,2}} + \frac{128}{81}\frac{\ell_2}{\ell_1^{\,2}}.$$

A comparison showing the accuracy of the latter two functions is shown in Reference [7].

Just as in the previous work, the equations for the model governing the conditions at maximum load are for the force equilibrium of each superdislocation and for the cancellation of the singularity. The latter implies that crack growth has occurred on the increasing load part of the load cycle and that, when the growth ceases, the crack-driving force is just zero. For this reason, it is <u>inappropriate</u> to impose the singularity cancelling equation at the minimum load as was done previously. Hence, this is no longer done. Another major change in the model formulation is to allow a repositioning of residual superdislocations at the minimum load as discussed above. This is based on the idea that a superdislocation represents the "center of gravity" of a dislocation pile-up. In such a pile-up, the dislocations near the crack will slip backwards, vanishing into the crack as the applied stress is reduced. The remaining dislocations cannot overcome the friction stress and are locked in position. Thus, using the center of gravity point of view, the superdislocation representing the residual plasticity at the minimum load must be further from the crack plane and will have a somewhat reduced strength.

To obtain a solution for the steady-state situation, consider that the residual superdislocation is located at a position L, the nascent superdislocation at a position ℓ. A solution exists if, and only if, the nascent superdislocation is in force equilibrium and the net stress-intensity factor

is zero. For the latter condition to hold with a nonnegative value of the strength of the nascent superdislocation, there will be a threshold value of the applied stress. From Equation (5), for the residual superdislocation strength held constant, this is

$$\sigma_{th} = \left(\frac{L_o}{L}\right)^{\frac{1}{2}} \sigma_{max} \quad , \tag{21}$$

where L/L_o is the ratio of the adjusted position to the initial position of the residual superdislocation. Now writing

$$(\Delta K)_{th} = (\sigma_{th} - \sigma_{min})(\pi a)^{\frac{1}{2}} \quad , \tag{22}$$

it can be seen that

$$(\Delta K)_{th} = K_{max}\left\{\left(\frac{L_o}{L}\right)^{\frac{1}{2}} - R\right\} \quad , \tag{23}$$

where, as usual, $R = K_{min}/K_{max}$.

A "threshold" will exist in the model if the right-hand side of Equation (23) is positive. This will be the case if

$$\frac{L}{L_o} < \frac{1}{R^2} \quad .$$

Using the values of L/L_o given in Table 3, Figure 7 shows that the inequality is always satisfied for all $R < 1$. Thus, the threshold effect does exist in the model.

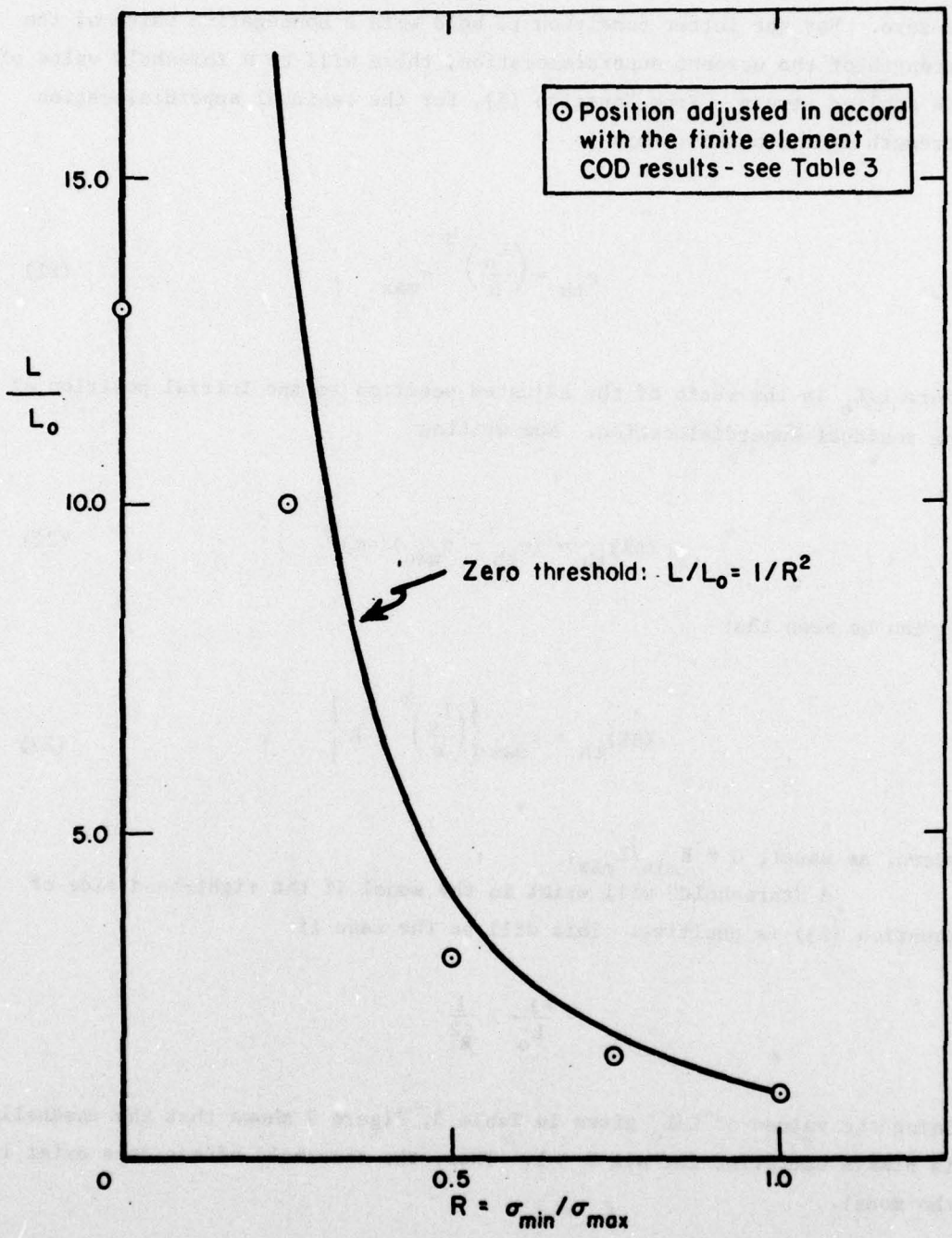

FIGURE 7. COMPARISON OF THE RESIDUAL SUPERDISLOCATION POSITION WITH VALUES FOR ZERO THRESHOLD

It might be noted that this arises strictly from consideration of the residual compressive stresses exerted on the crack tip by the plasticity generated in previous load cycles and is independent of a crack-closure condition. It can be further seen that there is nothing in the nature of a material property associated with the threshold as some researchers have suggested.

The final step in the formulation of the steady-state solution is to determine b. Then, by associating the crack-advance increment with the length of new crack surface projected along the original crack plane

$$\Delta a = 2k\,b\,\cos\theta \quad , \tag{24}$$

where k is taken to be an environment-material constant. The parameter k is intended to account for the experimentally observed fact that "rewelding" of the crack surfaces can occur and, further, that the extent to which this occurs depends on the environment. Thus, $0 < k \leq 1$. In benign evironments, k would be expected to be quite small. In agressive environments, it would approach unity.

Steady-State Crack-Growth Rate

Using the simplified two dislocation model of Figure 6, a prediction of steady-state fatigue crack growth can be made. For definitness, the following parameters will be used:

B = strength of the residual superdislocation
b = strength of the nascent superdislocation
L = position of the residual superdislocation along the slip plane
ℓ = position of the superdislocation along the slip plane
c = distance from the crack tip to the residual superdislocation slip plane.

It will be considered that B, L, and c are fixed by the prior load history; e.g., independently by finite element or other computations. The variables to be determined are b and ℓ. This is done by satisfying the equations for the equilibrium of the nascent superdislocation and for the cancellation of the singularity at the maximum load in the cycle. Thus, from Equations (8) and (9)

$$\tau_i = \sigma_{max}\, h(\ell) + \frac{Eb}{8\pi}\left\{g(\ell,\ell) + k(\ell,\ell)\right\} + \frac{EB}{8\pi}\left\{g(L,\ell) + k\,(L,\ell)\right\} \tag{25}$$

and

$$a\,\sigma_{max} = \frac{E}{8\pi}\ \{bf(\ell) + Bf(L)\} \quad . \tag{26}$$

The parameter b can be determined from Equation (26) as

$$b = \frac{1}{f(\ell)}\left\{\frac{8\pi}{E}\ a\,\sigma_{max} - Bf(L)\right\} \quad . \tag{27}$$

Then, by using Equation(27) to eliminate b from Equation (25), ℓ can be determined. The result, in terms of the linearized versions of the functions f, h, g, and k as given by Equations (10-13), is

$$\ell = \left\{ \frac{1}{6}\left(\frac{a}{2}\right)^{\frac{1}{2}}\ \sigma_{max}\left[3 \sin\theta \cos\frac{\theta}{2} - \frac{1}{\sin\theta \cos\frac{\theta}{2}}\right] + \right.$$

$$\left. \frac{1}{8\pi}\frac{EB}{L^{\frac{1}{2}}}\left[1 - 3\sin^2\theta\cos^2\frac{\theta}{2}\right]\right\}^2 \cdot$$

$$\cdot\left\{\tau_i - \sigma_{max}\sin\theta\cos\theta + \frac{2\,(1-\cos 4\theta)}{8\pi}\ \frac{EB}{L}\right\}^{-2} \quad . \tag{28}$$

The equivalent linearized version of Equation (27) is

$$b = \frac{8\pi}{E}\left\{\frac{1}{6}\left(\frac{a}{2}\right)^{\frac{1}{2}}\frac{\sigma_{max}}{\sin\theta\cos\frac{\theta}{2}} - \frac{EB}{8\pi}\frac{1}{L^{\frac{1}{2}}}\right\}\ell^{\frac{1}{2}} \quad . \tag{29}$$

Combining Equations (28) and (29) then gives

$$b = \frac{1}{9E}\left[3 - \frac{1}{\sin^2\theta\cos^2\frac{\theta}{2}}\right]\left\{\sigma_{max}\,(\pi a)^{\frac{1}{2}} - \left(\frac{9}{8\pi}\right)^{\frac{1}{2}}\sin\theta\cos\frac{\theta}{2}\frac{EB}{L^{\frac{1}{2}}}\right\}^2 \cdot$$

$$\cdot\left\{\tau_i - \sigma_{max}\sin\theta\cos\theta + \frac{1-\cos 4\theta}{4\pi}\frac{EB}{L}\right\}^{-1} \quad . \tag{30}$$

Setting $K_{max} = \sigma_{max} (\pi a)^{\frac{1}{2}}$ and $\tau_i = Y \sin\theta \cos\theta$ then gives

$$b = \frac{1}{9EY \sin\theta \cos\theta} \left[3 - \frac{1}{\sin^2\theta \cos^2\frac{\theta}{2}}\right] \left[K_{max} - K_{th}\right]^2 \cdot$$

$$\cdot \left[1 - \frac{\sigma_{max}}{Y} + \frac{1}{4\pi}\left(\frac{1 - \cos 4\theta}{\sin\theta \cos\theta}\right)\frac{EB}{YL}\right]^{-1} , \qquad (31)$$

where

$$K_{th} = \left(\frac{9}{8\pi}\right)^{\frac{1}{2}} \frac{EB}{L^{\frac{1}{2}}} \sin\theta \cos\frac{\theta}{2} . \qquad (32)$$

Further progress can be made by relating B and L to the values for fixed load conditions. Call these B_o and L_o, respectively. *It is readily found that*

$$B_o = \frac{K_{max}^2}{9EY \sin\theta \cos\theta} \left[3 - \frac{1}{\sin^2\theta \cos^2\frac{\theta}{2}}\right] \left[1 - \frac{\sigma_{max}}{Y}\right]^{-1} \qquad (33)$$

and

$$L_o = \frac{K_{max}^2}{72\pi Y^2 \sin^2\theta \cos^2\theta} \left[3 \sin\theta \cos\frac{\theta}{2} - \frac{1}{\sin\theta \cos\frac{\theta}{2}}\right]^2 \left[1 - \frac{\sigma_{max}}{Y}\right]^{-2} . \qquad (34)$$

Key parameters are seen to be the ratios B/B_o and L/L_o. These can be conveniently expressed in terms of dimensionless parameters β and λ, defined as

$$\beta = \left(\frac{B}{B_o}\right) , \qquad (35)$$

and

$$\lambda = \left(\frac{L}{L_o}\right) \qquad (36)$$

which fix the residual plasticity in this model.

Before specializing the results for $\theta = \cos^{-1}(1/3)$, it might be emphasized that, in order for the model to correctly predict general yielding when the applied stress is equal to the tensile yield stress Y, the friction stress was taken equal to $Y \sin\theta \cos\theta = 0.314\ Y$. Further note that plane stress conditions are used and that the equations have been linearized; i.e., by taking $\ell \ll L \ll a$, and neglecting the distance between the two slip planes. Under these conditions, substituting Equation (31) into Equation (24) then gives

$$\frac{da}{dN} = \frac{7}{32\sqrt{2}} \frac{k}{EY}\left\{K_{max} - K_{th}\right\}^2 \left\{1 - \frac{\sigma_{max}}{Y} + \frac{4\sqrt{2}}{9\pi}\frac{EB}{YL}\right\}^{-1} . \tag{37}$$

The introduction of expressions for B and L can be facilitated by expressing them in terms of the values obtained for a single load application through the use of Equations (33-36). In particular

$$B = \frac{21}{32\sqrt{2}} \frac{K^2_{max}}{EY} \beta \left(1 - \frac{\sigma_{max}}{Y}\right)^{-1} \tag{38}$$

and

$$L = \frac{147}{1024\pi} \frac{K^2_{max}}{Y^2} \lambda \left(1 - \frac{\sigma_{max}}{Y}\right)^{-2} \tag{39}$$

where β and λ, as above, denote the ratios of B and L for a growing crack (i.e., one with a wake of plasticity) to their values for a single load application.

Using Equations (38) and (39) to eliminate b and L in Equation (37) then gives a result that can be written as

$$\frac{da}{dN} = \frac{A}{EY}\left\{K_{max} - K_{th}\right\}^2 \left\{1 - \frac{\sigma_{max}}{Y}\right\}^{-1} , \tag{40}$$

where

$$K_{th} = \frac{\beta}{\lambda^{\frac{1}{2}}} K_{max} \tag{41}$$

and

$$A = \frac{7k}{32\sqrt{2}} \left\{ 1 + \frac{128}{63} \frac{\beta}{\lambda} \right\}^{-1} . \tag{42}$$

Because $K_{max} - K_{th} = (K_{max} - K_{min}) - (K_{th} - K_{min}) = K - (\Delta K)_T$, for small applied stresses, Equation (40) can be seen to be qualitatively consistent with Equation (1). Quantitative comparisons will depend on the exact form of the functions β and λ. While these are expected to be principally dependent on R and on Y/E, general relations have not yet been determined. However, it is interesting to note that, if β/λ is on the order of unity and k = 1, then, from Equation (42), A will be approximately equal to .05, a value in quite good agreement with McEvily's findings for crack growth in air.

There are some important differences between Equation (1) and (40) also. First, in this work, K_{th} emerges as a variable which reflects a load history effect. In contrast, the conventional view of the threshold is that it is a material property. Determinations of this quantity are made in such a way as to minimize the load history effect by gradually diminishing the stress amplitude to determine the limit of zero crack growth. Clearly, the value given by Equation (41) is appropriate to a particular load history, not to this limiting case.

A second difference is that, while a K_c term does not appear in the model, an explicit dependence on σ_{max}/Y does emerge from this approach.* It is possible that another crack growth mode combines with the sliding off mode being considered here at high K_{max} values. But, it is difficult to see how this could be connected with a K_c value in a logical self-consistent manner.

---

* As shown in Reference [11], Equation (1) can be generalized to take account of accelerated crack growth as net section yielding is approached.

The Crack Closure Condition

An essential difference between the previous work and the present is with regard to the crack-closure prediction capability of the model. It was stated in Reference 7 that the imposition of the singularity cancelling equation forces the crack faces to close smoothly at the tip and, consequently, that this is a necessary condition for crack closure to occur. But, as the work given in Appendix A shows, the interpretation of the crack-opening displacement relations giving rise to this conclusion was faulty.

It is now clear that a step change (of height equal to the superdislocation strength) occurs in the crack-opening displacement.* Thus, while cancelling the crack-tip singularity still forces the crack faces to be parallel, they will not touch each other except in the limiting case where the superdislocation strength is zero. It can be shown, in fact, that no impingement of the surfaces is possible at any point along the crack flanks for a positive superdislocation strength. Proof of this statement is given in Appendix A of this report. However, while it may appear that crack closure is impossible in this model, that this is not the case can be made clear, as follows.

For a superdislocation on a slip plane that intersects the crack faces at the crack tip, no crack closure is possible. However, the possibility of crack closure does exist if the slip plane intersects the crack faces at any other point. This is illustrated in Figure 8. This can be demonstrated quantitatively by use of the linearized version of the crack-opening displacement at the point of intersection. The key is the relation

$$d(L,a-c) = -\frac{6}{\pi}\left(\frac{c}{L}\right)^{\frac{1}{2}} \cos\frac{\theta}{2} \qquad (43)$$

where c denotes the distance between the crack tip and the point of intersection of the superdislocation slip plane and the crack face; i.e., the point $x = a - c$. Note that Equation (43) is based on the assumption that $c \ll L$ as well as that $L << a$.

* The relations exhibited in References [7-9] are all correct provided the Heaviside step function H(x) replaces the Dirac delta function $\delta(x)$ in the crack-opening displacement equations.

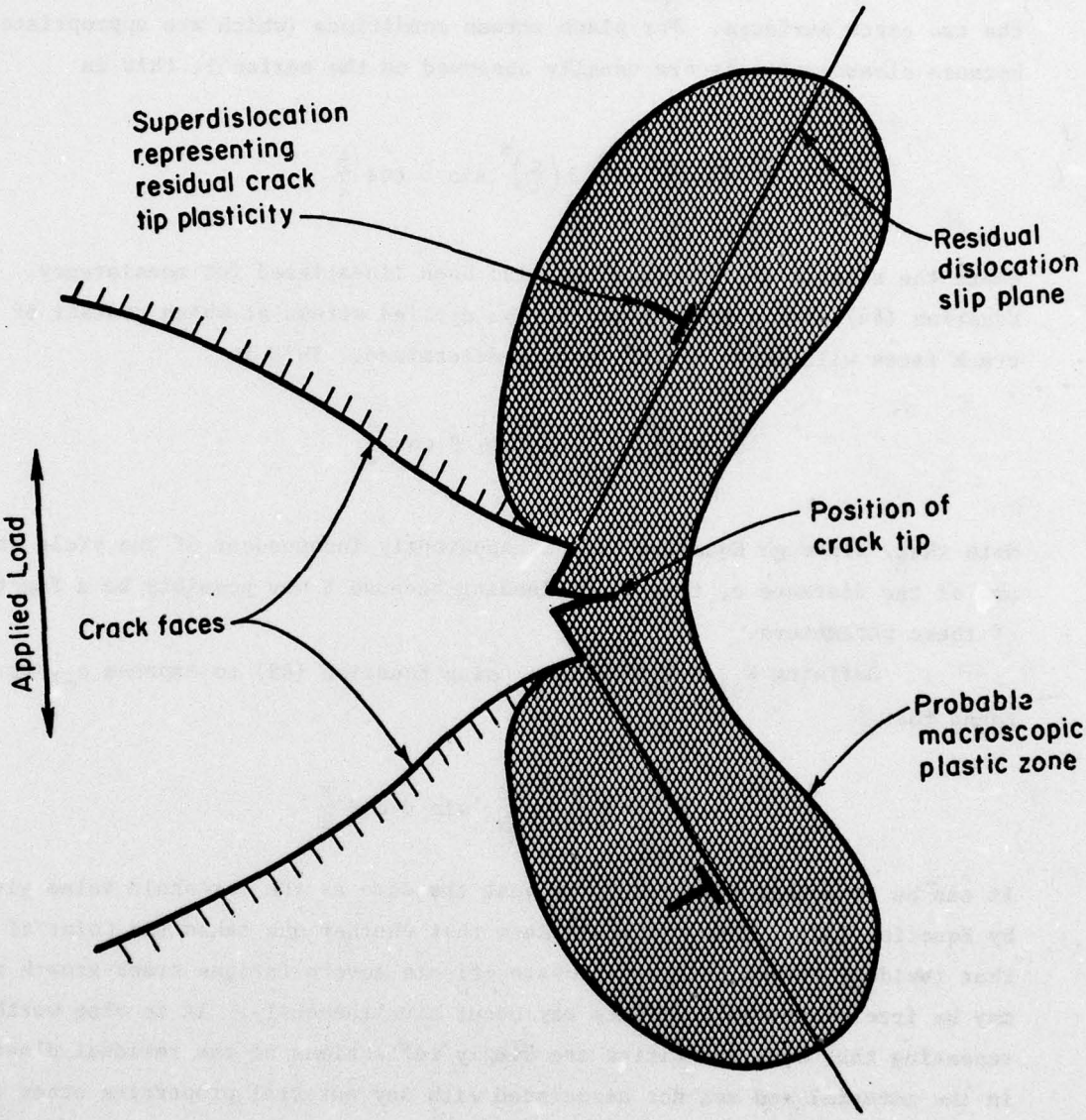

FIGURE 8. SUPERDISLOCATION MODEL OF RESIDUAL CRACK-TIP PLASTICITY SHOWING THE POSSIBILITY OF CRACK CLOSURE

Substituting Equation (43) into Equation (7) will give an expression for the crack-opening displacement at the potential point of contact between the two crack surfaces. For plane stress conditions (which are appropriate because closure effects are usually observed on the surface), this is

$$\frac{1}{2} v = \frac{2\sigma}{E} (2ac)^{\frac{1}{2}} - \frac{3}{\pi} B \left(\frac{c}{L}\right)^{\frac{1}{2}} \sin \theta \cos \frac{\theta}{2} \quad , \tag{44}$$

where the elastic contribution has also been linearized for consistency. Using Equation (44), for a given B and L, the applied stress at which contact of the crack faces will occur can be readily determined. This is

$$\sigma_c = \frac{3}{2\pi} \frac{EB}{(2aL)^{\frac{1}{2}}} \sin \theta \cos \frac{\theta}{2} \quad . \tag{45}$$

Note that, although Equation (45) is apparently independent of the yield stress and of the distance c, this is misleading because B may possibly be a function of these parameters.

Defining $K_{c\ell} = \sigma_c (\pi a)^{\frac{1}{2}}$ and using Equation (45) to express σ_c, it is found that

$$K_{c\ell} = \left(\frac{9}{8\pi}\right)^{\frac{1}{2}} \frac{EB}{L^{\frac{1}{2}}} \sin \theta \cos \frac{\theta}{2} \tag{46}$$

It can be seen that this result is just the same as the threshold value given by Equation (32). Thus, it would seem that whether one takes the point of view that residual stress or crack-closure effects govern fatigue crack-growth rates may be irrelevant--both effects may occur simultaneously. It is also worth repeating that both quantities are simply reflections of the residual plasticity in the material and are not associated with any material properties other than the usual mechanical parameters.

To reiterate, while the crack-closure condition arising previously in the model is now inoperative, the phenomenon is contained in the present model in another way. Again, this occurs in the model in a natural way and is not forced upon it as a basic postulate.

Comparison with Experimental Results

The strength and position of the residual superdislocation obviously exert strong influences on the crack-growth rate. It is believed that, by extending the procedure described in Section 3 of this report, the values of these parameters can be determined by comparison with elastic-plastic finite element solutions. Specifically, a series of load, crack growth, unload computations can be performed in which growth progresses (by releasing nodes) with load shedding to achieve a constant K value. Values of β and λ can then be determined by matching the crack-face displacements during the unloading. This has not yet been accomplished, however.

As an expedient, to test the results of the model against experimental results on constant amplitude fatigue crack growth, an alternative approach will be used to set values of β and λ. Guided by the results described in Section 3, for simplicity, it can be assumed that $\beta = 1$. The well known experimental result of Elber [12] can then be used to evaluate λ. Specifically, Elber found for 2024-T3 aluminum alloy that

$$U = \frac{K_{max} - K_{op}}{K_{max} - K_{min}} = 0.5 + 0.4R$$

or

$$K_{op} = (0.5 + 0.1R + 0.4R^2)\, K_{max} \quad . \tag{47}$$

It is also possible to determine K_{op} from the model. As shown in the foregoing, this is done by determining the load level at which the COD at the point of intersection of the residual slip plane with the crack is just equal to zero; cf, Equation (46). Using Equations (38) and (39) then gives

$$K_{op} = \frac{\beta}{\lambda^{\frac{1}{2}}} K_{max} \quad . \tag{48}$$

Combining Equations (47) and (48), setting $\beta = 1$, gives

$$\lambda = (0.5 + 0.1R + 0.4R^2)^{-2} \quad . \tag{49}$$

Finally, substituting Equation (49) into Equation (40), making use of (41) and (42), then gives the prediction

$$\frac{da}{dN} = \frac{0.155}{EY}\left[\frac{0.5 - 0.1R - 0.4\,R^2}{1 + 2.03\,(0.5 + 0.1R + 0.4R^2)^2}\right]\frac{K_{max}^2}{(1 - \sigma_{max}/Y)} \qquad (50)$$

for the steady-state crack growth rate resulting from constant amplitude loading.

A particularly well documented set of experimental data that can be used to test Equation (50) is that of von Euw, et al [13] on 2024-T3 aluminum. Their data were obtained from a 3-inch wide SEN specimen at two different crack length to specimen width ratios, a/w. As they pointed out, the conventional view is that, for the same values of K_{max} and K_{min}, the same crack growth should be obtained for all a/w values. However, this was not the case. To determine if Equation (50) could account for their observed differences, the $(1 - \sigma_{max}/Y)^{-1}$ terms was interpreted as a net section value with σ_{max} calculated from the given K_{max} values via

$$\sigma_{max} = K_{max}\left\{w^{1/2}\left(\frac{a}{w}\right)^{1/2}\left(1 - \frac{a}{w}\right) f\left(\frac{a}{w}\right)\right\}^{-1} \quad ,$$

where $f(a/w)$ is the finite width correction for the SEN specimen used in Reference [13]. In particular, $f(0.25) = 2.308$ and $f(0.45) = 4.989$ which gives $\sigma_{max} = K_{max}/78.7$ and $\sigma_{max} = K_{max}/167.4$ for $a/w = 0.25$ and 0.45, respectively. Other values used in the calculation are $E = 10^7$ ksi and $Y = 52.5$ ksi, also as given in Reference [13].

Comparisons between the prediction of Equation (50) and the results of von Euw, et al for two different kinds of tests are shown in Figures 9 and 10. In Figure 9 R is a constant while Figure 10 shows a case where ΔK is constant. In both comparisons it can be seen that the model does an excellent job of predicting the growth rates. Also, the previously unexplained difference between the results for the two different a/w ratios is now accounted for.

Note that the data used in Figures 9 and 10 are just the same as those used to test the earlier version of the model--see Figures 5.8 and 5.9 (page 56 and 57) of Reference [7]. In fact, the discrepancies obtained were a primary

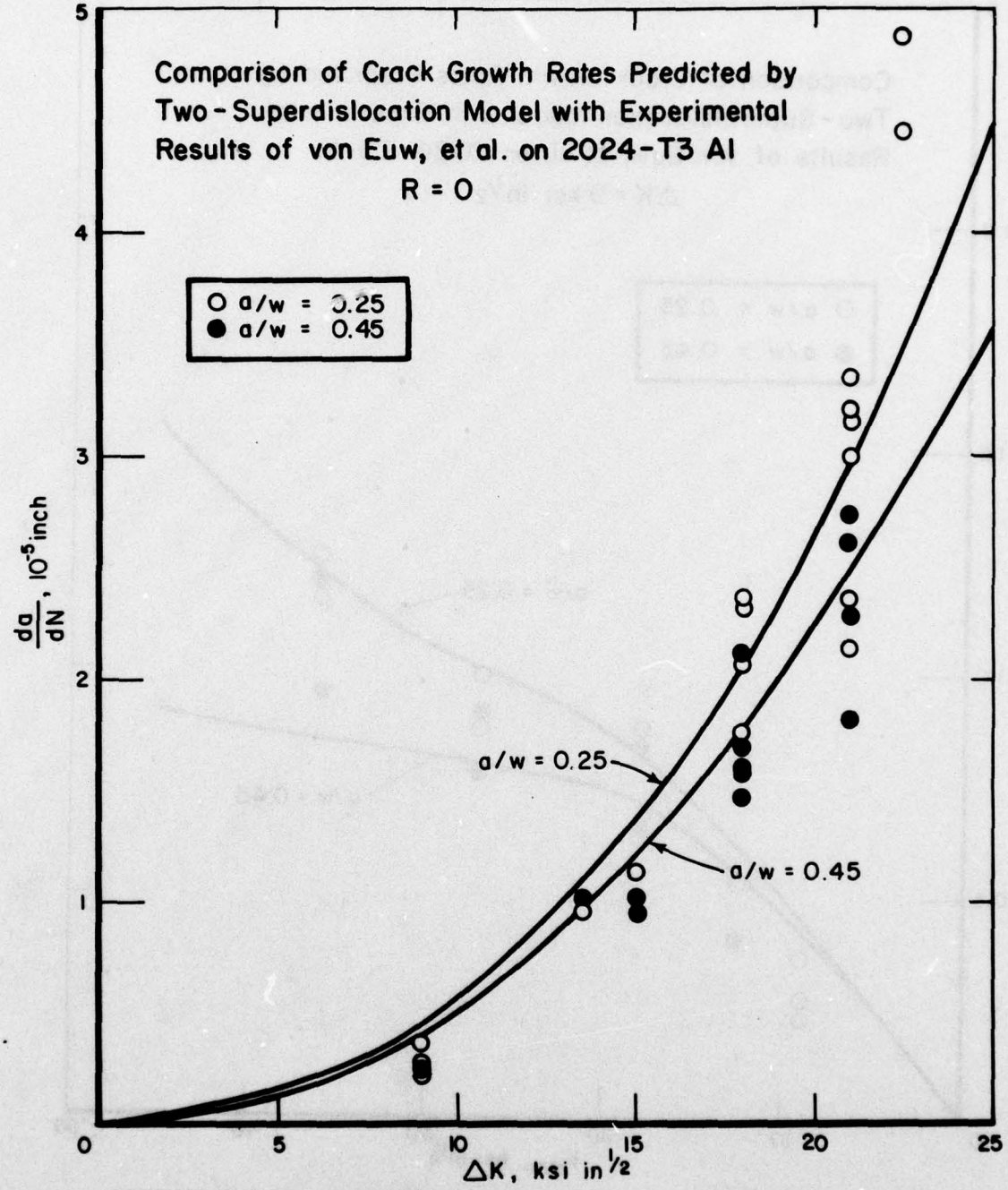

FIGURE 9. COMPARISON OF CRACK GROWTH RATES PREDICTED BY TWO-SUPERDISLOCATION MODEL WITH EXPERIMENTAL RESULTS OF VON EUW, el al ON 2024-T3 Al FOR R = 0

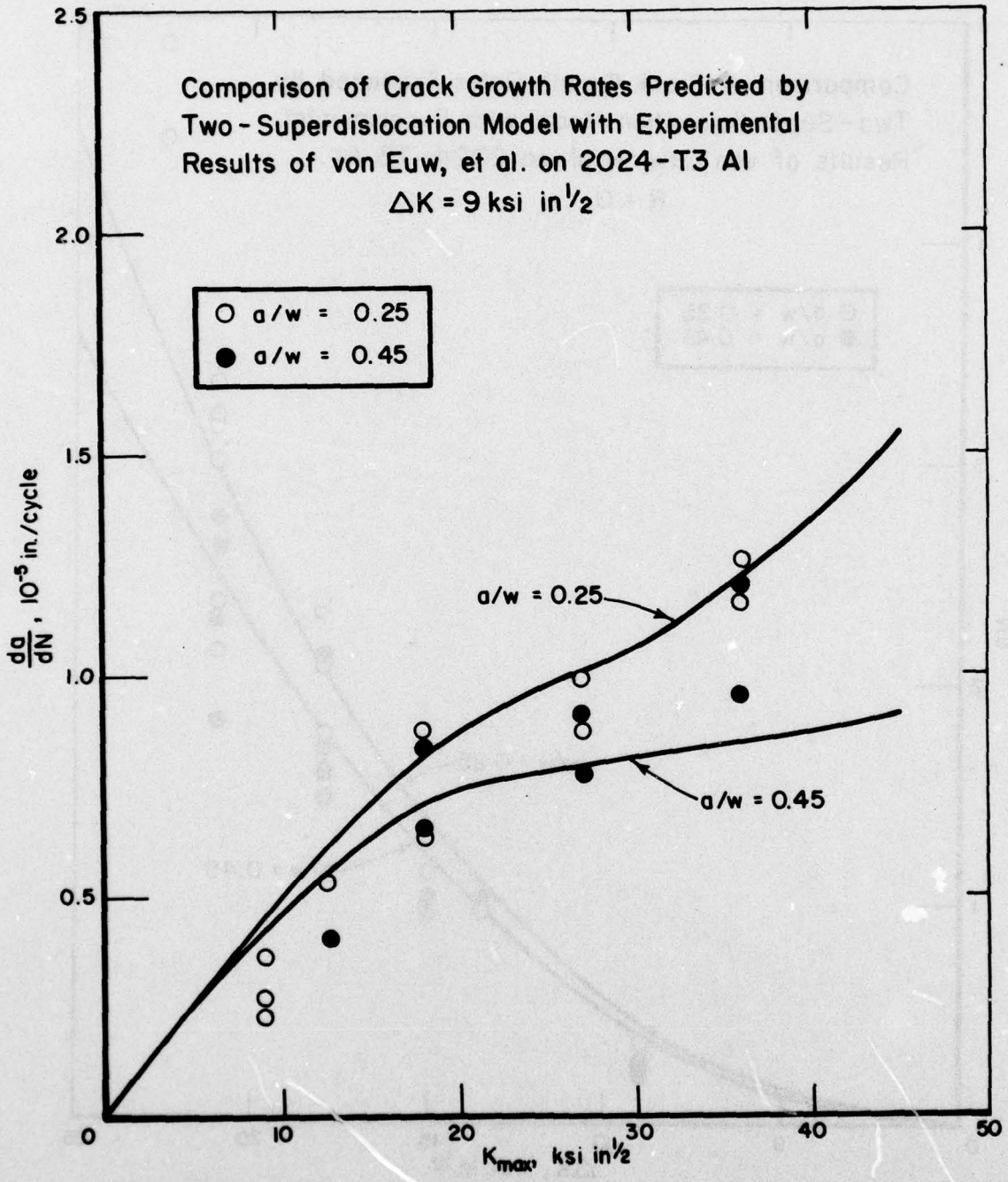

FIGURE 10. COMPARISON OF CRACK GROWTH RATES PREDICTED BY TWO-SUPERDISLOCATION MODEL WITH EXPERIMENTAL RESULTS OF VON EUW, et al ON 2024-T3 Al FOR ΔK = 9 KSI IN. $^{1}/_{2}$

motivation for the further development that has led to the present model. Clearly, the model is now in complete accord with the well-established experimental trends exemplified by the data of von Euw, et al.

It should perhaps be emphasized that the development given in this section applies only to constant amplitude loading. While the model can certainly be applied to variable amplitude loading--and this is the ultimate goal of the work--such computations will require that additional degrees of freedom be allowed; i.e., more than just one residual superdislocation pair. It is now clear how this can be done. As for example, as described in pages 58-62 of Reference [7], heuristic calculations indicate that meaningful results will be obtained. However, more detailed calculations such as these are beyond the scope of this work.

5. DISCUSSION, CONCLUSIONS, AND RECOMMENDATIONS

The work described herein was directed at the satisfactory completion of the following major goals:

(1) Prediction of constant crack-growth rates for load levels that are uniform from cycle to cycle that are in satisfactory agreement with experimental results.

(2) Predictions that properly reflect the effect of mechanical properties on fatigue crack-growth rates.

(3) Computational efficiency such that a large number of load cycles can be performed in a reasonable amount of time.

In addition, as has been the intent from the beginning of the work, the mathematical model incorporates only material properties for which data can readily be found for the materials of interest in engineering applications. While the model is not yet complete in all respects, the results provided in this report demonstrate that these goals have essentially been met.

One criticism of the results presented in Reference [7] was that the crack-growth rate always turned out to be inversely proportional to the yield stress. While there is no decisive body of experimental evidence which reveals the proper dependence on Y, there are some data which indicate that a Y^{-1} dependence is not universal. The present results partly alleviate this deficiency in that the yield stress dependence now differs from the Y^{-1} types of dependence; see, for example, Equation (40). Further improvements are also possible, as follows.

The current model represents crack-tip plasticity only in terms of the yield stress of the material. This means that it is confined to elastic-perfectly plastic behavior. More realistic material behavior might be incorporated into the model by following a suggestion made by Rice [14]. This is, for a power law hardening material, i.e., stress proportional to strain to the N^{th} power in the plastic regime, the tensile flow strength corresponding to the Mises equivalent shear strain N/(1+N) can be used. This is

$$\sigma_{flow} = Y\left[\frac{\sqrt{3}}{2(1+\nu)}\ \frac{N}{(1+N)Y/E}\right]^N ,$$

where Y is the yield stress, E is the elastic modulus, and ν is Poisson's ratio. A more convenient form is obtained by using the shear modulus G. This is

$$\sigma_{flow} = (3)^{N/2}\left(\frac{N}{1+N}\right)^{N} Y^{1-N} G^{N} \quad .$$

Note that, as $N \to 0$, $\left(\frac{N}{1+N}\right)^{N} \to 1$. Consequently, the latter form clearly shows that for a nonstrain hardening material, $\sigma_{flow} = Y$. The introduction of such a relation into the model would require four basic mechanical properties to specify material behavior: G, ν, Y, N.

The above provides one means by which more realistic elastic-plastic behavior could be incorporated into the model. Another is to use cyclic stress-strain properties rather than the monotonic values. In terms of the simple two-superdislocation model developed in the above, the same value of τ_i need not be used for each superdislocation. For example, the residual superdislocation can be associated with the uniaxial tensile yield stress, while the nascent superdislocation can be associated with the cyclic value. This may produce a delayed minimum in the crack-growth retardation following an overload as the location of the nascent dislocation changes from virgin material to cyclically deformed material. There are of course other explanations for a delayed minimum; e.g., difference between crack closure at the surface and in the interior. The point here is that such freedom exists and can be exploited in subsequent stages of development of the model.

A number of other research efforts currently in progress are also aimed at developing a general fatigue crack-growth model. These all utilize either a simplified representation of the crack-tip plasticity or incorporate a mechanism for the crack-closure condition or both. Evans [15] uses a simplified version of the superdislocation concept in his model for stress corrosion cracking and fatigue. Paris and Herman [16] have developed an approximate dislocation based model that predicts crack-closure and, hence, an effective ΔK that appears to be in good accord with experimental results. Newman [17] has devised a ligament model based on finite element calculations [18] which leaves plastically deformed material in the wake of the advancing crack. Most recently, Budiansky and Hutchinson [19] have extended a Dugdale model crack-tip plasticity representation to calculate crack-closure effects in steady-state crack growth.

The essential difference between the work described in this report and the work of others is that the latter are not able to incorporate a crack-growth criterion directly into their models. The model described here appears to be uniquely capable of providing this key feature. As a consequence, the reliance on a postulated controlling mechanism (e.g., crack-closure, residual plasticity) otherwise necessary is avoided. These mechanisms are automatically included in this model and make their contribution in a natural way. It might further be noted that experimental observations of fatigue crack tips also provide support for the formulation of the model. The mechanisms observed by Lankford and Kusenberger [20] and by Neumann [21] can be cited in this regard.

In conclusion, in this report, two areas in which the formulation of the model were inadequate have been identified and improved upon. These improvements have led to a "steady-state" fatigue crack-growth model that is in good agreement with experimental data. Because these predictions can be made with a simple two-superdislocation model, it appears that the desired computational convenience is also at hand. However, further work is needed to qualify the model for routine engineering calculations. Two specific recommendations can be made. The first is required in order to cope with variable amplitude loading, the second to cope with environmental effects. These are as follows.

Variable amplitude loading will produce residual plasticity behind the tip of a fatigue crack that will depend upon the details of the load history. The model cannot be expected to reflect this with only a single residual superdislocation pair as was possible for constant amplitude loading. But, the manner in which the simple model can most effectively be expanded to treat nonuniform loads without requiring the complexity of a full cycle-by-cycle representation of crack-tip plasticity is not yet established. Further work is needed to develop a set of rules for combining and repositioning superdislocations to represent the residual plasticity in high-to-low and low-to-high sequences. This offers the possibility of treating multiple and block overloads, negative excursions, and other complications involved in service conditions. The authors believe that the model described in this report is uniquely capable of providing this generality.

A key feature of fatigue is the quite important role played by the environment. The model developed here could account for this by taking the internal friction stress to depend on the environment. Alternatively, a more

useful approach may be simply to take some fraction of the crack-tip crack-opening displacement as the crack-advance increment. The physical basis for the latter is simply that the CTOD represents new surface area which can be attacked by the environment to which it is exposed. Thus, "rewelding" of the surfaces as observed in the experimental work of Neumann, et al [21,22], can be directly taken into account. Benign environments producing little deterent to rewelding will have low growth ratios while detrimental environments will produce large growth ratios. Further work is needed in which the predictions of the model are tested by detailed comparisons with experimental results to implement and verify this approach.

6. REFERENCES

1. Broek, D., Elementary Engineering Fracture Mechanics, Noordhoff Int. Publishing, Leyden, The Netherlands, 1974.

2. Hertzberg, R. W., Deformation and Fracture Mechanics of Engineering Materials, Wiley, New York, 1976.

3. Rolfe, S. T. and Barsom, J. M., Fracture and Fatigue Control in Structures, Prentice-Hall, Englewood Cliffs, New Jersey, 1977.

4. Nelson, D. V., "Review of Fatigue-Crack-Growth Prediction Methods", Exp. Mech., Feb, 1977.

5. Purcell, A. H., "Dislocations and Fatigue Cracking", Ind. Research, April, 1977.

6. Crooker, T. W., "Fracture Mechanics Fatigue Design", Mech. Eng., June, 1977.

7. Kanninen, M. F., Feddersen, C. E., and Atkinson, C., Initial Development of Fatigue-Crack-Retardation Model, NADC-76076-30, January 31, 1976.

8. Kanninen, M. F., Atkinson, C., and Feddersen, C. E., "A Fatigue Crack-Growth Analysis Method Based on a Simple Representation of Crack-Tip Plasticity", Cyclic Stress-Strain and Plastic Deformation Aspects of Fatigue Crack Growth, ASTM-STP, 637, 1977.

9. Atkinson, C. and Kanninen, M. F., "A Simple Representation of Crack-Tip Plasticity: The Inclined Strip-Yield Superdislocation Model", Int. J. Fracture, Vol 13, 1977, p 151.

10. McEvily, A. J. and Groeger, J., "On the Threshold for Fatigue-Crack Growth", Proc. 4th Int. Conf. Fracture, Vol 2, p 1293, Univ. Waterloo Press, 1977.

11. McEvily, A. J., Bunkelmann, D., and Tanaka, K., "Effect of Large-Scale Yielding on Fatigue Crack Propagation", Strength and Structure of Solid Materials, Noordhoff Int. Pub, 1976, p 275.

12. Elber, W. "The Significance of Fatigue Crack Closure", Damage Tolerance in Aircraft Structure, ASTM STP 406, American Society for Testing Materials, Philadelphia, 1971, p 230.

13. von Euw, E.F.J., Hertzberg, R. W., and Roberts, R., "Delay Effects in Fatigue-Crack Propagation", Stress Analysis and Growth of Cracks, ASTM STP 513, American Society for Testing Materials, Philadelphia, 1972, p 230.

14. Rice, J. R., "Elastic-Plastic Fracutre Mechanics", in The Mechanics of Fracture, Edited by F. Erodgan, ASME AMD Publication, Vol 19, 1976, p 32.

15. Evans, J. T., "Time-Dependent Plastic Relaxation at a Crack Tip", Acta Met, in press, 1977.

16. Paris, P. C. and Herman, L., "Measurements and ANalytical Models for Crack Closure in Fatigue", 14th IUTAM Congress, 1977.

17. Newman, J. C., Jr., "Correlation of Fatigue-Crack-Growth Rates Using a Simple Crack-Closure Model", SESA Spring Meeting, May, 1977.

18. Newman, J. C., Jr., "A Finite Element Analysis of Fatigue Crack Closure", Mechanics of Crack Growth, ASTM STP 590, p 281, 1976.

19. Budiansky, B. and Hutchinson, J. W., "Analysis of Closure in Fatigue Crack Growth", Harvard University Report, June 1977.

20. Lankford, J. and Kusenberger, F. N., "On Crack Tip Yielding During Fatigue Cycling of a High Strength Steel", Phil. Mag., Vol 26, 1972, p 1485.

21. Neumann, P., "The Geometry of Slip Processes at a Propagating Fatigue Crack", Acta Met, Vol 22, 1974, p 1167.

22. Neumann, P., Vehoff, H., and Fuhbrott, H., "On the Mechanisms of Fatigue Crack Growth", Proc 4th Int. Conf. on Fracture, Vol 2, Univ. Waterloo Press, 1977, p 1293.

APPENDIX A

ADAPTATIONS OF FORMULAS FOR THE STRIP-YIELD SUPERDISLOCATION MODEL FOR CRACK-TIP PLASTICITY

APPENDIX A

ADAPTATIONS OF FORMULAS FOR THE STRIP-YIELD SUPERDISLOCATION MODEL FOR CRACK-TIP PLASTICITY

Introduction

The fatigue crack propagation model described in this report depends on calculations from formulas based on the strip-yield superdislocation model for crack-tip plasticity given in Reference [A-1]. The formulas are derived as complex functions of a complex variable. Hence, computations from them tend to be slow and may possibly involve obscure ambiguities. The formulas are subjected here to rearrangement into real form in the hope of finding ways to verify the results to shorten computations based on them, and to facilitate the development of simple approximate relations.

From one point of view, the formulas of Reference [A-1] are based on the presumption of superdislocations of semi-infinite length interacting with a crack. To obtain correct results, the "tails" of the superdislocations--i.e., the position of the slip plane on the opposite side of the crack plane from the superdislocation--must therefore be abolished. There is another point of view, however. This is that the previously derived relations can be equally well derived in terms of slip planes terminating in the crack plane. This gives the same stresses, but alters the displacements. To verify this, the following proceeds from the first point of view.

Background

Consider that the crack is stress free while a load normal to the crack is applied remotely. All the superdislocations are inclined to the crack by the same angle or its supplement, depending on the quadrant in which the branch point of the superdislocation lies. The entire configuration is symmetric about the plane and center of the crack. The strength of each superdislocation is presumed to be uniform throughout the entire length of that superdislocation. The notation used for a single set of superdislocations is shown in Figure A-1.

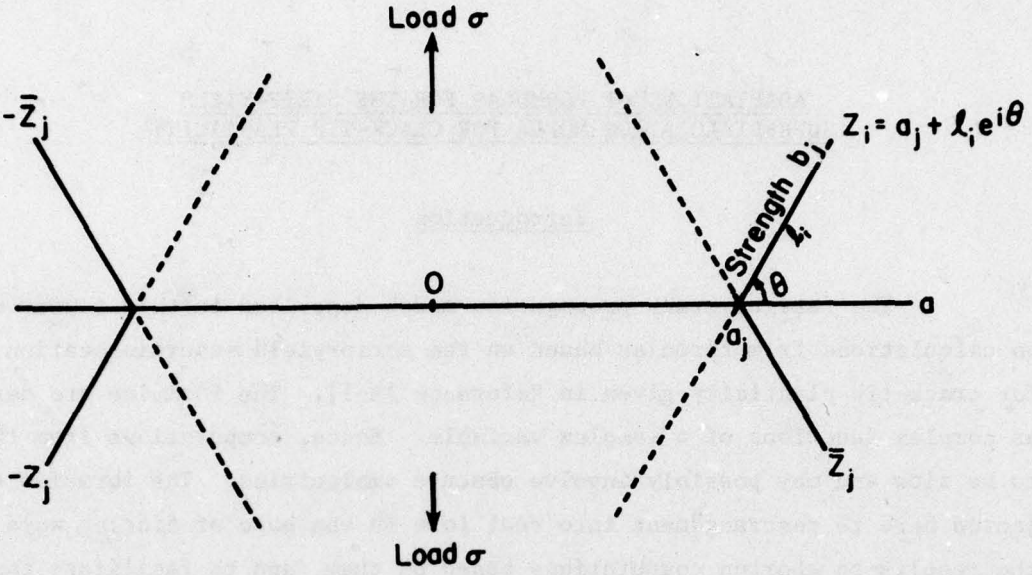

FIGURE A-1. POSITIONS OF SUPERDISLOCATIONS IN ONE SYMMETRY SET

The equations of interest furnish terms for a possible singularity cancelling equation (for stress at the crack tip considering effects of all sets of superdislocations) and for determination of the shear stress τ active along each superdislocation at its branch point (considering effects of the load and all sets of superdislocations). In particular, with M sets of superdislocations, terms f_j, k_n, k_{jn} are to be supplied for the conditions

$$\sigma a = \frac{G(1-\gamma)}{4\pi(1-\nu)} \sum_{j=1}^{M} b_j f_j \quad , \tag{A-1}$$

$$\tau_n = \sigma h_n + \frac{G}{4\pi(1-\nu)} \sum_{j=1}^{M} b_j (k_{jn} + g_{jn}) \quad , \quad n = 1,2, \ldots, M \quad . \tag{A-2}$$

The factor $(1-\gamma)$ is introduced in case only partial satisfaction of the singularity cancelling equation is desired. In addition, terms d_j are to be supplied to allow calculation of the crack-opening displacement

$$\Delta u_2 = \frac{\sigma(\kappa+1)}{2G} (a^2-x^2)^{\frac{1}{2}} + \sin\theta \sum_{j=1}^{M} b_j d_j \quad . \tag{A-3}$$

Before proceeding further, it may be observed that the superdislocations presumed in the derivation of the formulas shown in Reference [A-1[had semi-infinite length which is not really desired. To make the superdislocations terminate at the crack plane, one needs only to subtract effects contributed by the tails beyond the crack plane (that is the dotted parts of the lines). These effects can be found from the existing formulas by letting $\ell \to 0$ for influential (as opposed to influenced) dislocations.* A second observation is that in their only relevant context, the functions k_{jn} and g_{jn} are added, so that they lack individual significance. Yet another observation is that effects of the superdislocations at the left end of the crack apparently have been omitted from many parts of the formulas on the presumption that they are too remote from the right end (the end actually considered) to be significant. This latter presumption can account for defects of symmetry about the origin observable in some of the formulas.

---

* It may be noted that limits of functions f_j, h_n, k_{jn}, g_{jn}, and d_j so found will still be based on the presumption of a stress-free crack. They are not to be confused with contributions arising simply from superdislocations terminating on the crack. Unmitigated effects from such superdislocations could imply infinite stresses on the crack, but those will be missing from limits of functions for which the surface stresses are always required to be cancelled.

The aim of the present work then is to make the References [A-1,A-2] formulas better founded, more readily interpretable, and if possible more easily computable by presenting and examining several alternative formulation of them.

Some Auxiliary Quantities

It is helpful to begin adaptation of the References [A-1,A-2] formulas by introducing several quantities which facilitate their expression in real form. A starting point is to observe that a recurring quantity in their formulas is $(z_j^2 - a^2)^{\frac{1}{2}}$, in which

$$z_j = a_j + \ell_j e^{i\theta} = a(\alpha_j + \lambda_j e^{i\theta}) \quad , \tag{A-4}$$

where by definition $\alpha_j = a_j/a$ and $\lambda_j = \ell_j/a$. To get a polar representation of this radical, one may seek real functions $f_1(\lambda_j,\theta)$ and $f_2(\lambda_j,\theta)$ such that

$$f_1 + i\, f_2 = (z_j^2 - a^2)^{\frac{1}{2}}/a \quad .$$

If this is to hold, then squaring both sides and equating their real parts and their imaginary parts shows

$$f_1^2 - f_2^2 = -(1-\alpha_j^2) + 2\alpha_j\lambda_j \cos\theta + \lambda_j^2 \cos 2\theta \quad ,$$

$$2f_1 f_2 = 2\alpha_j\lambda_j \sin\theta + \lambda_j^2 \sin 2\theta \quad .$$

Squaring and adding these quantities shows

$$(f_1^2 + f_2^2)^2 = (1-\alpha_j^2)^2 - 2\lambda_j^2 (1-\alpha_j^2)(2\alpha_j \cos\theta + \lambda_j \cos 2\theta) + 4\alpha_j^2\lambda_j^2 + 4\alpha_j\lambda_j^3 \cos\theta + \lambda_j^4$$

which can be shown to be equivalent to

$$f_1^2 + f_2^2 = D_j^2 \quad , \quad \text{where}$$

$$D_j = \{[(\lambda_j^2+1-\alpha_j^2)\ \sin\theta]^2 + [2\alpha_j\lambda_j+(\lambda_j^2-1+\alpha_j^2)\ \cos\theta]^2\}^{\frac{1}{4}} \quad . \qquad (A\text{-}5)$$

Rearrangement of the above $f_1^2 - f_2^2$ also shows

$$f_1^2 - f_2^2 = -(\lambda_j^2+1-\alpha_j^2)\ \sin\theta.\ \sin\theta + [2\alpha_j\lambda_j+(\lambda_j^2-1+\alpha_j^2)\ \cos\theta]\ \cos\theta,$$

so

$$2f_1^2 = -(\lambda_j+1-\alpha_j^2)\ \sin\theta.\ \sin\theta + [2\alpha_j\lambda_j + (\lambda_j^2-1+\alpha_j^2)\ \cos\theta]\ \cos\theta + D_j^2 \quad .$$

Let β_j be the angle in the range $-\pi < \beta_j \leq \pi$ for which

$$\sin\beta_j = \frac{(\lambda_j^2+1-\alpha_j^2)\ \sin\theta}{D_j^2}\ ,\ \cos\beta_j = \frac{2\alpha_j\ \lambda_j + (\lambda_j^2-1+\alpha_j^2)\ \cos\theta}{D_j^2} \quad . \qquad (A\text{-}6)$$

Presuming $\lambda_j \geq 0$, $0 \leq \alpha_j \leq 1$ and $0 \leq \theta \leq \frac{\pi}{2}$ so that $\sin\beta_j \geq 0$, it follows

$$\beta_j = \arccos\frac{2\alpha_j\lambda_j + (\lambda_j^2-1+\alpha_j^2)\ \cos\theta}{D_j^2} \quad . \qquad (A\text{-}6')$$

It can be shown also that $\sin(\theta+\beta_j) \geq 0$, so it is implied that $0 \leq \beta_j \leq \pi - \theta$. Now

$$2f_1^2 = D_j^2\ [\cos\theta\cos\beta_j - \sin\theta\sin\beta_j + 1] = 2D_j^2\cos^2\frac{\theta+\beta_j}{2} \quad .$$

Thus $f_1 = \pm D_j \cos\frac{\theta+\beta_j}{2}$, and since $f_1^2 + f_2^2 = D_j^2$, it follows that $f_2 = \pm D_j \sin\frac{\theta+\beta_j}{2}$. To have $2f_1f_2 = 2\alpha_j\lambda_j \sin\theta + \lambda_j^2 \sin 2\theta$, it is necessary that the ambiguous signs for f_1 and f_2 be alike, and to have $(z_j^2 - a^2)^{\frac{1}{2}}$ in the right half plane (as apparently was presumed for the formulas being considered) that sign must be positive.

Thus,

$$f_1 = D_j \cos\frac{\theta+\beta_j}{2} \quad , \qquad f_2 = D_j \sin\frac{\theta+\beta_j}{2} \quad ,$$

and then

$$(z_j^2 - a^2)^{\frac{1}{2}}/a = D_j \left[\cos\frac{\theta+\beta_j}{2} + i \sin\frac{\theta+\beta_j}{2}\right] = D_j\, e^{i(\theta+\beta_j)/2} \quad . \tag{A-7}$$

This expression holds for all values of θ, λ_j, and α_j in the ranges that were presumed for them.

Letting $\rho_j = 1-\alpha_j = (a-a_j)a$, one can interpret D_j by showing

$$D_j^2 = \delta_j\, \delta_j' \quad , \quad \text{where}$$

$$\delta_j = [\rho_j^2 - 2\rho_j\lambda_j \cos\theta + \lambda_j^2]^{\frac{1}{2}} = (\text{distance from } z_j \text{ to } a)/a,$$

$$\delta_j' = [(2-\rho_j)^2 + 2\lambda\,(2-\rho_j)\cos\theta + \lambda_j^2] = (\text{distance from } z_j \text{ to } -a)/a. \tag{A-8}$$

These distances are illustrated in Figure A-2a. The angle β_j is harder to interpret, but it can be approximated by the angle between the lines from z_j to a_j and from z_j to a. Other quantities of occasional interest include R_j and ψ_j, the polar coordinates of z_j, which are also shown.

A second radical which arises is $(\bar{z}_j^2 - a^2)^{\frac{1}{2}}$. To reexpress it, one may show that

$$(\bar{z}_j^2 - a^2)(z_j^2 - a^2) = D_j^4\, a^4 \quad .$$

Thus,

$$(\bar{z}_j^2 - a^2)^{\frac{1}{2}}/a = \pm D_j^2\, a/(z_j^2 - a^2)^{\frac{1}{2}} = \pm D_j\, e^{-i(\theta+\beta_j)/2} \quad . \tag{A-9}$$

Since this radical too seems to have been presumed to lie in the right half plane, the ambiguous sign here will be taken to be positive.

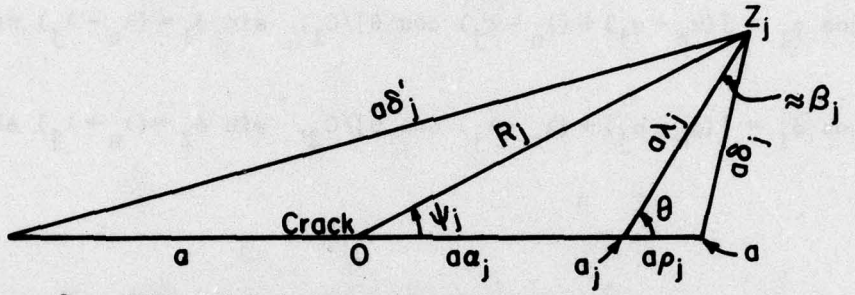

a. Quantities related to one superdislocation

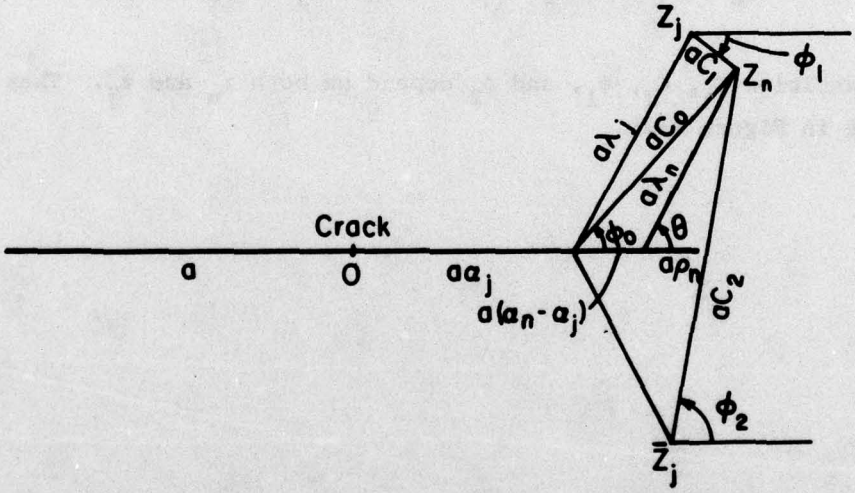

b. Quantities involved in interaction of superdislocations

FIGURE A-2. INTERPRETATION OF AUXILIARY QUANTITIES

To prepare for handling the quantities $(z_n - z_j)$ and $(z_n - \bar{z}_j)$, let

$$C_1 = \{[(\alpha_n - \alpha_j) + (\lambda_n - \lambda_j)\cos\theta]^2 + [(\lambda_n - \lambda_j)\sin\theta]^2\}^{\frac{1}{2}} ,$$

$$C_2 = \{[(\alpha_n - \alpha_j) + (\lambda_n - \lambda_j)\cos\theta]^2 + [\lambda_n + \lambda_j)\sin\theta]^2\}^{\frac{1}{2}} , \quad \text{(A-10)}$$

and let ϕ_1 and ϕ_2 be angles in the range $-\pi < \phi \leq \pi$ for which

$$\cos\phi_1 = [(\alpha_n - \alpha_j) + (\lambda_n - \lambda_j)\cos\theta]/C_1, \quad \sin\phi_1 = (\lambda_n - \lambda_j)\sin\theta/C_1 ,$$

$$\cos\phi_1 = [(\alpha_n - \alpha_j) + (\lambda_n - \lambda_j)\cos\theta]/C_2, \quad \sin\phi_2 = (\lambda_n + \lambda_j)\sin\theta/C_2 . \quad \text{(A-11)}$$

Then

$$(z_n - z_j)/a = C_1 e^{i\phi 1} , \quad (z_n - \bar{z}_j) = C_2 e^{i\phi_2} . \quad \text{(A-12)}$$

The new quantities C_1, C_2, ϕ_1, and ϕ_2 depend on both z_n and z_j. They are illustrated in Figure A-2b.

Functions Related to Stresses

Turn now to the functions determined in References [A-1,A-2] to define the stress of five

$$f_n = 4 \sin\theta \left[\mathrm{Re}\left\{ \frac{(z_n^2 - a^2)^{\frac{1}{2}}}{z_n - a} \right\} + a\,\ell_n\, \mathrm{Re}\left\{ \frac{e^{i\theta}}{(z_n - a)(z_n^2 - a^2)^{\frac{1}{2}}} \right\} \right] \quad . \qquad \text{(A-13)}$$

Using results found above, one now finds

$$\mathrm{Re}\left\{ \frac{(z_n^2 - a^2)^{\frac{1}{2}}}{z_n - a} \right\} = \mathrm{Re}\left\{ \frac{D_n\, e^{i(\theta+\beta_n)^{\frac{1}{2}}}}{(-\rho_n + \lambda_n e^{i\theta})} \frac{(-\rho_n + \lambda_n e^{-i\theta})}{(-\rho_n + \lambda_n e^{i\theta})} \right\} = \frac{D_n \left[-\rho_n \cos\frac{\theta+\beta_n}{2} + \lambda_n \cos\frac{\theta-\beta_n}{2} \right]}{\delta_n^2} \quad ,$$

$$a\,\ell_n\, \mathrm{Re}\left\{ \frac{e^{i\theta}}{(z_n - a)(z_n^2 - a^2)^{\frac{1}{2}}} \right\} = \frac{\lambda_n}{D_n} \mathrm{Re}\left\{ \frac{e^{i(\theta-\beta_n)/2}(-\rho_n + \lambda_n e^{i\theta})}{(-\rho_n + \lambda_n e^{2\theta})(-\rho_n + \lambda_n e^{i\theta})} \right\} = \frac{\lambda_n \left[-\rho_n \cos\frac{\theta+\beta_n}{2} + \lambda_n \cos\frac{\theta+\beta_n}{2} \right]}{D_n\, \delta_n^2} \quad .$$

Thus the function f_n is equivalent to

$$f_n = \frac{4 \sin\theta}{D_n\, \delta_n^2} \left[(\lambda_n^2 - \rho_n D_n^2) \cos\frac{\theta+\beta_n}{2} + \lambda_n (D_n^2 - \rho_n) \cos\frac{\theta-\beta_n}{2} \right] \quad . \qquad \text{(A-14)}$$

This function represents the contribution that the superdislocations at z_n and $\bar{z}_n$ make to the singularity cancelling equation. However, those superdislocations were presumed to have semi-infinite tails which are not relevant. We can find an adjustment to delete the tail effects by taking $-\lim_{\lambda_n \to 0} f_n$. Note that this adjustment does not violate boundary conditions on the crack since it, like f_n, is based on the presumption that no stress is transmitted across the crack. Now as $\lambda_n \to 0$, one has $\delta_n \to \rho_n$, $D_n^2 \to 1-\alpha_n^2$ and $\beta_n \to \pi - \theta$, so

$$-\lim_{\lambda_n \to 0} f_n = \frac{4 \sin\theta}{\rho_n^2 \sqrt{1-\alpha_n^2}} \left[-\rho_n (1-\alpha_n^2) \cos\frac{\pi}{2} + 0 \right] = 0 \quad . \qquad \text{(A-15)}$$

Since this adjustment vanishes, the function f_n applies also when the superdislocations are presumed to lack the semi-infinite tail.

The function f_n given above is an abbreviated form based on the presumption that contributions from the superdislocations at the left end of the crack are negligible for the singularity cancelling equation for the right end of the crack. For some purposes this approximation is unacceptable, and then a fuller form of f_n based on an entire set of four superdislocations is desirable. To find the fuller form (say f_n^T), one may use the form of the singularity-cancelling equation given on page 78 of Reference [A-1]. That form (for plane strain) is

$$\sigma_a = \frac{G\,b}{4\pi(1-\nu)}\ \mathrm{Im}\left\{\sum_{j=1}^{4}\mu_1\left[\frac{(z_j^2-a^2)^{1/2}}{z_j-a}+\frac{(\bar{z}_j^2-a^2)^{1/2}}{\bar{z}_j-a}\right]+a\sum_{j=1}^{4}\bar{\mu}_j\frac{(\bar{z}_j-z_j)}{(\bar{z}_j-a)(\bar{z}_j^2-a^2)^{1/2}}\right\}, \qquad \text{(A-16)}$$

and appropriate locations z_j can be taken to be z_1, $\bar{z}_1$, $-z_1$, $-\bar{z}_1$ while the appropriate strengths seem to be respectively $e^{i\theta}$, $-e^{-i\theta}$, $e^{i\theta}$, $-e^{-i\theta}$. With these specifications, one finds

$$f_n^T = 4\sin\theta\left[\mathrm{Re}\left\{\frac{2a}{(z_n^2-a^2)^{1/2}}\right\}+2a\,\ell_n\,\mathrm{Re}\left\{\frac{e^{i\theta}}{(z_n^2-a^2)^{3/2}}\right\}\right], \qquad \text{(A-17)}$$

and the real form becomes

$$f_n^T = \frac{8\sin\theta}{D_n}\left[\cos\frac{\theta+\beta_n}{2}+\frac{\alpha_n\lambda_n}{D_n^2}\cos\frac{\theta+3\beta_n}{2}+\frac{\lambda_n^2}{D_n^2}\cos\frac{\theta-3\beta_n}{2}\right]. \qquad \text{(A-18)}$$

As $\lambda_n \to 0$, this function vanishes, so here too the deletion of the tail effects does not change the function. It may be noted that this fuller function, though it involves more superdislocations, has a simpler real form than does the function based on only two superdislocations.

The second stress-related function is

$$h_n = \sin\theta\left[\cos\theta + a^2\,\ell_n\,\mathrm{Re}\left\{\frac{e^{2i\theta}}{(z_n^2-a^2)^{3/2}}\right\}\right] \quad . \tag{A-19}$$

Now

$$a^2\,\ell_n\,\mathrm{Re}\left\{\frac{e^{2i\theta}}{(z_n^2-a^2)^{3/2}}\right\} = \lambda_n\,\mathrm{Re}\left\{\frac{e^{2i\theta}}{D_n^3 e^{i(3\theta+3\beta_n)/2}}\right\} = \frac{\lambda_n}{D_n^3}\cos\frac{\theta-3\beta_n}{2} \quad ,$$

so the real form of h_n is

$$h_n = \sin\theta\left[\cos\theta + \frac{\lambda_n}{D_n^3}\cos\frac{\theta-3\beta_n}{2}\right] \quad . \tag{A-20}$$

This function represents contributions the applied load makes to shear stress along the slip plane at z_n. Since these contributions are not made by the dislocation, there are no tail effects to be adjusted.

Before considering the function k_{nn}, it is well to consider k_{jn} for $j \neq n$. This is given as

$$k_{jn} = -\,\mathrm{Re}\left\{e^{2i\theta}\left[\frac{e^{i\theta}(\bar{z}_j-\bar{z}_n)+e^{-i\theta}(z_j-z_n)}{(z_j-z_n)^2} - \frac{e^{i\theta}(\bar{z}_j-z_n)+e^{-i\theta}(\bar{z}_j-z_n)}{(\bar{z}_j-z_n)^2}\right]\right\} \quad . \tag{A-21}$$

Using quantities defined above, one now finds the real form

$$k_{jn} = \frac{1}{a}\left[\frac{2}{C_1}\cos(\theta-\phi_1)\cos(2\theta-2\phi_1) - \frac{2}{C_2}\cos(\theta+\phi_2)\cos(2\theta-2\phi_2)\right] \quad . \tag{A-22}$$

To get an adjustment for the undesired tail effects, note that as $\lambda_n \to 0$:

$$\begin{aligned} C_1 \to C_2 \to C_o &\equiv \left[(\alpha_n-\alpha_j)^2 + 2(\alpha_n-\alpha_j)\lambda_n\cos\theta + \lambda_n^2\right]^{1/2} \\ &= (\text{distance from } a_j \text{ to } z_n)/a \quad , \end{aligned} \tag{A-23}$$

and $\phi_1 \to \phi_2 \to \phi_o$, where

$$\cos \phi_o = \frac{(\alpha_n - \alpha_j) + \lambda_n \cos \theta}{C_o} \quad , \quad \sin \lambda_o = \frac{\lambda_n \sin \theta}{C_o} \quad . \tag{A-24}$$

The quantities C_o and ϕ_o are included in Figure A-2b. Using them, the adjustment needed for tail effects in k_{jn} is seen to be

$$-\lim_{\lambda_n \to 0} k_{jn} = -\frac{2}{aC_o}\left[\cos(\theta - \phi_o) - \cos(\theta + \phi_o)\right] \cos(2\theta - 2\phi_o)$$

$$= -\frac{4}{aC_o} \sin\theta \sin\phi_o \cos(2\theta - 2\phi) = -\frac{4\lambda_n \sin^2\theta}{aC_o^2} \cos(2\theta - 2\phi_o) \quad . \tag{A-25}$$

This adjustment for tail effects in k_{jn} is not trivial, but its ultimate effect is yet to be found since k_{jn} in practice is always added to g_{jn}, which is yet to be discussed. We add the observation that k_{jn} represents contributions that the dislocations at z_j and $\bar{z}_j$ make to stress on the slip plane at z_n. If effects from dislocations at $-z_j$ and $-\bar{z}_j$ were included, k_{jn} would be changed slightly in its value but perhaps more noticeably in its form.

For the function k_{nn}, it has been shown that

$$k_{nn} = -\frac{1}{\ell_n} \cos 2\theta \quad . \tag{A-26}$$

This function excludes the shear stress contributed at z_n by the dislocation at z_n, since the dislocation is not considered to drive itself forward, but the contribution from the dislocation at $\bar{z}_n$ is included. In adjusting for tail effects, however, it seems appropriate to exclude effects from tails of both the dislocations at z_n and $\bar{z}_n$. We can find the adjustment required here from that found for k_{jn} by considering there a case for which $a_j = a_n$ and $\ell_n > 0$ but letting $\ell_j \to 0$. Since then $C_o \to \lambda_n$ and $\phi_o \to \theta$, it follow that

$$\text{tail adjustment for } k_{nn} = -\frac{4 \sin^2 \theta}{\ell_n} \quad . \tag{A-27}$$

Again the ultimate effect of this adjustment is tied to an adjustment to g_{nn} which is yet to be discussed.

Before considering the function g_{nn}, it is well to consider the function g_{jn} for $j \neq n$. This is

$$g_{jn} = 2_n \sin^{-2} \mathrm{Re}\left[\frac{e^{2i\theta}}{(z_n^2-a^2)^{\frac{1}{2}}}\left\{\frac{(z_j^2-a^2)^{\frac{1}{2}}-(z_n^2-a^2)^{\frac{1}{2}}}{(z_n-z_j)^2}+\frac{(\bar{z}_j^2-a^2)^{\frac{1}{2}}-(\bar{z}_n^2-a^2)^{\frac{1}{2}}}{(z_n-\bar{z}_j)^2}\right.\right.$$

$$\left.+\frac{z_n}{z_n^2-a^2}\left[\frac{(z_j^2-a^2)^{\frac{1}{2}}}{z_n-z_j}+\frac{(\bar{z}_j^2-a^2)^{\frac{1}{2}}}{z_n-\bar{z}_j}\right]\right\}$$

$$+\frac{\ell_j e^{2i\theta}}{(z_n^2-a^2)^{\frac{1}{2}}}\left\{\frac{e^{i\theta}}{(z_n-z_j)^2(z_j^2-a^2)^{\frac{1}{2}}}\left[\frac{a^2(z_n-z_j)}{z_n^2-a^2}+2\frac{(z_n^2-a^2)^{\frac{1}{2}}(z_j^2-a^2)^{\frac{1}{2}}+a^2-z_jz_n}{z_n-z_j}\right]\right. \qquad \text{(A-28)}$$

$$\left.\left.+\frac{e^{i\theta}}{(z_n-\bar{z}_j)^2(\bar{z}_j^2-a^2)^{\frac{1}{2}}}\left[\frac{a^2(z_n-\bar{z}_j)}{z_n^2-a^2}+2\frac{(z_n^2-a^2)^{\frac{1}{2}}(\bar{z}_j^2-a^2)^{\frac{1}{2}}+a^2-\bar{z}_jz_n}{z_n-\bar{z}_j}\right]\right\}\right] .$$

Using quantities defined above, this g_{jn} can be expressed in the real form:

$$g_{jn}=\frac{2\lambda_n \sin^2\theta}{a\,D_n}\left\{\frac{D_j}{C_1^2}\cos\frac{4\theta+\beta_j-\beta_n-4\phi_1}{2}-\frac{D_n}{C_1^2}\cos(2\theta-2\phi_1)+\frac{D_j}{C_2^2}\cos\frac{2\theta-\beta_j-\beta_n-4\phi_2}{2}-\frac{D_n}{C_2^2}\cos(2\theta-2\phi_2)\right.$$

$$+\frac{\alpha_n D_j}{C_1 D_n^2}\cos\frac{2\theta+\beta_j-3\beta_n-2\phi_1}{2}+\frac{\alpha_n D_j}{C_2 D_n^2}\cos\frac{\beta_j+3\beta_n+2\phi_2}{2}+\frac{\lambda_n D_j}{C_1 D_n^2}\cos\frac{4\theta+\beta_j-3\beta_n-2\phi_1}{2}$$

$$\left.+\frac{\lambda_n D_j}{C_2 D_n^2}\cos\frac{2\theta-\beta_j-3\beta_n-2\phi_2}{2}+\frac{\lambda_j}{C_2 D_j D_n^2}\cos\frac{2\theta-\beta_j-3\beta_n-2\phi_1}{2}+\frac{2\lambda_j D_n}{C_1^3}\cos(3\theta-3\phi_1)+\right.$$

$$+\frac{2\lambda_j}{C_1^3 D_j}\left[(1-\alpha_j\alpha_n)\cos\frac{4\theta-\beta_j-\beta_n-6\phi_1}{2}-(\alpha_n\lambda_j+\alpha_j\lambda_n)\cos\frac{6\theta-\beta_j-\beta_n-6\phi_1}{2}-\lambda_j\lambda_n\cos\frac{8\theta-\beta_j-\beta_n-6\phi_1}{2}\right]$$

$$+\frac{\lambda_j}{C_2 D_j D_n^2}\cos\frac{\beta_j-3\beta_n-2\phi_2}{2}+\frac{2\lambda_j D_n}{C_2^3}\cos(\theta-3\phi_2) \qquad \text{(A-29)}$$

$$+\frac{2\lambda_j}{C_2^3 D_j}\left[(1-\alpha_j\alpha_n-\lambda_j\lambda_n)\cos\frac{2\theta+\beta_j-\beta_n-6\phi_2}{2}-\alpha_j\lambda_n\cos\frac{4\theta+\beta_j-\beta_n-6\phi_2}{2}-\alpha_n\lambda_j\cos\frac{\beta_j-\beta_n-6\phi_2}{2}\right]\Bigg\}$$

To find the adjustment needed to cancel effects from the unwanted tails of the dislocations with branch points at z_j and $\bar{z}_j$, note that if $\lambda_j \to 0$ then $C_1 \to C_2 \to C_0$, $\phi_1 \to \phi_2 \to \phi_0$, $D_j \to D_{j0} = (1-\alpha_j^2)^{1/2}$ and $\beta_j \to \pi - \theta$. Then the desired adjustment proves to be

$$-\lim_{\lambda_j \to o} g_{jn} = \frac{4\lambda_n \sin^2\theta}{a C_o^2}\cos(2\theta-2\phi_o) \qquad \text{(A-30)}$$

This adjustment too is not trivial, but it is the negative of the adjustment for k_{jn}, so the adjustment needed for $g_{jn}+k_{jn}$ is zero. Since g_{jn} and k_{jn} are always summed in being used, this implies that the unadjusted formulas for them can be used in practice, even though they are questionable when viewed individually. It should be observed also that g_{jn} as shown here refers only to contributions to slip plane shear stresses at z_n arising from forces required on the crack to abolish the stresses caused by the dislocations at z_j and $\bar{z}_j$. If effects of the dislocations at $-z_j$ and $-\bar{z}_j$ were included, there would be small additions to g_{jn}. In view of the long real expression for g_{jn}, it is to be hoped that such addition would provide a simpler overall sum, as may well be possible.

Finally, turn to g_{nn}. This is

$$g_{nn} = 2\ell_n \sin^2\theta\, \mathrm{Re}\left[\frac{e^{2i\theta}}{(z_n^2-a^2)^{1/2}}\left\{-\frac{2z_n^2+a^2}{2(z_n^2-a^2)^{3/2}}+\frac{z_n(\bar{z}_n^2-a^2)^{1/2}}{(z_n^2-a^2)(z_n-\bar{z}_n)}+\frac{(\bar{z}_n^2-a^2)^{1/2}-(z_n^2-a^2)^{1/2}}{(z_n-\bar{z}_n)^2}\right\}+\right.$$

$$+\frac{\ell_n e^{2i\theta}}{(z_n^2-a^2)^{\frac{1}{2}}}\left\{-\frac{a^2 z_n e^{i\theta}}{(z_n^2-a^2)^{5/2}}+\frac{e^{-i\theta}}{(z_n-\bar{z}_n)^2(z_n^2-a^2)^{\frac{1}{2}}}\left[\frac{a^2(z_n-\bar{z}_n)}{z_j^2-a^2}+2\,\frac{(z_n^2-a^2)^{\frac{1}{2}}\,(\bar{z}_n^2-a^2)^{\frac{1}{2}}+a^2-z_n\bar{z}_n}{z_n-\bar{z}_n}\right]\right\}\Bigg] . \tag{A-31}$$

Again using quantities defined above, this g_{nn} can be expressed in the real form

$$g_{nn}=\frac{2\lambda_n \sin^2\theta}{D_n^2}\left[-\frac{(2\alpha_n^2+1)}{2D_n^2}\cos 2\beta_n-\frac{2\alpha_n\lambda_n}{D_n^2}\cos(\theta-2\beta_n)-\frac{\lambda_n^2}{D_n^2}\cos(2\theta-2\beta_n)-\frac{\alpha_n \sin 2\beta_n}{2\lambda_n \sin\theta}\right. \tag{A-32}$$

$$\left.+\frac{\sin(\theta-2\beta_n)}{2\sin\theta}-\frac{\alpha_n\lambda_n}{D_n^4}\cos 3\beta_n-\frac{\lambda_n^2}{D_n^4}\cos(\theta-3\beta_n)-\frac{\sin\beta_n}{2D_n^2\sin\theta}-\frac{D_n^2+1-\alpha_n^2}{2\lambda_n^2}\right] .$$

One cannot manipulate this function itself to find its unwanted tail effects, but an adjustment for them can be found by beginning with g_{jn} and assuming $\alpha_j = \alpha_n$, but taking $\lambda_n > \lambda_j$. This assumption alone makes $C_1 = \lambda_n - \lambda_j$ and $\phi_1 = \theta$, and thereby simplifies g_{jn}. Continuing by letting $\lambda_j \to 0$, so that also $C_1 \to C_2 \to \lambda_n$, $\phi_2 \to \theta$, $D_j \to D_{jo} = (1-\alpha_n^2)^{\frac{1}{2}}$ and $\beta_j \to \pi-\theta$, one finds the adjustment

$$-\lim_{\lambda_j \to 0} g_{jn} = \frac{4\sin^2\theta}{\ell_n} = \text{adjustment for } g_{nn}. \tag{A-33}$$

This adjustment is the negative of that required for k_{nn}. Since g_{nn} and k_{nn} are always added in use, their adjustments cancel each other. However, here too the effects of the dislocations at $-z_n$ and $-\bar{z}_n$ were omitted, and including them could make minor changes in value and perhaps substantial changes in form.

Discussion of the Functions Related to Stresses

Up to this point, the effort to make the stress related functions (f_n, h_n, k_{jn}, k_{nn}, g_{jn}, and g_{nn}) more manageable has provided real expressions for them and has shown how they would be changed by elimination of effects from the unwanted tails of the dislocations. The real expressions are given in

Equations (14), (20), (22), (26), (29), and (32), respectively, using new symbols defined in Equations (4) to (8), (10), (11), (23), and (24) and interpreted in Figures 1 and 2. Nontrivial adjustments for tail effects were found for the last four functions, as shown by Equations (25), (27), (30), and (33), but these adjustments cancel each other when k_{jn} and g_{jn} (or k_{nn} and g_{nn}) are added, as they always are in actual use. It was observed that the given stress related functions are based on effects from the pair of dislocations at one end of the crack, but not from the pair at the other end since they were regarded as remote. For one function (f_n), revised forms were deduced to include effects from all four dislocations of the symmetry set. Surprisingly, the form of f_n based on four dislocations [as in Equations (17) and (18)] is simpler than that based on two [as in Equations (13) and (14)], though that might not be true for the other functions.

The complexity of these stress related functions prompts a desire for simplified forms, especially for g_{jn}, but care must be exercised that any simplified form is at least approximately valid over the range of its parameters for which it is used. The functions differ in complexity, so they will be considered separately. The aim, of course, can be either to make the formulas more comprehensible or to make them more rapidly computable.

The form of f_n based on four dislocations [as in Equation (18)] is the simpler one for f_n, so consider it first. It has three terms, of which the first two have essentially the same magnitude while the third is smaller, since α_n and λ_n/D_n^2 have the order of unity while λ_n is smaller. To combine the terms of highest order, we may use the identity

$$\frac{\alpha_n \lambda_n}{D_n^2} \cos\frac{\theta+3\beta_n}{2} = \frac{1}{2}\left[\cos\frac{\theta+\beta_n}{2} - \frac{\lambda_n^2}{D_n^2}\cos\frac{\theta-3\beta_n}{2} + \frac{1-\alpha_n^2}{D_n^2}\cos\frac{3\theta+3\beta_n}{2}\right] \quad . \qquad \text{(A-34)}$$

Use of this identity shows

$$f_n^T = \frac{8\sin\theta}{D_n}\left[\frac{3}{2}\cos\frac{\theta+\beta_n}{2} + \frac{\lambda_n^2}{2D_n^2}\cos\frac{\theta-3\beta_n}{2} + \frac{1-\alpha_n^2}{2D_n^2}\cos\frac{3\theta+3\beta_n}{2}\right] \quad . \qquad \text{(A-35)}$$

Here the first term should be dominant, since λ_n and $\frac{1-\alpha_n^2}{2\lambda_n}$ ($\approx\frac{1-\alpha_n}{\lambda_n}$) are expected to be small, while $\frac{\lambda_n}{2D_n^2}$ has the order of unity. Indeed if $(1-\alpha_n)/\lambda_n$ is small (that is $(a-a_n)/\ell_n$ is small), then from Equation (5)

$$D_n \approx \sqrt{2\lambda_n} \quad ,$$

and from equation (6)

$$\beta_n \approx (\frac{\lambda_n}{2} + \frac{1-\alpha_n}{\lambda_n}) \sin\theta \quad ,$$

which is small. It can be seen that the first order approximation is

$$f_n^T \approx 6\sqrt{\frac{2}{\lambda_n}} \sin\theta \cos\frac{\theta}{2} \quad , \qquad \text{(A-36)}$$

in agreement with the approximation given in References [A-1,A-2]. If, however, one wishes to account somewhat for the distance $1-\alpha_n$ ($\equiv\rho_n$), some of its effect can be seen in each of the terms in the brackets of Equation (35) as well as in D_n. Letting

$$\varepsilon_n = \rho_n/\lambda_n = (1-\alpha_n)/\lambda_n \quad ,$$

and keeping terms of order λ_n and ε_n, one finds from Equations (5) and (6):

$$D_n \approx \sqrt{2\lambda_n}\,[1+\frac{1}{4}(\lambda_n-2\varepsilon_n)\cos\theta] \quad ,$$

$$\beta_n \approx \frac{\lambda_n+2\varepsilon_n}{2}\sin\theta \; .$$

Using these approximations, Equation (35) yields the approximation

$$f_n^T \approx 6\sqrt{\frac{2}{\lambda_n}} \sin\theta \cos\frac{\theta}{2}\left[1 - \frac{\lambda_n}{12} - \frac{5\epsilon_n}{6}(1 - 2\cos\theta)\right] . \qquad \text{(A-37)}$$

This approximation to f_n^T provides some insight concerning the relative effect of the distance ρ_n under the presumption that λ_n and ρ_n/λ_n are small, though its computational advantage over the exact form in Equation (35) may be small.

It is important now to note that if the function f_n as given by Equation (14) is approximated to the same degree as f_n^T is in Equation (37), one finds

$$f_n \approx 6\sqrt{\frac{2}{\lambda_n}} \sin\theta \cos\frac{\theta}{2}\left[1 + \frac{\lambda_n}{12} - \frac{5\epsilon_n}{6}(1 - 2\cos\theta)\right] . \qquad \text{(A-38)}$$

This approximation differs from that for f_n^T by a term of order λ_n in the brackets. The difference between these approximations must be due to the difference between the original complex representations for f_n and f_n^T as given by Equations (13) and (17). Since Equation (17) has better justification (from using all four dislocations of the symmetry set instead of only two), the approximation (37) must be regarded as better than (37). Thus, in this sense, Equation (13) does not support the degree of approximation shown in Equation (38). Since the complex representations of k_{jn}, k_{nn}, g_{jn}, and g_{nn} as given originally by equations (21), (26), (28), and (31) are based on the same neglect of the two more remote dislocations, it must be considered doubtful that they would support a higher order approximation as typified by Equation (37), though they should support first order approximations as typified by Equation (36). Since the first influence of ϵ_n is the same in both Equations (37) and (38), it might be hoped that the first influence of ϵ_n could be correct for the other stress related functions even though the formulas are based on two dislocations, but use of four-dislocation forms would make calculations more secure.

To get an approximate form of h_n from Equation (20) to accuracy comparable to that in Equation (37), one may reuse the same approximations for D_n and β_n and thus show

$$h_n \simeq \sin\theta\cos\theta + \frac{1}{4}\sqrt{\frac{2}{\lambda_n}}\cos\frac{\theta}{2}\left[1 + \frac{3\lambda_n}{4}(1-2\cos\theta) + \frac{3\varepsilon_n}{2}\right] \quad . \qquad \text{(A-39)}$$

The first two terms of this approximation agree with those given in References [A-1,A-2]. Since this function represents effects from the applied load which are not dependent on how many dislocations were employed, the higher order terms here should also be valid.

Approximation of the function k_{jn} given by Equation (22) involves consideration of more parameters since there are two sets of dislocations. In order to express the results more compactly, let

$$A_d = \alpha_n - \alpha_j, \quad L_d = \lambda_n - \lambda_j, \quad L_s = \lambda_n + \lambda_j \quad .$$

Using these quantities, one may express the component parts of Equation (22) exactly and thus rewrite that equation in the form

$$ak_{jn} = \frac{1}{C_1^2}(A_d\cos\theta + L_d)\left[1 - \frac{2A_d^2\sin^2\theta}{C_1^2}\right]$$

$$- \frac{1}{C_2^2}[A_d\cos\theta + L_d\cos^2\theta - L_s\sin^2\theta]\left\{\frac{2}{C_2^2}[A_d\cos\theta + L_d\cos^2\theta + L_s\sin^2\theta]^2 - 1\right\} \quad ,$$

where

$$C_1^2 = A_d^2 + 2A_dL_d\cos\theta + L_d^2 \quad ,$$

$$C_2^2 = A_d^2 + 2A_dL_d\cos\theta + L_d^2\cos^2\theta + L_s^2\sin^{-2} \quad .$$

To simplify this result, it will be assumed that A_d is of smaller order than L_s or L_d. Expanding the various parts of the expression for k_{jn} as series in (A_d/L_s) or (A_d/L_d) truncated after terms of order 1, one finds at last that

$$ak_{jn} \approx \frac{2}{L_d} - \frac{2(L_d\cos^2\theta - L_s\sin^2\theta)[2(L_d\cos^2\theta + L_s\sin^2\theta)^2 - (L_d^2\cos^2\theta + L_s^2\sin^2\theta)]}{(L_d^2\cos^2\theta + L_s^2\sin^{-2}\theta)^2}$$

$$- 2A_d\cos\theta\left[\frac{1}{L_d^2} - \frac{2(L_d\cos^2\theta + L_s\sin^2\theta)(L_d\cos^2\theta - 3L_s\sin^2\theta) + (L_d+L_s)^2\sin^2\theta - L_d^2}{(L_d^2\cos^2\theta + L_s^2\sin^2\theta)^2}\right] \qquad \text{(A-40)}$$

It can be seen that if $\lambda_j \to 0$ so that $L_d = L_s = \lambda_n$, this equation reduces to

$$ak_{jn} \approx 2\left[\frac{1}{\lambda_n} - \frac{\cos 2\theta}{\lambda_n}\right] - 2A_d\cos\theta\ \frac{4\sin^2\theta}{\lambda_n^2},$$

a form in which the term $-\cos 2\theta/\lambda_n$ is like one given in References [A-1,A-2], while the term $1/\lambda_n$ reminds one of the deleted self-driving effects in k_{nn}. There was no term corresponding to that involving A_d. Thus, the k_{jn} of Equation (40) is fairly plausible. The accuracy of approximations using the second order term may be doubtful, however, since the two more remote dislocations were neglected in the original formula (21), though the contribution of the term involving A_d may be nearly right.

The value of k_{nn} given by Equation (26) needs no approximation.

The function of g_{jn} as expressed by Equation (29) contains all the quantities appearing in the preceding functions, including two distances D and angles β corresponding to the two points z_j and z_n. Some formal simplifications of the function can be had by introducing also (R_j, ψ_j) and (R_n, ψ_n), the polar coordinates of z_j and z_n. Thus, g_{jn} can be written as

$$g_{jn} = \frac{2\lambda_n\sin^2\theta}{aD_n}\left\{\frac{D_j}{C_1^2}\cos\frac{4\theta + \beta_j - \beta_n - 4\theta_1}{2} - \frac{D_n}{C_1^2}\cos(2\theta - 2\phi_1) + \right.$$

$$\left. + \frac{D_j}{C_2^2}\cos\frac{2\theta - \beta_j - \beta_n - 4\phi_2}{2} - \frac{D_n}{C_2^2}\cos(2\theta - 2\phi_2) + \right. \qquad \text{(A-41)}$$

$$+\frac{D_j R_n}{C_1 D_n^2}\cos\frac{2\theta+\beta_j-3\beta_n-2\phi_1+2\psi_n}{2}+\frac{D_j R_n}{C_2 D_n^2}\cos\frac{\beta_j+3\beta_n-2\phi_2-2\psi_n}{2}$$

$$+\frac{\lambda_j}{C_1 D_j D_n^2}\cos\frac{2\theta-\beta_j-3\beta_n-2\phi_1}{2}+\frac{2\lambda_j D_n}{C_1^3}\cos(3\theta-3\phi_1)$$

$$+\frac{2\lambda_j}{C_1^3 D_j}\left[\cos\frac{4\theta-\beta_j-\beta_n-6\phi_1}{2}-R_n R_j\cos\frac{4\theta-\beta_j-\beta_n-6\phi_1+2\psi+2\psi_j}{2}\right]$$

$$+\frac{\lambda_j}{C_2 D_j D_n^2}\cos\frac{\beta_j-3\beta_n-2\phi_2}{2}+\frac{2\lambda_j D_n}{C_2^3}\cos(\theta-3\phi_2)$$

$$+\frac{2\lambda_j}{C_2^3 D_j}\left[\cos\frac{2\theta+\beta_j-\beta_n-6\theta_2}{2}-R_n R_j\cos\frac{2\theta+\beta_j-\beta_n-6\phi_2+2\psi_n-2\psi_j}{2}\right]\Bigg\}\ .$$

It is helpful to note that all the angles β_j, β_n, ψ_j, and ψ_n are small to the order of the relevant λ and $\varepsilon(=\rho/\lambda)$. The two bracketed quantities in Equation (41) are also small to this order, so that all terms in the braces have order approximately like $\lambda^{-3/2}$.

Approximation of the function g_{jn} for small values of selected parameters is much more tedious than the process for the earlier stress-related functions, since g_{jn} involves so many parameters, and because it has so many terms, including a great variety of trigommetric functions. In order to make the approximation possible, all these parameters were treated as being small to the same order: λ_j, λ_n, L_d, L_s, β_j, β_n, ψ_j, ψ_n, and A_d/L_d (that is, A_d was treated as small to higher order). In addition, a new quantity L_t was defined to be

$$L_t = (L_d^2\cos^2\theta + L_s^2\sin^2\theta)^{\frac{1}{2}}\ ,$$

so that it also is small to the same order. With these assumptions and much algebra, it was found that the first approximation to g_{jn} is

$$g_{jn} \approx \frac{\sqrt{2\lambda_n}\sin^2\theta}{a}\left\{-\frac{(2\lambda_j)^{3/2}}{L_d^3}-\frac{(2\lambda_j)^{3/2}L_d\cos\theta}{L_t^4}\left[1+\frac{4L_s^2\sin^2\theta}{L_t^2}\right]+\frac{3\sqrt{2\lambda_j}}{4\lambda_n L_d}+\frac{3L_d\sqrt{2\lambda_j}\cos\theta}{4\lambda_n L_t^2}\right.$$

$$\left.+\frac{\sqrt{2\lambda_n}}{L_d^3}(2\lambda_j-L_d)+\frac{\sqrt{2\lambda_n}}{L_t^4}\left[L_sL_d-2(L_d\cos^2\theta+L_s\sin^2\theta)^2-\frac{4L_sL_d(L_s-L_d)^2\sin^2\theta\cos^2\theta}{L_t^2}\right]\right\} . \quad (42)$$

These terms have order equivalent to that of λ_j^{-1}. The terms of next higher order (like that of λ_j^0) are several times more voluminous, and they also have doubtful relevance since their general magnitude is expectedly like that of discrepancies due to omission of effects from the two more remote dislocations of the symmetry set. Therefore, those terms have been relegated to the end of this Appendix. Equation (42) also lacks the term which could be added to compensate for the unwanted tail effects. Since $C_o^2 = \lambda_n^2+2A_d\lambda_n\cos\theta + A_d^2$, and

$$\cos(2\theta-2\phi_0) = 1 - 2\sin^2(\theta-\phi_0) = 1 - 2A_d^2\sin^2\theta/C_0^2 ,$$

one finds from Equation (30) that that compensating term would be

$$-\lim_{\lambda_n\to 0} g_{jn} = \frac{4\lambda_n\sin^2\theta(\lambda_n^2+2A_d\cos\theta+A_d^2\cos 2\theta)}{(\lambda_n^2+2A_d\lambda_n\cos\theta+A_d^2)^2} \approx \frac{4\sin^2\theta}{\lambda_n}\left[1-\frac{2A_d}{\lambda_n}\cos\theta\right] . \quad (A-43)$$

The remaining stress-related function to be approximated is g_{nn}. Beginning from Equation (32), assuming λ_n, ε_n, and β_n to be small of the same order [where again $\varepsilon_n = (1-\alpha_n)/\lambda_n$], and keeping terms of the first two orders, one can show

$$g_{nn} \approx -\frac{2\sin^2\theta}{\lambda_n a}\left[1+\frac{1}{16}(\lambda_n+18\,\varepsilon_n)(1+\cos\theta)\right] . \quad (A-44)$$

It is appropriate to compare the approximations given here with some given in Reference [A-1]. There it was assumed that $a_j = a_n$, and either

that $\lambda_j \gg \lambda_n$ or that $\lambda_n \gg \lambda_j$. Here, by taking $a_j = a_n$ (so that $A_d = 0$) and $\lambda_j \gg \lambda_n$, one finds from Equations (40) and (42) that

$$k_{jn} \approx -\frac{2(1-\cos 4\theta)}{\ell_j} \quad , \quad \text{and } g_{jn} \approx -\frac{3\sin^2\theta}{2\sqrt{\ell_n \ell_j}} \sin^2\theta \quad . \tag{A-45}$$

Adding these results provides the same approximation as is shown for $g_{12} + k_{12}$ on Page 37 of Reference [A-1]. The case with $a_j = a_n$ and $\lambda_n \gg \lambda_j$ is somewhat more delicate, since the leading terms of the respective approximations cancel each other. Therefore, it is necessary to keep terms of the first two orders in λ_n. [This is not to be confused with the first two orders over all the parameters, as governed the approximations leading to Equations (4) and (42). This is merely a way of selecting the remaining major terms in those two equations.] With this in view, Equations (40) and (42) yield for $\lambda_n >> \lambda_j$.

$$\begin{aligned} k_{jn} &\approx \frac{4\sin^2\theta}{\ell_n} + \frac{2\ell_j(1-\cos 4\theta)}{\ell_n^2} \quad , \\ g_{jn} &\approx -\frac{4\sin^2\theta}{\ell_n} + \frac{3\sqrt{\ell_j}}{2\ell_n^{3/2}}(1+\cos\theta)\sin^2\theta \quad . \end{aligned} \tag{A-46}$$

In the sum $k_{jn} + g_{jn}$, the leading terms here cancel each other, and the resulting sum is the same approximation as is shown for $k_{21} + g_{21}$ on Page 37 of Reference [A-1]. The leading terms which here cancel each other are, of course, the quantities which would have been removed alternatively by the compensation for tail effects in the functions k_{jn} and g_{jn}.

It may be observed also that the distinction between the approximations offered by Equations (40) and (42) and those cited from Reference [A-1] consists mainly in the more general lengths ℓ_j and ℓ_n allowed by Equations (40) and (42).

It is implicit here that accounting for finite values of both these lengths is more important than is the separation between the slip planes, which determines $A_d = (a_n - a_j)/a$. This order of importance is quite plausible except if ℓ_j and ℓ_n are nearly equal, but such cases were ruled out for Equations (40) and (42) when it was assumed that A_d/L_d is also small, that is that $(a_n - a_j)/(\ell_n - \ell_j)$ is small. This assumption should be remembered in applying these approximations.

The great abundance of parameters entering these stress-related functions places a great burden on the organization of any approximation process. This is well illustrated by the complexity of the second order terms of g_{jn} given later. Some simplification might yet be found for the sum of those terms, but it probably would be minor unless some other drastic assumption is made, such as taking $\lambda_j >> \lambda_n$ or $\lambda_n >> \lambda_j$. Assumptions such as those could be imposed readily on the second order terms for g_{jn}, but they probably would still yield terms competing in magnitude with the discrepancy allowed when the two remote dislocations were discounted. This illustrates the caution needed in approximation of these functions. It is good that exact, real expressions exist for all the stress-related functions, and but for g_{jn} they are simple.

Formulas for Crack-Opening Displacements

The Equation (3) for the crack-opening displacement employs a function d_j for which Reference [A-1] gives the complex form

$$d_j = 2\delta(a_j - |x|) - \frac{4}{\pi}\ell_j(a^2-x^2)^{\frac{1}{2}}\,\mathrm{Re}\left\{\frac{z_j e^{i\theta}}{(z_j^2-a^2)^{\frac{1}{2}}(z_j^2-x^2)}\right\}$$

$$+\frac{1}{\pi}\,\mathrm{Im}\left\{\log\left[\frac{a^2-xz_j+i(z_j^2-a^2)^{\frac{1}{2}}(a^2-x^2)^{\frac{1}{2}}}{a^2-xz_j-i(z_j^2-a^2)^{\frac{1}{2}}(a^2-x^2)^{\frac{1}{2}}}\right]+\log\left[\frac{a^2+xz_j+i(z_j^2-a^2)^{\frac{1}{2}}(a^2-x^2)^{\frac{1}{2}}}{a^2+xz_j-i(z_j^2-a^2)^{\frac{1}{2}}(a^2-x^2)^{\frac{1}{2}}}\right]\right\}. \qquad \text{(A-47)}$$

This d_j multiplied by $b_j \sin\theta$ represents the contribution to the crack-opening displacement at position x (for $x^2 \le a^2$) made by the set of four dislocations symmetric to the one with branch point at z_j, each extending semi-infinitely.

To begin to find d_j in real form, one may show first that in terms of the quantities introduced above and the position variable

$$v_j = \left(1 - \frac{x^2}{a^2}\right)^{\frac{1}{2}} / D_j \quad ,$$

one finds

$$\frac{4}{\pi} \ell_j (a^2-x^2)^{\frac{1}{2}} \operatorname{Re}\left\{ \frac{z_j e^{i\theta}}{(z_j^2-a^2)^{\frac{1}{2}} (z_j^2-x^2)} \right\} = \tag{A-49}$$

$$= \frac{4\lambda_j v_j}{\pi D_j^2} \frac{\left[\alpha_j \cos \frac{\theta+3\beta_j}{2} + \lambda_j \cos \frac{\theta-3\beta_j}{2}\right] + v_j^2\left[\alpha_j \cos \frac{\theta-\beta_j}{2} + \lambda_j \cos \frac{3\theta-\beta_j}{2}\right]}{[1 + 2 v_j^2 \cos (\theta + \beta_j) + v_j^4]}$$

To prepare for treating the logarithmic terms in d_j, consider any real numbers a and b, and define ϕ (where $-\pi < \phi \leq \pi$) so that

$$\cos \phi = \frac{a}{\sqrt{a^2+b^2}}, \qquad \sin \phi = \frac{b}{\sqrt{a^2+b^2}} \quad ,$$

that is so that

$$\phi = \operatorname{sgn} (b) \arccos \frac{a}{\sqrt{a^2+b^2}} \quad .$$

Then

$$\log (a+ib) = \log (\cos \phi + i \sin \phi) + \log \sqrt{a^2+b^2}$$

$$= \log e^{i\theta} + \log \sqrt{a^2+b^2} = i\phi + \log \sqrt{a^2+b^2}$$

and

$$\operatorname{Im} [\log(a+ib)] = \phi = \operatorname{sgn} (b) \arccos \frac{a}{\sqrt{a^2+b^2}} \quad . \tag{A-50}$$

Applying this to terms to appear in d_j, and letting $s = x/a$, one finds

$$\frac{1}{\pi}\,\mathrm{Im}\left\{\log\left[\frac{a^2-xz_j+i(z_j^2-a^2)^{\frac{1}{2}}(a^2-x^2)^{\frac{1}{2}}}{a^2-xz_j-i(z_j^2-a^2)^{\frac{1}{2}}(a^2-x^2)^{\frac{1}{2}}}\right]+\log\left[\frac{a^2+xz_j+i(z_j^2-a^2)^{\frac{1}{2}}(a^2-x^2)^{\frac{1}{2}}}{a^2+xz_j-i(z_j^2-a^2)^{\frac{1}{2}}(a^2-x^2)^{\frac{1}{2}}}\right]\right\}$$

$$=\frac{1}{\pi}\,\mathrm{Im}\left\{\log\frac{\left\{\left[a^2+i(z_j^2-a^2)^{\frac{1}{2}}(a^2-x^2)^{\frac{1}{2}}\right]-xz_j\right\}\left\{\left[a^2+i(z_j^2-a^2)^{\frac{1}{2}}(a^2-x^2)^{\frac{1}{2}}\right]+xz_j\right\}}{\left\{\left[a^2-i(z_j^2-a^2)^{\frac{1}{2}}(a^2-x^2)^{\frac{1}{2}}\right]-xz_j\right\}\left\{\left[a^2-i(z_j^2+a^2)^{\frac{1}{2}}(a^2-x^2)^{\frac{1}{2}}\right]+xz_j\right\}}\right\}$$

$$=\frac{1}{\pi}\,\mathrm{Im}\left\{\log\frac{\left[a^2+i(z_j^2-a^2)^{\frac{1}{2}}(a^2-x^2)^{\frac{1}{2}}\right]^2-x^2z_j^2}{\left[a^2-i(z_j^2-a^2)^{\frac{1}{2}}(a^2-x^2)^{\frac{1}{2}}\right]^2-x^2z_j^2}\right\}=\frac{1}{\pi}\,\mathrm{Im}\left\{\log\frac{(a^2-x^2)+2i(a^2-x^2)^{\frac{1}{2}}(z_j^2-a^2)^{\frac{1}{2}}+i^2(z_j^2-a^2)}{(a^2-x^2)-2i(a^2-x^2)^{\frac{1}{2}}(z_j^2-a^2)^{\frac{1}{2}}+i^2(z_j^2-a^2)}\right\}$$

$$=\frac{1}{\pi}\,\mathrm{Im}\left\{\log\left[\frac{(a^2-x^2)^{\frac{1}{2}}+i(z_j^2-a^2)^{\frac{1}{2}}}{(a^2-x^2)^{\frac{1}{2}}-i(z_j^2-a^2)^{\frac{1}{2}}}\right]^2\right\}=\frac{1}{\pi}\,\mathrm{Im}\left\{\log\left[\frac{(a^2-x^2)^{\frac{1}{2}}+i\,a(f_1+i\,f_2)}{(a^2-x^2)^{\frac{1}{2}}-i\,a(f_1+i\,f_2)}\right]^2\right\}$$

$$=\frac{2}{\pi}\,\mathrm{Im}\left\{\log\left[\frac{(\sqrt{1-s^2}-f_2)+i\,f_1}{(\sqrt{1-s^2}+f_2)-i\,f_1}\right]\right\}=\frac{2}{\pi}\left[\arccos\frac{\sqrt{1-s^2}-f_2}{\sqrt{(\sqrt{1-s^2}-f_2)^2+f_1^2}}+\arccos\frac{\sqrt{1-s^2}-f_2}{\sqrt{(\sqrt{1-s^2}+f_2)^2+f_1^2}}\right]$$

$$=\frac{2}{\pi}\arccos\frac{1-s^2-f_1^2-f_2^2}{\sqrt{(1-s^2-f_1^2-f_2^2)^2+4f_1^2(1-s^2)}}=\frac{2}{\pi}\arccos\frac{v^2-1}{\sqrt{(v^2-1)^2+4v^2\cos\frac{\theta+\beta}{2}}}$$

$$=\frac{2}{\pi}\arccos\frac{v^2-1}{\sqrt{v^4+2v^2\cos(\theta+\beta)+1}}\quad,\quad\text{where}\quad v=\sqrt{1-s^2}/D\quad.\qquad\text{(A-51)}$$

For all relevant λ, α, θ, and x (that is $x^2 \leq a^2$), this last expression is a continuous function which should be valid and which avoids the many-valued nature of the original logarithms. This is the function intended in the Reference [A-1] analysis. The variable v appears to be a natural variable to replace x, and it can be seen that it varies nearly in proportion to $(a-x)^{1/2}$ for x near a.

Combining the above results, one finds that Equation (47) is equivalent to

$$d_j = 2\delta(a_j-|x|) - \frac{4\lambda_j v_j}{\pi D_j^2}\frac{\left[\alpha_j \cos\frac{\theta+3\beta_j}{2}+\lambda_j\cos\frac{\theta-3\beta_j}{2}\right]+v_j^2\left[\alpha_j\cos\frac{\theta-\beta_j}{2}+\lambda_j\cos\frac{3\theta-\beta_j}{2}\right]}{[1+2v_j^2\cos(\theta+\beta_j)+v_j^4]}$$

$$-\frac{2}{\pi}\arccos\frac{1-v_j^2}{\sqrt{1+2v_j^2\cos(\theta+\beta_j)+v_j^4}} \quad . \tag{A-52}$$

To find adjustment to compensate for the unwanted tails of the dislocations, we note that as $\lambda_j \to 0$ one has $D_j^2 \to 1-\alpha_j^2$, $\beta_j \to \pi-\theta$, and

$$-\lim_{\lambda_j\to 0} d_j = -2\delta(a_j-|x|)+2H(a_j-|x|) \quad ,$$

here $H(a_j - |x|)$ is the Heaviside step function. Adding this adjustment to d_j gives the compensated form

$$d_{jc} = 2H(a_j-|x|) - \frac{4\lambda_j v_j}{\pi D_j^2}\frac{\left[\alpha_j\cos\frac{\theta+3\beta_j}{2}+\lambda_j\cos\frac{\theta-3\beta_j}{2}\right]+v_j^2\left[\alpha_j\cos\frac{\theta-\beta_j}{2}+\lambda_j\cos\frac{3\theta-\beta_j}{2}\right]}{[1+2v_j^2\cos(\theta+\beta_j)+v_j^4]}$$

$$-\frac{2}{\pi}\arccos\frac{1-v_j^2}{\sqrt{1+2v_j^2\cos(\theta+\beta_j)+v_j^4}} \quad . \tag{A-53}$$

To this, we may add the observation that if $v_j^2 < 1$, then

$$-\frac{2}{\pi}\arccos\frac{1-v_j^2}{\sqrt{1+2v_j^2\cos(\theta+\beta_j)+v_j^4}} = -\frac{2}{\pi}\arctan\frac{2v_j\cos\frac{\theta+\beta_j}{2}}{1-v_j^2} \quad . \tag{A-54}$$

This latter form may have computational advantages, but it has an unwanted step if v_j^2 increases through 1.

The desired function d_{jc} is represented exactly by Equation (53), but if one wishes to examine the behavior of d_j for small values of v_j, say $|v_j|<|$ (that is $|x|>a_j$), he may alter d_j by using the expansions

$$\frac{\cos\alpha' + v^2\cos\beta'}{1+2v^2\cos(\alpha'+\beta')+v^4} = \sum_{n=o}^{\infty}(-v^2)\cos[(n+1)\alpha'+\beta'] \quad , \text{ and}$$

$$\arctan\left[\frac{2v\cos\frac{\theta+\beta}{2}}{1-v^2}\right] = 2v\sum_{n=o}^{\infty}\frac{(-v^2)^n}{2n+1}\cos\frac{(2n+1)(\theta+\beta)}{2} \quad . \tag{A-55}$$

From these, it follows

$$d_{jc} = 2H(a_j-|x|) - \frac{4\lambda_j v_j}{\pi D_j^2}\sum_{n=o}^{\infty}(-v_j^2)^n\left[\alpha_j\cos\frac{(2n+1)\theta+(2n+3)\beta_j}{2}+\lambda_j\cos\frac{(2n-1)\theta+(2n+3)\beta_j}{2}\right]$$

$$-\frac{4v_j}{\pi}\sum_{n=o}^{\infty}\frac{(-v_j^2)^n}{2n+1}\cos\frac{(2n+1)(\theta+\beta_j)}{2} \quad , \text{ for } |v_j|<| \quad . \tag{A-56}$$

To get simple approximation for d_j, take the first two terms of each of the series. This shows

$$d_{jc} = 2H(a_j-|x|) - \frac{4v_j}{\pi}\left\{\left[\cos\frac{\theta+\beta_j}{2}+\frac{\alpha_j\lambda_j}{D_j^2}\cos\frac{\theta+3\beta_j}{2}+\frac{\lambda_j^2}{D_j^2}\cos\frac{\theta-3\beta_j}{2}\right]\right.$$

$$\left. - v_j^2\left[\frac{1}{3}\cos\frac{3\theta+3\beta_j}{2}+\frac{\alpha_j\lambda_j}{D_j^2}\cos\frac{3\theta+5\beta_j}{2}+\frac{\lambda_j^2}{2_j}\cos\frac{\theta+3\beta_j}{2}\right]+\ldots\right\} \quad . \tag{A-57}$$

Inspection shows that the first bracketed term here is equal to $f_n^T D_n/(8 \sin\theta)$. This is precisely the relationship needed to make the terms of order v_j cancel in the equation for Δu_2 provided σ and b are related by the singularity cancelling equation. Satisfaction of this relation shows again that f_n^T is a more satisfactory function than f_n. To arrange the bracketed quantities in Equation (57) into terms of descending magnitude, use Equation (34) and the relation

$$\frac{\alpha_j \lambda_j}{D_j^2} \cos\frac{3\theta+5\beta_j}{2} = \frac{1}{2}\left[\cos\frac{3\theta+3\beta_j}{2} - \frac{\lambda_j^2}{D_j^2}\cos\frac{\theta+5\beta_j}{2} + \frac{1-\alpha_j^2}{D_j^2}\cos\frac{5\theta+5\beta_j}{2}\right] \quad . \qquad \text{(A-58)}$$

Then equation (57) becomes

$$d_{jc} = 2H(a_j - |x|) - \frac{4v_j}{\pi}\left\{\left[\frac{3}{2}\cos\frac{\theta+\beta_j}{2} + \frac{\lambda_j^2}{2D_j^2}\cos\frac{\theta-3\beta_j}{2} + \frac{1-\alpha_j^2}{2D_j^2}\cos\frac{3\theta+3\beta_j}{2}\right]\right.$$
$$\left. - v_j^2\left[\frac{5}{6}\cos\frac{3\theta+3\beta_j}{2} + \frac{\lambda_j^2}{2D_j^2}\cos\frac{3\theta+5\beta_j}{2} + \frac{1-\alpha_j^2}{2D_j^2}\cos\frac{5\theta+5\beta_j}{2}\right] + \ldots\right\} .$$

Then, assuming that λ_j and ε_j $(\equiv \rho_j/\lambda_j)$ are small, an approximation including effects up to levels included in Equation (37) is

$$d_{jc} \approx 2H(a_j - |x|) - \frac{4v_j}{\pi}\cos\frac{\theta}{2}\left[\left[\frac{3}{2} - \frac{\lambda_j}{8}(1-3\cos\theta) - \frac{\varepsilon_j}{4}(5 - 7\cos\theta)\right]\right. \qquad \text{(A-59)}$$

$$- v_j^2\left\{\frac{5}{6}(2\cos\theta-1) + \frac{\lambda_j}{8}(2\cos\theta-1)\left[2-5\,\frac{1-\cos 3\theta}{3-4\sin^2\theta}\right]+\right.$$

$$\left.\left. + \frac{\varepsilon_j}{2}\left[2\cos 2\theta - 2\cos\theta + H - \frac{5}{2}(2\cos\theta - 1)\frac{1-\cos 3\theta}{3-4\sin^2\theta}\right]\right\} \ldots\right] ,$$

provided that also $v_j^2 << 1$.

A particular value of d_j which may be of interest is that for which $x \to a_j^+$, this being the position for which d_j should be smallest. Assuming that λ_j and ε_j are small, we see that

$$D_j^2 \approx 2\,\lambda_j \quad \text{and} \quad 1-\alpha_j^2 \approx 2(1-\alpha_j) = 2\,\varepsilon_1\,\lambda_j \approx \varepsilon_j\,D_j^2 \ , \text{ so that}$$

$$v_j^2 \approx \left[1-\frac{x^2}{a^2}\right]\ \varepsilon_j/(1-\alpha_j^2) \quad .$$

Letting $x \to a_j^+$ makes $v_j^2 \to \varepsilon_j$. Using this value in Equation (55) shows

$$\lim_{x\to a_j^+} d_{jc} \approx -\frac{4\,\varepsilon_j^{1/2}}{\pi}\cos\frac{\theta}{2}\left[\frac{3}{2}-\frac{\lambda_j}{2}\,(1-3\cos\theta)-\frac{\varepsilon_j}{12}\,(5-\cos\theta)\right] \approx -\frac{6\,\varepsilon_j^{1/2}}{\pi}\cos\frac{\theta}{2} \quad . \quad \text{(A-60)}$$

This limit, multiplied by $b_j \sin\theta$, represents the interference between the surfaces which this dislocation would cause in the absence of an applied load and with no other dislocations.

The function d_{jc} is the one that is needed to define Equation (3) which is used to represent crack-opening displacement. We have here provided an exact, real representation of it in Equation (53), and this representation is one which should be readily computable as well as moderately well comprehensible. An alternative series representation of the exact form is given by Equation (56), and it leads to approximations such as that offered by Equation (59). That approximation must be used only in view of the assumptions that v_j and ε_j [$\equiv(a-a_j)/\ell_j$] are small, so its use in computing must be restricted accordingly, but it also offers opportunities for interpretation such as that in Equation (60).

It may be remarked that computations of d_j based on the complex Equation (47) are apt to produce misplaced steps in the results, since the individual logarithmic terms can have steps for values of x quite different from where the entire function should have its step. This difficulty has been overcome in the real formulations shown here.

Towards Some Simple Theorems on the Displacements Produced on the Crack Due to Dislocation Crack Interactions

This report emphasizes how a simple model of plastic relaxation at a crack tip may be useful in trying to give a quantitative description of fatigue crack growth. It is envisioned that, as the crack progresses, dislocations are emitted from the crack tip leaving in their wake a displacement discontinuity equal to the strength of the super dislocation. That is, when dislocations leave the crack tip, they leave behind a stress on the crack. Using superposition, the resulting displacement can be added to the displacement field produced by the opening of the crack due to the applied stress and residual stress of the dislocation.

A question of some importance with regard to the prediction of a crack-closure effect in fatigue is the effect on the crack face displacements of the compressive stress due to the dislocations. To bound this, consider the following agrument. The compressive stress due to an arrangement of dislocations cannot be greater than when the superdislocation pairs are right at the crack tip. This arrangement gives

$$\sigma_{yy} = -2A\left\{\frac{b}{(x-X)} - \frac{b}{x+X}\right\} = -\frac{2Ab\ X}{(x^2-X^2)} \quad ,$$

where, for $\kappa = 3-4\nu$ (plane strain) or $\frac{3-\nu}{1+\nu}$ (plane stress)

$$A = \frac{2G}{\pi(\kappa+1)} \quad .$$

Solving this limit problem using a continuous distribution of dislocations, or via a direct simple argument, shows that it gives a displacement field of

$$v = -2b\ H\ [X^2-x^2] \quad ,$$

so if $|x| < |X|$, then $v = -2b$. Hence, the net effect of dislocations emanating from the crack tip together with the applied stress cannot ever be negative.

Addendum

Sum of second order terms for approximation of g_{jn} [cf, Equation (42)]:

$$\text{Sum} = \frac{\sqrt{2\lambda_n}\sin^2\theta}{a}\left\{\frac{\sqrt{2\lambda_j}}{L_d^2}\,\frac{\cos\theta}{4}\left(\lambda_j - 2\varepsilon_j - \frac{8A}{L_d}\right) - \frac{\sqrt{2\lambda_n}}{L_d^2}\,\frac{\cos\theta}{4}\left(\lambda_n - 2\varepsilon_n - \frac{8A_d}{L_d}\right)\right.$$

$$+\frac{\sqrt{2\lambda_j}}{L_t^2}\left\{\frac{\cos^2\theta}{4}\left[1+\frac{2L_s(L_d-L_s)\sin^2\theta}{L_t^2}\right]\left(\lambda_j-2\varepsilon_j-\frac{8A_dL_d}{L_d^2}\right)+\right.$$

$$\left.\frac{2AL_s\sin^2\theta}{L_t^2}\left[1+\frac{2L_d(L_s-L_d)\cos^2\theta}{L_t^2}\right]+\frac{\sin^2\theta}{2}\left(\frac{L_s}{2}+\varepsilon_j+\varepsilon_n\right)\left[1-\frac{2L_s(L_s\sin^2\theta+L_d\cos^2\theta}{L_t^2}\right]\right\}$$

$$-\frac{\sqrt{2\lambda_n}}{L_t^2}\left[\frac{\cos\theta}{4}\left(\lambda_n-2\varepsilon_n-\frac{8A_dL_d}{L_t^2}\right)\left\{\cos 2\theta\left[1-\frac{2L_s^2\sin^2\theta}{L_t^2}\right]+\frac{4L_sL_d\sin^2\theta\cos^2\theta}{L_t^2}\right\}\right.$$

$$\left.+\frac{4A_dL_s\sin^2\theta\cos\theta}{L_t^2}\left[1+\frac{L_d(L_s\cos 2\theta-2L_d\cos^2\theta)}{L_t^2}\right]\right]$$

$$+\frac{\sqrt{2\lambda_j}}{2\lambda_nL_d}\cos\theta\left[\frac{1}{4}(\lambda_j-2\varepsilon_j)+\frac{1}{2}(\lambda_n+2\varepsilon_n)-\frac{A_d}{L_d}\right]$$

$$+\frac{\sqrt{2\lambda_j}}{2\lambda_nL_t}\left\{\frac{L_d\cos^2\theta}{L_t}\left[\frac{1}{4}(\lambda_j-\varepsilon_j)+\frac{1}{2}(\lambda_n+2\varepsilon_n)-\frac{A_dL_d}{L_t^2}\right]+\right.$$

$$\left.+\frac{A_d}{L_t}+-\left(\frac{L_d}{4}+\frac{\varepsilon_j}{2}+\frac{3\varepsilon_n}{2}\right)\frac{L_s\sin^2\theta}{L_t}-\frac{A_dL_d^2\cos^2\theta}{L_t^3}\right\}+$$

$$-\frac{\sqrt{2\lambda_j}}{4\lambda_n L_d}\cos\theta\left[\frac{\lambda_j-2\varepsilon_j}{4}+\frac{\lambda_n-2\varepsilon_n}{2}+\frac{A_d}{L_d}\right]+\frac{2\lambda_j\sqrt{2\lambda_n}}{L_d^3}\cos\theta\left[\frac{\lambda_n-2\varepsilon_n}{2}-\frac{3A_d}{L_d}\right]$$

$$+\frac{\sqrt{2\lambda_n}}{L_d^3}\cos\theta\left[L_s\left(\frac{\lambda_j-\varepsilon_j}{4}+\frac{3A}{L_d}\right)+(\lambda_n\varepsilon_n+\lambda_j\varepsilon_j-\lambda_n\lambda_j)\right]$$

$$+\frac{L_d\sqrt{2\lambda_j}}{4\lambda_n L_t^2}\left\{\frac{4A_d+(\lambda_j+2\varepsilon_j-3\lambda_n-6\varepsilon_n)L_s\sin^2\theta}{4L_d}-\frac{A_dL_d}{L_t^2}\cos^2\theta-\cos^2\theta\left[\frac{\lambda_j-2\varepsilon_j}{4}+\frac{\lambda_n-2\varepsilon_n}{2}+\frac{A_dL_d}{L_t^2}\right]\right\}$$

$$+\frac{2L_s\lambda_j\sqrt{2\lambda_n}}{L_t^4}\cos\theta\left\{\left(\frac{\lambda_n-2\varepsilon_n}{4}-\frac{4A_dL_d}{L_t^2}\right)\left[\frac{L_d\cos^2\theta-L_s\sin^2\theta}{L_s}+\frac{4L_d(L_d-L_s)\sin^2\theta\cos^2\theta}{L_t^2}\right]+\right.$$

$$\left.+\frac{A_d\cos\theta}{L_s}\left[1+\frac{4L_s^2\sin^2\theta}{L_t^2}-\frac{8L_s^2(L_s-L_d)\sin^4\theta}{L_t^4}\right]\right\}$$

$$+\frac{\sqrt{2\lambda_j}}{L_t^4}\left\{-\cos^2\theta\left\{-L_sL_d+(L_s-L_d)^2\sin^2\theta+\frac{4L_s^2L_d(L_s-L_d)\sin^2\theta}{L_t^2}\right\}\left(\frac{\lambda_j-2\varepsilon_j}{4}+\frac{4A_dL_d}{L_t^2}\right)\right.$$

$$-A_dL_s\cos^2\theta\left[1+\frac{4L_s^2\sin^2\theta}{L_t^2}-\frac{8L_s^3(L_s-L_d)\sin^4\theta}{L_t^4}\right]+$$

$$\left.+\left[-L_d(L_d+2\overline{\varepsilon_n-\varepsilon_j})\frac{\sin^4\theta}{4}+(\rho_n+\rho_j-\lambda_n\lambda_j)\right]\left[L_d\cos^2\theta-L_s\sin^2\theta+\frac{4L_dL_s(L_d-L_s)\sin^2\theta\cos^2\theta}{L_t^2}\right]+\right.$$

$$+ A_d L_d \sin^2\theta \left[1 - \frac{4L_s^2 \sin^2\theta}{L_t^2} - \frac{8L_s^2(L_s-L_d)\sin^4\theta}{L_t^4}\right] -$$

$$- L_s \left[L_d + 2(\varepsilon_n - \varepsilon_j)\right] \frac{\sin\theta\cos\theta}{4} \left[-(3L_s - L_d)\sin\theta\cos + \frac{4L_s^2(L_s-L_d)\sin^3\theta\cos\theta}{L_t^2}\right] \Bigg\} \Bigg\}$$

$$+ \frac{\sqrt{2\lambda_n}\sin^2\theta}{a} \left[-\frac{\cos\theta}{4}(\lambda_n - 2\varepsilon_n)\right] \Bigg\{ \frac{\sqrt{2\lambda_n}}{L_d^3}(L_d - L_s) + \frac{\sqrt{2\lambda_n}}{L_d^3}(2\lambda_j - L_d) +$$

$$+ \frac{\sqrt{2\lambda_j}}{L_t^4}(L_d - L_s)L_d \cos\theta \left[1 + \frac{4L_s^2\sin^2\theta}{L_t^2}\right] + \frac{3\sqrt{2\lambda_j}}{4\lambda_n L_d}$$

$$+ \frac{3L_d\sqrt{2\lambda_j}\cos\theta}{4\lambda_n L_t^2} + \frac{\sqrt{2\lambda_n}}{L_t^4}\left[L_s L_d - 2(L_d\cos^2\theta + L_s\sin^2\theta)^2 - \frac{4L_s L_d(L_s-L_d)^2\sin^2\theta\cos^2\theta}{L_t^2}\right] \Bigg\}$$

REFERENCES

A-1. Kanninen, M. F., Fedderson, C. E., and Atkinson, C., "Initial Development of a Fatigue-Crack-Retardation Model", NADC-76076-30, Prepared for Naval Air Development Center by Battelle's Columbus Laboratories, Jan. 31, 1976.

A-2. Atkinson, C., and Kanninen, M. F., "A Simple Representation of Crack-Tip Plasticity: The Inclined Strip-Yield Superdislocation Model", International Journal of Fracture, in press, 1977.

APPENDIX B

COMPUTATION OF CRACK-OPENING DISPLACEMENTS WITH AN INCREMENTAL ELASTIC-PLASTIC FINITE-ELEMENT METHOD

APPENDIX B

COMPUTATION OF CRACK OPENING DISPLACEMENTS WITH AN INCREMENTAL ELASTIC-PLASTIC FINITE ELEMENT METHOD

Introduction

Crack-opening displacements for a 12-inch wide, 0.25-inch thick panel with a 1.04-inch center crack have been computed using an elastic-plastic finite-element computer program. Three different panel materials - aluminum, titanium and carbon steel - were analyzed. The properties for each of these materials are summarized in Table B-1.

Two types of stress loads were applied to the panels. One series of analyses were made loading each of the three material panels to half their yield strength and removing the load. A second series of six analyses were conducted only for the aluminum material. The aluminum panels were cyclically loaded to stress states of varying amplitude and mean stress. The center crack was analytically propagated in one analysis and held constant in the other five analyses. Table B-2 summarizes the loading conditions for each of the six cyclic analyses.

The following presents a description of the finite-element program and tables of crack-opening displacements for each analysis.

Description of the Finite-Element Computer Program

A Battelle finite-element computer program has been developed for the specific purpose of solving elastic-plastic fracture problems. The code is an extensively modified version of the AXISOL code developed by Wilson [B-1]. The program uses triangular or quadralateral constant-strain elements formulated by the conventional stiffness approach. Each triangular element is allotted six degrees of freedom by the program. The quadralateral elements are comprised of four triangular elements defined by the four corner nodes of the quadralateral element and a centroidal node. A plane stress or plane strain state can be modeled with the program.

The final solution for a problem is obtained by adding solutions for discrete load increments. Element stiffnesses are recalculated for each load increment. Elastic loading from an elastic-plastic stress state can be modeled with the program. Linear or piecewise-linear hardening is currently employed by the program. No Bauschinger effect is considered.

The program can simulate crack growth by relaxing node forces at the node representing the crack tip. Five relaxation steps are employed to release the crack-tip force. The relaxation procedure is conceptually that used by McClintock [B-2] and by Andersson [B-3].

Computed Crack-Opening Displacements

The following tables present crack-opening displacements for the aluminum, titanium, and carbon steel panels subjected to one load-unload cycle and for aluminum panels subjected to varied cyclic stress loads. Tables B-3 through B-5 list the displacements for the aluminum, titanium, and carbon steel panels, respectively. Tables B-6 through B-11 list the displacements for the cyclically loaded aluminum panels.

References

B-1 Wilson, E. L., "Structural Analysis of Axisymmetric Solids", AIAA Journal, Vol. 3, No. 12, Dec. 1965, pp. 2269-2274.

B-2 McClintock, F. A., Fracture (edited by Liebowitz, D.), Vol. 3: Engineering Fundamentals and Environmental Effects, p. 47. Academic Press, New York.

B-3 Andersson, H., "Finite-Element Treatment of Uniformly Moving Crack-Tip", J. Mech. Phys. Solids, Vol. 22 (1974), pp. 285-308.

TABLE B-1. MATERIAL PROPERTIES FOR CENTER-CRACKED PANELS

Material	Yield Stress, ksi	Elastic Modulus, ksi	Plastic Modulus, ksi	Poisson's Ratio
Aluminum	52.5	10,300	309	0.34
Titanium	120	16,000	480	0.34
Carbon Steel	52.5	29,500	885	0.30

TABLE B-2. CYCLIC APPLIED STRESS LOAD LEVELS FOR ALUMINUM CENTER-CRACKED PANELS

Analysis Number	Mean Stress, psi	Stress Amplitude, psi	Table of Displacements
1	13,125	13,125	B-1, B-6
2	19,688	6,562	B-7
3	26,250	13,125	B-8
4	19,688	6,562	B-9
5	19,688	19,688	B-10
6*	13,125	13,125	B-11

* Center crack extended in this analysis.

TABLE B-3. CRACK OPENING DISPLACEMENTS FOR Al 2024-T3 CENTER-CRACKED PANELS FOR A LOAD-UNLOAD SEQUENCE OBTAINED FROM AN ELASTIC-PLASTIC FINITE ELEMENT ANALYSIS (Plane Stress)

a = 0.52 inches w = 12 inches

Applied Stress, psi	Crack Opening Displacement (Inches) At Various Positions On Crack Face (Inches From Center)					
	x=0	x=.1	x=.2	x=.3	x=.4	x=.461
Maximum Applied Stress = 26,250 psi						
Loading Phase						
22,875	.00220	.00215	.00201	.00176	.00133	.00090
24,000	.00232	.00228	.00213	.00187	.00142	.00098
25,125	.00244	.00240	.00225	.00198	.00152	.00107
26,250	.00257	.00252	.00237	.00209	.00161	.00115
Unloading Phase						
22,495	.00221	.00217	.00204	.00180	.00140	.00101
18,746	.00186	.00182	.00171	.00151	.00118	.00086
14,997	.00150	.00147	.00138	.00123	.00097	.00072
11,248	.00114	.00112	.00106	.00094	.00075	.00058
7,499	.00078	.00077	.00073	.00065	.00054	.00043
3,749	.00042	.00041	.00040	.00037	.00032	.00029
0	.00006	.00007	.00007	.00008	.00011	.00015

TABLE B-4. CRACK OPENING DISPLACEMENTS FOR Ti-6Aℓ-4V CENTER-CRACKED PANELS FOR A LOAD-UNLOAD SEQUENCE OBTAINED FROM AN ELASTIC-PLASTIC FINITE ELEMENT ANALYSIS (Plane Stress)

a = 0.52 inches w = 12 inches

Applied Stress, psi	Crack Opening Displacement (Inches) At Various Positions On Crack Face (Inches from Center)					
	x=0	x=.1	x=.2	x=.3	x=.4	x=.461
Maximum Applied Stress = 60,000 psi						
			Loading Phase			
52,417	.00325	.00318	.00298	.00261	.00197	.00134
54,945	.00343	.00336	.00315	.00276	.00211	.00146
57,472	.00362	.00354	.00332	.00292	.00224	.00158
60,000	.00380	.00372	.00350	.00308	.00238	.00170
			Unloading Phase			
51,424	.00327	.00321	.00301	.00266	.00206	.00149
42,854	.00274	.00269	.00253	.00223	.00175	.00128
34,283	.00221	.00217	.00204	.00181	.00143	.00106
25,712	.00168	.00165	.00156	.00139	.00111	.00085
17,141	.00115	.00113	.00107	.00096	.00079	.00064
8,571	.00062	.00061	.00059	.00054	.00048	.00043
0	.00009	.00010	.00010	.00012	.00016	.00021

AD-A051 584 BATTELLE COLUMBUS LABS OHIO F/G 20/11
THE DEVELOPMENT OF AN ANALYTICAL PREDICTION TECHNIQUE FOR VARIA--ETC(U)
JUN 77 M F KANNINEN, C ATKINSON, J C BELL N62269-76-C-0316
UNCLASSIFIED BATT-8-6490 NADC-77255-30 NL

2 OF 2
AD A051584

END
DATE FILMED
4 -78
DDC

TABLE B-5. CRACK OPENING DISPLACEMENTS FOR CARBON STEEL CENTER-CRACKED PANELS FOR A LOAD-UNLOAD SEQUENCE OBTAINED FROM AN ELASTIC-PLASTIC FINITE ELEMENT ANALYSIS (Plane Stress)

a = 0.52 inches w = 12 inches

Applied Stress, psi	Crack Opening Displacement (Inches) At Various Positions On Crack Face (Inches from Center)					
	x=0	x=.1	x=.2	x=.3	x=.4	x=.461
Maximum Applied Stress = 26,250 psi						
Loading Phase						
18,712	.00045	.00044	.00041	.00036	.00026	.00018
21,225	.00050	.00049	.00045	.00039	.00029	.00019
23,737	.00055	.00054	.00051	.00044	.00032	.00020
26,250	.00061	.00059	.00055	.00048	.00035	.00022
Unloading Phase						
22,496	.00051	.00050	.00047	.00040	.00029	.00019
18,746	.00042	.00041	.00039	.00033	.00023	.00015
14,997	.00033	.00032	.00030	.00025	.00018	.00011
11,247	.00024	.00023	.00022	.00018	.00013	.00007
7,499	.00014	.00014	.00013	.00011	.00007	.00003
3,749	.00052	.00052	.00005	.00003	.00002	.00001
0	.00004	.00004	.00004	.00005	.00004	.00004

TABLE B-6. CRACK OPENING DISPLACEMENTS FOR Al 2024-T3 CENTER-CRACKED PANELS FOR A CYCLIC LOADS OBTAINED FROM AN ELASTIC-PLASTIC FINITE ELEMENT ANALYSIS

a = 0.52 inches w = 12 inches

Applied Stress, psi	Crack Opening Displacement (Inches) At Various Positions On Crack Face (Inches from Center)					
	x=0	x=.1	x=.2	x=.3	x=.4	x=.461
CYCLE 2*						
Mean Stress = 13,125 psi			Stress Amplitude = 13,125 psi			
Loading Phase						
3,281	.00038	.00037	.00036	.00033	.00029	.00027
6,562	.00069	.00068	.00065	.00058	.00048	.00040
9,844	.00100	.00099	.00093	.00083	.00067	.00052
13,125	.00131	.00129	.00122	.00108	.00086	.00065
16,406	.00163	.00160	.00151	.00133	.00105	.00077
19,688	.00195	.00191	.00179	.00158	.00124	.00090
22,969	.00226	.00222	.00208	.00183	.00142	.00102
26,250	.00257	.00252	.00237	.00209	.00161	.00115
Unloading Phase						
22,496	.00221	.00217	.00204	.00180	.00139	.00101
18,746	.00186	.00182	.00171	.00151	.00118	.00086
14,997	.00150	.00147	.00138	.00123	.00097	.00072
11,248	.00114	.00112	.00105	.00094	.00075	.00058
7,498	.00078	.00077	.00073	.00065	.00054	.00043
3,749	.00042	.00042	.00040	.00037	.00032	.00029
0	.00006	.00007	.00007	.00008	.00011	.00015

* Results for Cycle 1 listed in Table B.

TABLE B-7. CRACK OPENING DISPLACEMENTS FOR Al 2024-T3 CENTER-CRACKED PANELS FOR CYCLIC STRESS LOADING OBTAINED FROM AN ELASTIC-PLASTIC FINITE ELEMENT ANALYSIS (Plane Stress)

a = 0.52 inches w= 12 inches

Applied Stress, psi	Crack Opening Displacement (Inches) At Various Positions On Crack Face (Inches) From Center					
	x=0	x=.1	x=.2	x=.3	x=.4	x=.461
CYCLE 1						
Mean Stress = 19,688 psi			Stress Amplitude = 6,562 psi			
Loading Phase						
22,875	.00220	.00215	.00201	.00176	.00133	.00090
24,000	.00232	.00228	.00213	.00187	.00142	.00098
25,125	.00245	.00240	.00225	.00198	.00152	.00170
26,250	.00257	.00252	.00237	.00209	.00161	.00115
Unloading Phase						
21,872	.00216	.00211	.00198	.00175	.00136	.00098
17,498	.00174	.00170	.00160	.00142	.00111	.00082
13,125	.00132	.00129	.00122	.00108	.00086	.00065
CYCLE 2						
Loading Phase						
16,406	.00163	.00160	.00151	.00133	.00105	.00077
19,688	.00195	.00191	.00179	.00158	.00124	.00090
22,968	.00226	.00222	.00208	.00184	.00142	.00102
26,250	.00264	.00257	.00237	.00209	.00161	.00115
Unloading Phase						
21,872	.00216	.00211	.00198	.00175	.00136	.00098
17,498	.00174	.00170	.00160	.00142	.00111	.00082
13,125	.00132	.00129	.00122	.00108	.00086	.00065

TABLE B-8. CRACK OPENING DISPLACEMENTS FOR Al 2024-T3 CENTER-CRACKED PANELS FOR CYCLIC STRESS LOADING OBTAINED FROM AN ELASTIC-PLASTIC FINITE ELEMENT ANALYSIS (Plane Stress)

a = 0.52 inches w = 12 inches

Applied Stress, psi	Crack Opening Displacements (Inches) At Various Positions On Crack Face (Inches From Center)					
	x=0	x=.1	x=.2	x=.3	x=.4	x=.461
CYCLE 1						
Mean Stress = 26,250 psi			Stress Amplitude = 13,125 psi			
Loading Phase						
23,954	.00232	.00227	.00212	.00186	.00142	.00098
26,156	.00256	.00251	.00236	.00208	.00160	.00114
28,360	.00282	.00276	.00260	.00230	.00180	.00132
30,563	.00309	.00303	.00285	.00254	.00251	.00152
32,766	.00337	.00331	.00313	.00280	.00225	.00174
34,968	.00369	.00362	.00343	.00309	.00252	.00198
37,172	.00403	.00397	.00377	.00342	.00283	.00226
39,375	.00442	.00435	.00415	.00379	.00318	.00258
Unloading Phase						
35,620	.00404	.00398	.00381	.00349	.00296	.00243
31,871	.00369	.00364	.00348	.00320	.00274	.00229
28,122	.00333	.00328	.00315	.00291	.00253	.00214
24,373	.00297	.00293	.00282	.00263	.00231	.00200
20,624	.00261	.00258	.00249	.00234	.00210	.00186
16,874	.00225	.00223	.00217	.00205	.00189	.00171
13,125	.00190	.00188	.00184	.00177	.00167	.00157

TABLE B-8 (Continued) CRACK OPENING DISPLACEMENTS FOR Al 2024-T3 CENTER-CRACKED PANELS FOR CYCLIC STRESS LOADING OBTAINED FROM AN ELASTIC-PLASTIC FINITE ELEMENT ANALYSIS (Plane Stress)

Applied Stress, psi	a = 0.52 inches w = 12 inches Crack Opening Displacements (Inches) At Various Positions On Crack Face (Inches From Center)					
	x=0	x=.1	x=.2	x=.3	x=.4	x=.461
CYCLE 2						
Mean Stress = 26,250 psi			Stress Amplitude = 13,125 psi			
Loading Phase						
16,406	.00220	.00219	.00212	.00202	.00186	.00169
19,688	.00252	.00250	.00241	.00227	.00205	.00182
22,968	.00284	.00280	.00270	.00252	.00223	.00195
26,250	.00215	.00311	.00299	.00277	.00242	.00207
29,531	.00346	.00342	.00327	.00302	.00261	.00220
32,812	.00378	.00372	.00356	.00327	.00280	.00232
36,094	.00409	.00403	.00385	.00352	.00299	.00245
39,375	.00441	.00435	.00414	.00378	.00318	.00257
Unloading Phase						
35,620	.00406	.00400	.00381	.00349	.00296	.00243
31,871	.00369	.00364	.00349	.00321	.00275	.00229
28,122	.00334	.00329	.00316	.00292	.00254	.00215
24,373	.00299	.00294	.00283	.00263	.00232	.00200
20,624	.00262	.00259	.00250	.00235	.00211	.00186
16,874	.00226	.00224	.00217	.00206	.00189	.00172
13,125	.00191	.00189	.00186	.00178	.00170	.00158

TABLE B-8 (Continued) CRACK OPENING DISPLACEMENTS FOR Al 2024-T3 CENTER-CRACKED PANELS FOR CYCLIC STRESS LOADING OBTAINED FROM AN ELASTIC-PLASTIC FINITE ELEMENT ANALYSIS (Plane Stress)

a = 0.52 inches w = 12 inches

Applied Stress, psi	Crack Opening Displacements (Inches) At Various Positions On Crack Face (Inches From Center)					
	x=0	x=.1	x=.2	x=.3	x=.4	x=.461
CYCLE 3						
Mean Stress = 26,250 psi			Stress Amplitude = 13,125 psi			
Loading Phase						
16,406	.00222	.00220	.00213	.00202	.00186	.00167
19,688	.00253	.00250	.00242	.00228	.00225	.00182
22,968	.00284	.00281	.00271	.00253	.00224	.00195
26,250	.00316	.00312	.00299	.00278	.00243	.00207
29,531	.00247	.00342	.00328	.00303	.00262	.00220
32,812	.00378	.00373	.00357	.00328	.00280	.00233
36,094	.00410	.00404	.00386	.00353	.00299	.00245
39,375	.00441	.00435	.00414	.00378	.00318	.00258
Unloading Phase						
35,620	.00405	.00399	.00381	.00349	.00296	.00243
31,871	.00369	.00364	.00349	.00320	.00275	.00229
28,122	.00334	.00329	.00316	.00292	.00253	.00215
24,373	.00298	.00294	.00283	.00263	.00232	.00200
20,624	.00262	.00259	.00250	.00235	.00210	.00186
16,874	.00226	.00224	.00217	.00206	.00189	.00172
13,125	.00190	.00189	.00184	.00177	.00168	.00157

TABLE B-9. CRACK OPENING DISPLACEMENTS FOR Al 2024-T3 CENTER-CRACKED PANELS FOR CYCLIC STRESS LOADING OBTAINED FROM AN ELASTIC-PLASTIC FINITE ELEMENT ANALYSIS (Plane Stress)

a = 0.52 inches w = 12 inches

Applied Stress, psi	Crack Opening Displacements (Inches) At Various Positions On Crack Face (Inches From Center)					
	x=0	x=.1	x=.2	x=.3	x=.4	x=.461
CYCLE 1						
Mean Stress = 26,250 psi			Stress Amplitude = 13,125 psi			
Loading Phase						
23,954	.00232	.00227	.00212	.00186	.00142	.00098
26,156	.00256	.00251	.00236	.00208	.00160	.00114
28,360	.00282	.00276	.00260	.00230	.00180	.00132
30,563	.00309	.00303	.00285	.00254	.00201	.00152
32,766	.00337	.00331	.00313	.00280	.00225	.00174
34,968	.00369	.00362	.00343	.00309	.00252	.00198
37,172	.00403	.00397	.00377	.00342	.00283	.00226
39,375	.00442	.00435	.00415	.00379	.00318	.00258
Unloading Phase						
35,620	.00404	.00398	.00381	.00349	.00296	.00243
31,871	.00369	.00364	.00348	.00320	.00274	.00229
28,122	.00333	.00328	.00315	.00291	.00253	.00214
24,373	.00297	.00293	.00282	.00263	.00231	.00200
20,624	.00261	.00258	.00249	.00234	.00210	.00186
16,874	.00225	.00223	.00217	.00205	.00189	.00171
13,125	.00190	.00188	.00184	.00177	.00167	.00157

TABLE B-9. (Continued) CRACK OPENING DISPLACEMENTS FOR A1 2024-T3 CENTER-CRACKED PANELS FOR CYCLIC STRESS LOADING OBTAINED FROM AN ELASTIC-PLASTIC FINITE ELEMENT ANALYSIS (Plane Stress)

a = 0.52 inches w = 12 inches

Applied Stress, psi	Crack Opening Displacements (Inches) At Various Positions On Crack Face (Inches From Center)					
	x=0	x=.1	x=.2	x=.3	x=.4	x=.461
CYCLE 2						
Mean Stress = 19,688 psi		Stress Amplitude = 6,562, psi				
Loading Phase						
16,406	.00221	.00219	.00212	.00202	.00186	.00169
19,688	.00252	.00250	.00241	.00227	.00205	.00182
22,969	.00284	.00280	.00270	.00252	.00223	.00195
26,250	.00315	.00311	.00299	.00277	.00242	.00207
Unloading Phase						
21,872	.00273	.00270	.00260	.00244	.00217	.00190
17,498	.00231	.00229	.00222	.00210	.00192	.00174
13,125	.00190	.00188	.00184	.00178	.00167	.00157

TABLE B-10. CRACK OPENING DISPLACEMENT FOR Al 2024-T3 CENTER-CRACKED PANELS FOR CYCLIC STRESS LOADING OBTAINED FROM AN ELASTIC-PLASTIC FINITE ELEMENT ANALYSIS (Plane Stress)

a = 0.52 inches w = 12 inches

Applied Stress, psi	Crack Opening Displacements (Inches) At Various Positions On Crack Face (Inches From Center)					
	x=0	x=.1	x=.2	x=.3	x=.4	x=.461
CYCLE 1						
Mean Stress = 19,688 psi			Stress Amplitude = 19,688 psi			
Loading Phase						
23,954	.00232	.00227	.00212	.00186	.00142	.00098
26,156	.00256	.00251	.00236	.00208	.00160	.00114
28,360	.00282	.00276	.00260	.00230	.00180	.00132
30,563	.00309	.00303	.00285	.00254	.00201	.00152
32,766	.00337	.00331	.00313	.00280	.00225	.00174
34,968	.00369	.00362	.00343	.00309	.00252	.00198
37,172	.00403	.00397	.00377	.00342	.00283	.00226
39,375	.00442	.00435	.00415	.00379	.00318	.00258
Unloading Phase						
35,620	.00404	.00398	.00381	.00349	.00296	.00243
31,871	.00369	.00364	.00348	.00320	.00274	.00229
28,122	.00333	.00328	.00315	.00291	.00253	.00214
24,373	.00297	.00293	.00282	.00263	.00231	.00200
20,624	.00261	.00258	.00249	.00234	.00210	.00186
16,874	.00225	.00223	.00217	.00205	.00189	.00171
13,125	.00190	.00188	.00184	.00177	.00167	.00157
9,844	.00158	.00157	.00155	.00152	.00148	.00144
6,562	.00127	.00127	.00126	.00127	.00129	.00132
3,281	.00095	.00096	.00098	.00101	.00111	.00119
0	.00064	.00065	.00069	.00076	.00092	.00107

TABLE B-10. (Continued) CRACK OPENING DISPLACEMENT FOR Al 2024-T3 CENTER-CRACKED PANELS FOR CYCLIC STRESS LOADING OBTAINED FROM AN ELASTIC-PLASTIC FINITE ELEMENT ANALYSIS (Plane Stress)

a = 0.52 inches w = 12 inches

Applied Stress, psi	Crack Opening Displacements (Inches) At Various Positions On Crack Face (Inches From Center)					
	x=0	x=.1	x=.2	x=.3	x=.4	x=.461
CYCLE 2						
Mean Stress = 19,688 psi			Stress Amplitude = 19,688 psi			
Loading Phase						
3,281	.00095	.00096	.00098	.00101	.00111	.00119
6,562	.00127	.00127	.00126	.00127	.00129	.00132
9,844	.00158	.00157	.00155	.00152	.00148	.00144
13,125	.00190	.00188	.00184	.00177	.00167	.00157
16,406	.00221	.00219	.00212	.00202	.00186	.00169
19,688	.00252	.00250	.00241	.00227	.00205	.00182
22,969	.00284	.00280	.00270	.00252	.00223	.00195
26,250	.00215	.00311	.00299	.00277	.00242	.00207
29,531	.00346	.00342	.00327	.00302	.00261	.00220
32,812	.00378	.00372	.00356	.00327	.00280	.00232
36,094	.00409	.00403	.00385	.00352	.00299	.00245
39,375	.00441	.00435	.00414	.00378	.00318	.00258
Unloading Phase						
35,796	.00407	.00401	.00383	.00351	.00297	.00244
32,212	.00373	.00368	.00352	.00323	.00277	.00230
28,633	.00338	.00334	.00320	.00296	.00256	.00217
25,054	.00304	.00301	.00289	.00268	.00236	.00203
21,475	.00270	.00267	.00258	.00241	.00215	.00189
17,895	.00236	.00233	.00226	.00214	.00195	.00175
14,316	.00202	.00200	.00195	.00186	.00174	.00162
10,737	.00167	.00166	.00164	.00159	.00154	.00148
7,158	.00133	.00133	.00132	.00132	.00133	.00134
3,579	.00099	.00099	.00101	.00104	.00113	.00121
0	.00065	.00066	.00070	.00077	.00092	.00107

TABLE B-11. CRACK OPENING DISPLACEMENTS FOR Al 2024-T3 CENTER-CRACKED PANEL FOR A CYCLIC STRESS LOAD OBTAINED FROM AN ELASTIC-PLASTIC FINITE ELEMENT ANALYSIS (Plane Stress)

a = 0.52 inches w = 12 inches

Applied Stress, psi	Crack Opening Displacements (Inches) At Various Positions On Crack Face (Inches From Center)					
	x=0	x=.1	x=.2	x=.3	x=.4	x=.461
CYCLE 1						
Mean Stress = 13,125 psi			Stress Amplitude = 13,125 psi			
Loading Phase						
22,875	.00220	.00215	.00201	.00176	.00133	.00090
24,000	.00238	.00232	.00213	.00187	.00142	.00098
25,125	.00245	.00240	.00225	.00198	.00152	.00107
26,250	.00257	.00252	.00237	.00209	.00161	.00115
Unloading Phase*						
22,500	.00249	.00245	.00233	.00212	.00180	.00151
18,750	.00208	.00205	.00196	.00179	.00152	.00129
15,000	.00168	.00166	.00151	.00145	.00124	.00106
11,250	.00128	.00126	.00121	.00111	.00096	.00083
7,500	.00088	.00087	.00083	.00077	.00068	.00061
3,750	.00048	.00047	.00046	.00043	.00040	.00038
0	.00008	.00008	.00008	.00008	.00012	.00015

* Unloaded after crack extension of 0.06 inches at maximum load.

TABLE B-11. (Continued) CRACK OPENING DISPLACEMENTS FOR Al 2024-T3 CENTER-CRACKED PANEL FOR A CYCLIC STRESS LOAD OBTAINED FROM AN ELASTIC-PLASTIC FINITE ELEMENT ANALYSIS (Plane Stress)

a = 0.52 inches w = 12 inches

Applied Stress, psi	Crack Opening Displacements (Inches) At Various Positions On Crack Face (Inches From Center)					
	x=0	x=.1	x=.2	x=.3	x=.4	x=.461
CYCLE 2						
Mean Stress = 13,125 psi			Stress Amplitude = 13, 125 psi			
Loading Phase						
3,281	.00043	.00043	.00041	.00039	.00036	.00035
6,582	.00078	.00077	.00074	.00069	.00061	.00055
9,844	.00113	.00112	.00107	.00098	.00085	.00075
13,125	.00148	.00146	.00139	.00128	.00110	.00095
16,406	.00183	.00181	.00172	.00157	.00134	.00114
19,688	.00218	.00215	.00205	.00187	.00159	.00134
22,969	.00254	.00250	.00238	.00217	.00183	.00154
26,250	.00289	.00284	.00271	.00246	.00208	.00174
Unloading Phase*						
22,500	.00277	.00274	.00263	.00245	.00218	.00195
18,750	.00233	.00230	.00221	.00207	.00184	.00166
15,000	.00188	.00186	.00179	.00168	.00150	.00137
11,250	.00144	.00142	.00137	.00129	.00117	.00107
7,500	.00100	.00099	.00095	.00090	.00083	.00077
3,750	.00055	.00055	.00053	.00051	.00049	.00048
0	.00011	.00011	.00011	.00012	.00015	.00018

* Unloaded after crack extension of 0.06 inches at maximum load.

TABLE B-11. (Continued) CRACK OPENING DISPLACEMENTS FOR Al 2024-T3 CENTER-CRACKED PANEL FOR A CYCLIC STRESS LOAD OBTAINED FROM AN ELASTIC-PLASTIC FINITE-ELEMENT ANALYSIS (Plane Stress)

a = 0.52 inches w = 12 inches

Applied Stress, psi	Crack Opening Displacements (Inches) At Various Positions On Crack Face (Inches From Center)					
	x=0	x=.1	x=.2	x=.3	x=.4	x=.461
CYCLE 3						
Mean Stress = 13,125 psi			**Stress Amplitude = 13, 125 psi**			
Loading Phase						
3,281	.00050	.00049	.00048	.00046	.00044	.00044
6,562	.00089	.00087	.00085	.00080	.00074	.00070
9,844	.00127	.00126	.00122	.00114	.00104	.00096
13,125	.00166	.00164	.00158	.00148	.00133	.00122
16,406	.00205	.00203	.00195	.00182	.00163	.00148
19,688	.00244	.00241	.00232	.00216	.00193	.00174
22,969	.00283	.00279	.00269	.00250	.00222	.00199
26,250	.00322	.00318	.00305	.00284	.00252	.00225
Unloading Phase*						
22,500	.00304	.00300	.00291	.00275	.00251	.00233
18,750	.00255	.00252	.00245	.00231	.00212	.00197
15,000	.00207	.00204	.00198	.00188	.00173	.00161
11,250	.00158	.00156	.00152	.00144	.00133	.00126
7,500	.00109	.00108	.00105	.00100	.00094	.00090
3,750	.000604	.000600	.000588	.000569	.000549	.000542
0	.000117	.000118	.000123	.000132	.000156	.000185

* Unloaded after crack extension of 0.06 inches at maximum load.

TABLE B-11. (Continued) CRACK OPENING DISPLACEMENTS FOR Al 2024-T3 CENTER-CRACKED PANEL FOR A CYCLIC STRESS LOAD OBTAINED FROM AN ELASTIC-PLASTIC FINITE ELEMENT ANALYSIS (Plane Stress)

a = 0.52 inches w = 12 inches

Applied Stress, psi	Crack Opening Displacements (Inches) At Various Positions On Crack Face (Inches From Center)					
	x=0	x=.1	x=.2	x=.3	x=.4	x=.461
CYCLE 4						
Mean Stress = 13,125 psi			Stress Amplitude = 13, 125 psi			
Loading Phase						
3,281	.00054	.00053	.00053	.00051	.00050	.00049
6,562	.00097	.00096	.00094	.00090	.00084	.00081
9,844	.00140	.00138	.00134	.00128	.00119	.00112
13,125	.00182	.00180	.00175	.00166	.00153	.00143
16,406	.00225	.00222	.00216	.00204	.00187	.00175
19,688	.00267	.00264	.00256	.00242	.00222	.00206
22,969	.00310	.00307	.00297	.00281	.00256	.00237
26,250	.00353	.00349	.00338	.00320	.00291	.00268
Unloading Phase*						
22,500	.00332	.00329	.00321	.00306	.00285	.00269
18,750	.00279	.00277	.00270	.00258	.00241	.00228
15,000	.00226	.00224	.00219	.00209	.00196	.00186
11,250	.00173	.00172	.00168	.00161	.00151	.00145
7,500	.00120	.00119	.00117	.00112	.00107	.00103
3,750	.000670	.000666	.000656	.000639	.000623	.000620
0	.000139	.000141	.000145	.000155	.000178	.000206

* Unloaded after crack extension of 0.06 inches at maximum load.

DISTRIBUTION LIST

REPORT NO. NADC-77255-30
AIRTASK NO. WR 02303001, WORK UNIT DG-602

	No. of Copies
NAVAIRSYSCOM, AIR-50174 (2 for retention, 2 for AIR-530, 1 for AIR-530215, 1 for AIR-530221C, 2 for AIR-320B)	8
NAVAIRTESTCEN, Patuxent River, Maryland	1
NAVAVNSAFECEN, NAS, Norfolk, Virginia	1
CNAVANTRA, NAS, Corpus Christi, Texas	1
CNABATRA, NAS, Pensacola, Florida	1
CNARESTRA, NAS, Glenview, Illinois	1
CNATRA, NAS, Pensacola, Florida	1
NAVAIRSYSCOMREPLANT	1
NAVAIRSYSCOMREPCENT	1
NAVAIRSYSCOMREPAC	1
NAVAIREWORKFAC, NAS, Alameda, California	1
NAVAIREWORKFAC, NAS, Jacksonville, Florida	1
NAVAIREWORKFAC, NAS, Norfolk, Virginia	1
NAVAIREWORKFAC, NAS, Pensacola, Florida	1
NAVAIREWORKFAC, NAS, Quonset Point, Rhode Island	1
NAVAIREWORKFAC, NAS, San Diego, California	1
NAVAIREWORKFAC, NAS, Cherry Point, North Carolina	1
COMNAVAIRLANT	1
COMNAVAIRPAC	1
NWL, Dahlgren, Virginia (Attention Mr. Morton)	1
USAF Systems Command, WPAFB, Ohio 45433	
Attention FBR	1
Attention FB	1
Attention LLD	1
Attention SEFS	1
Attention FYA	1
Attention LAM	1
Attention FBA	1
Attention LPH	1
USA AMMRC, Watertown, Massachusetts	1
USA APG, Aberdeen, Maryland	1
USA AMRDL, Fort Eustis, Virginia (Attention Mr. Berrisford)	1
USA AVSCOM, St. Louis, Missouri (Attention AMSAV-GR)	1
Defense Research and Development Staff, British Embassy, Washington, D.C., via NAVAIR (AIR-5302)	1
Canadian Joint Staff, Navy Member, Washington, D.C., via NAVAIR (AIR-5302)	1
Technical Advisory, AFIAS-B, Directorate of Aerospace Safety, Norton AFB, California	1
DDC	12
NAVSEASYSCOM, Washington, D.C. 20362 (Attention Mr. C. Pohler, Code 035)	1
NAVSHIPRADCEN, Bethesda, Maryland 20034 (Attention Mr. A. B. Stavovy 730)	1
Bell Aerosystems Co., Buffalo, New York 14205	1
Bell Helicopter Co., Fort Worth, Texas 76101	1
Boeing Co., Airplane Div., Seattle, Washington 98124 (Attention Mr. T. Porter)	1

DISTRIBUTION LIST (continued)

	No. of Copies
Boeing Co., Airplane Div., Wichita, Kansas 67210	1
Boeing Co., Vertol Div., Philadelphia, Pennsylvania 19142	1
McDonnell Douglas Aircraft Corp., Aircraft Div., Long Beach, California 90801	1
General Dynamics/Convair, San Diego, California 92112	1
General Dynamics Corp., Fort Worth, Texas 76101	1
Goodyear Aerospace Corp., Akron, Ohio 44305	1
Grumman Aerospace Corp., Bethpage, Long Island, New York 11714	1
Aircraft-Missiles Div., Fairchild-Hiller Corp.,	1
Hagerstown, Maryland 21740	1
Kaman Aircraft Corp., Bloomfield, Connecticut 06002	1
Lockheed Aircraft Corp., Lockheed-California Co., Burbank, California 91503	1
Lockheed Aircraft Corp., Lockheed-Georgia Co., Marietta, Georgia 30061	1
LTV Aerospace Corp., Dallas, Texas 75222	1
Martin Co., Baltimore, Maryland 21203	1
McDonnell Douglas Aircraft Corp., St. Louis, Missouri 63166	1
Rockwell International, Columbus Aircraft Div., Columbus, Ohio 43216 (Attention Mr. O. Acker)	1
Rockwell International, Los Angeles, California 90053 (Attention Mr. G. Fitch)	1
Northrop Corp., Aircraft Div., Hawthorne, California 90250	1
Republic Aviation Div., Fairchild-Hiller Corp., Farmingdale, Long Island, New York 11735	1
Sikorsky Aircraft Co., Stratford, Connecticut 06497	1
Hdqtrs., R&T Div., AFSC, Bolling AFB, Washington, D.C. 22209	1
Office of Aerospace Research, Arlington, Virginia 22209	1
FAA (FS-120), Washington, D.C., 20553	1
Scientific and Technical Information Facility, College Park, Maryland 20740 (NASA Rep.)	2
Administrator, NASA, Washington, D.C. 20546	1
NASA-Langley Research Center, Materials Div., Hampton Virginia 23365 (Attention Mr. H. F. Hardrath)	1
National BuStds, Washington, D.C. 20234	1
Office of Naval Research, Washington, D.C. 20362 (Attention Dr. N. Perrone)	1
Director, Naval Research Lab, Washington, D.C. 20390	1
Midwest Research Institute, Kansas City, Missouri 64110	1
University of Illinois, Urbana, Illinois 61803 (Attention Prof. T. J. Dolan and Prof. J. Morrow)	1 each
University of Kansas, Lawrence, Kansas 66044	1
University of Michigan, Ann Arbor, Michigan 48105	1
University of Minnesota, Minneapolis, Minnesota 55455	1
Alcoa, Alcoa Labs, Alcoa Center, Pennsylvania 15069 (Attention Mr. J. G. Kaufman)	1
Lehigh University, Bethlehem, Pennsylvania 18015 (Attention Prof. G. C. Sih)	1
Belfour-Stulen, Inc., Traverse City, Michigan 49684	1
Cornell Aero. Lab, Buffalo, New York 14221	1

DISTRIBUTION LIST (continued)

	No. of Copies
Metals & Ceramics Information Center, Battelle, Columbus Laboratories Columbus, Ohio 43201	1
NASA, Lewis Research Center, Cleveland, Ohio 44153 (Attention Technical Library)	1
Naval Postgraduate School, Monterey, California 93940 (Attention Prof. Lindsey)	1
Battelle, Pacific Northwest Laboratories, P. O. Box 999, Richland, Washington 99352 (Attention Mr. W. E. Anderson)	1
School of Engineering, George Washington University, Washington, D.C. 20006 (Attention Prof. H. Liebowitz)	1
Dept. of Metallurgy, University of Connecticut, Storrs, Connecticut 06268 (Attention Prof. A. J. McEvily)	1
Dept. of Mech. Eng., Washington University, St. Louis, Missouri (Attention Prof. P. C. Paris)	1
Materials Dept., 6531 Boelter Hall, University of California at Los Angeles, Los Angeles, California 90024 (Attention Prof. A. S. Tetelman)	1
National Transportation Safety Board, 800 Independence, Washington, D.C. 20594 (Attention Mr. W. D. Cowan)	1
Pratt and Whitney Aircraft, P. O. Box 611, Middletown, Connecticut (Attention Mr. C. A. Rau)	1
Aeronautics Dept., Delft University, Delft, Holland (Attention Prof. J. Schijve)	1
FAA, 800 Independence, Washington, D. C. 20594 (Attention Mr. D. Kemp)	1
Air Force Flight Dynamics Lab, WPAFB, Ohio 45433 (Attention Mr. R. M. Engle)	1
VanderBilt University, P. O. Box 3245 Station B, Nashville, Tennessee 37235 (Attention Prof. P. Packman)	1
Air Force Flight Dynamics Lab., Wright-Patterson Air Force Base, Ohio 45433, (Attention Mr. H. A. Wood)	1
NASA-Langley Research Center, Hampton, Virginia 23665 (Attention Dr. J. C. Newman, Jr.)	1
Max-Planck-Institut for Eisenforschung, 4000 Dusseldorf, Max-Planck-Strasse 1, Germany (Attention Prof. P. Neumann)	1
Lehigh University, Metallurgy and Materials Science, Bethlehem, Pennsylvania 18015 (Attention Prof. R. W. Hertzberg)	1
Southwest Research Institute, 8500 Culebra Rd., San Antonio, Texas 78228 (Attention Dr. J. Lankford)	1
Electric Power Research Institute, P.O. Box 10412, 3412 Hillview Avenue, Palo Alto, California 94303 (Attention K. Stahlkopf)	1
The University of Newcastle Upon Tyne, Newcastle Upon Tyne NE1 7RU England (Attention Dr. J. T. Evans, Dept. of Metallurgy)	1
United Kingdom Atomic Energy Authority, 11 Charles 2 St., SW1, London, England (Attention B. Tomkins)	1
Purdue University, Lafayette, Indiana 47907 (Attention B. M. Hillberry)	1
Massachusetts Institute of Technology, 77 Massachusetts Ave., Cambridge, Massachusetts 02139 (Attention R. M. Pelloux)	1
U.S. Naval Research Laboratory, 4555 Overlook Ave., SW, Washington, D.C., 20032, (Attention T. W. Crooker)	1

DISTRIBUTION LIST (continued)

	No. of Copies
University of Harvard, Cambridge, Massachusetts 02138 (Attention J. W. Hutchinson).	1
U.S. Nuclear Regulatory Commission, Washington, D.C., 20555 (Attention R. E. Johnson)	1
University of Iowa, Iowa City, Iowa, 52252 (Attension R. I. Stephens). .	1